EFFECT OF DUST DISPERSION AND MORPHOLOGY ON DUST DEFLAGRATION HAZARD

A Dissertation

by

PRANAV BAGARIA

Submitted to the Office of Graduate and Professional Studies of
Texas A&M University
in partial fulfillment of the requirements for the degree of

DOCTOR OF PHILOSOPHY

Chair of Committee,	Chad V. Mashuga
Committee Members,	James Holste
	Eric L. Petersen
	Zhengdong Cheng
Head of Department,	Nazmul M. Karim

May 2019

Major Subject: Chemical Engineering

ABSTRACT

Dust explosions have led to numerous fatalities, injuries and property loss. Standards (ASTM, ISO etc.) mention a 20 L or a 1 m^3 apparatus to measure explosion parameters. These standards assume the dust particle size distribution remains unaltered post-dispersion in these apparatus. Recent studies have shown that dispersion in the standard 20 L apparatus, widely used for dust explosion properties measurement, leads to significant particle breakage. Reduction in particle size distribution due to dispersion can lead to erroneous risk assessment due to association of explosion parameters with pre-dispersion particle size distribution.

This research investigates various factors that affect dust particle size reduction during dispersion and studies the effect of dust particle shape on minimum ignition energy (*MIE*). First, we explored the role of outlet valve, dispersion nozzle, cloud turbulence, and dust concentration on particle breakage. Also, the behavior of nanomaterial post-dispersion was analyzed. Results show significant particle breakage occurs due to outlet valve, nozzle, and cloud turbulence. An inverse relation between dust concentration and particle breakage was found. Nanomaterial de-agglomerates post-dispersion generating large surface area, thereby increasing explosion hazard. Second, we analyzed particle breakage due to dispersion in the *MIE* apparatus. Results show that *MIE* apparatus does not cause particle breakage but it alters the size distribution of electrostatic dusts significantly, which can affect ignition energy measurement of electrostatic dusts. Third, consequence of particle breakage due to dispersion on *MIE* was

studied. Results show significant reduction in the *MIE* value of the dust post-dispersion, highlighting increased risk. Fourth, dependence of size reduction due to dust dispersion on different materials was studied. A sigmoidal correlation between particle breakage due to dispersion and the mechanical properties (brittleness index) of materials was established allowing process industries to identify dusts susceptible to breakage during explosion testing. Finally, we examined the effect of particle morphology on *MIE* of dusts. By testing spherical and irregular shaped material with similar size distribution, we demonstrated that morphology significantly impacts the *MIE* of dusts and should be included as a factor in risk assessment.

This research will result in improved ASTM testing standards and accurate risk assessment for better safety measures.

DEDICATION

To

God

My parents Kanta Bagaria and Rajiv Lochan Bagaria

My siblings Divya Bagaria and Prakhar Bagaria

My extended family

My mentor (Late) Dr. M. Sam Mannan

My best friend Pranjali Shah

ACKNOWLEDGEMENTS

I would like to express my sincere gratitude to Dr. Mashuga for all the guidance and support throughout my PhD. I appreciate the challenges and experiences that helped me become a better researcher and a better person. I would like to thank my committee members, Dr. James Holste, Dr. Zhengdong Cheng, and Dr. Eric L. Petersen, for their inputs and guidance over the course of this research. Thanks to (Late) Dr. Sam Mannan for the motivation, guidance and providing me with plenty of opportunities to succeed. He has been integral to my personal and professional development. I acknowledge members of Mary Kay O'Connor Process Safety Center, especially Ms. Valerie Green, Ms. Alanna Scheinerman, and Ms. Sheera Helms for their administrative assistance.

I would like to thank Dr. Hans Pasman, and Dr. Maria Papadaki for sharing their expert knowledge and valuable experience. I would also like to thank Dr. Ashok Dastidar from Fauske & Associates, LLC. for his collaboration in this research. Usage of the Texas A&M University (TAMU) Materials Characterization Facility, and guidance of Dr. Yordanos Bisrat and Dr. Wilson Serem are acknowledged. I appreciate the staff of Chemical Engineering, especially Ms. Ashley Henley and Mr. Louis Muniz Jr. for their professional assistance.

Finally, special thanks to my mother, my father, my siblings and my extended family for their unconditional love, encouragement and support; and thanks to my best friend Ms. Pranjali Shah for supporting me, helping me achieve my goals and making this journey a little bit easier.

CONTRIBUTORS AND FUNDING SOURCES

This work was supervised by a dissertation committee consisting of Dr. Chad V. Mashuga [Committee Chair], Dr. James Holste [Committee Member], and Dr. Zhengdong Cheng [Committee Member] of the Department of Chemical Engineering and Dr. Eric L. Petersen [Committee Member] of the Department of Mechanical Engineering.

The dispersion experiments conducted in Chapter III were conducted in part by Mr. Gary Payne from Fauske & Associates, LLC. and Mr. Entao Yang from Tianjin University. The SEM images in Chapter III and Chapter IV were provided by Dr. Jiaqi Zhang of the Department of Chemical Engineering, Texas A&M University. The results of Chapter III and Chapter IV were published in 2016 and 2017, respectively. The dispersion experiments in Chapter V were conducted in part by Mr. Michael Lim and Mr. Mark Olinger from Fauske & Associates, LLC. Nanoindentation experiments in Chapter V were conducted in part by Dr. Qiang Li of the Department of Plant Pathology and Microbiology, Texas A&M University and Dr. Wilson Serem of the Material Characterization Facility (MCF), Texas A&M University. The results of Chapter V were published in 2019. Ignition energy testing in Chapter VI and Chapter VII was conducted in part by Mr. Ben Hall and Mr. Shrey Prasad of the Department of Chemical Engineering, Texas A&M University. The samples in Chapter VII were donated by ECKA Granules Australia Pty Ltd. and Henan Yuan Yang Aluminum Industry Co. Ltd.

All other work and analyses conducted for the dissertation was completed by the student independently.

Graduate study was supported by the startup fund from Texas A&M University for Dr. Chad V. Mashuga. The contents of this research are solely the responsibility of the authors and do not necessarily represent the official views of Texas A&M University.

TABLE OF CONTENTS

Page

LIST OF FIGURES

Page

LIST OF TABLES

Page

CHAPTER I

INTRODUCTION

1.1. Motivation for dust explosion research[*]

Since the first recorded dust explosion incident in 1785 [1], countless more have occurred on a frequent basis. Around 3500 dust explosion incidents occurred between 1980 and 2005 in the United States, out of which 281 were major events resulting in 119 fatalities and 718 worker injuries. In the U.S. agricultural sector from 1996 to 2005, a total of 106 incidents occurred, killing 16 people, injuring 126 and resulting in $162.8 million in facility damage [2]. Another 82 dust-related fires and explosions occurred between 2006 and 2008 in the U.S. [3]. During 2008–2012, 50 incidents occurred resulting in 29 fatalities and 161 injuries [4]. If averaged, the rate of dust explosion incident in the U.S. is > 1 per month between 1980 and 2012. These staggering statistics are only for the U.S., if global incidents are considered, the situation becomes much worse. Some of the recent major dust explosion incidents are shown in Table 1. The sheer number of incidents, fatalities, and losses depicts the seriousness of the industrial dust explosion problem and shows the need for increased hazard awareness and dedicated research to improve understanding of such events.

[*] [14] Reprinted with permission from "Effect of dust dispersion on particle breakage and size distribution in the minimum ignition energy apparatus" by Bagaria, P., Zhang, J., & Mashuga, C., 2018. Journal of Loss Prevention in the Process Industries, 56, 518-523, Copyright (2018) by Elsevier.

Table 1 Major dust explosion incidents between 2010 and 2015 [[4]-[8], [14]]. Reprinted with permission from "Effect of dust dispersion on particle breakage and size distribution in the minimum ignition energy apparatus" by Bagaria, P., Zhang, J., & Mashuga, C., 2018. Journal of Loss Prevention in the Process Industries, 56, 518-523, Copyright (2018) by Elsevier.

Incident	Location and Year	Material and Consequence
AL Solutions	U.S.A, 2010	Titanium-Zirconium Powder, 3 fatalities
Foxconn Plant Explosion	China, 2011	Aluminum Dust, 4 fatalities, 18 injuries
U.S. Ink Fire	U.S.A, 2012	Gilsonite, Carbon Black, and Petroleum Distillate Powder Mixture, 7 injuries
Kunshan Explosion	China, 2014	Metal Powder, 146 fatalities
Formosa Fun Coast	Taiwan, 2015	Colored Cornstarch, 15 fatalities, ~ 500 injuries

1.2. Dust explosion

Dust explosion is a process of rapid combustion of fine combustible particles suspended in air or oxidizing medium. The five necessary elements that are required for dust explosion to take place are combustible dust (fuel), oxygen, ignition, dispersion, and confinement. These necessary elements form the sides of a dust explosion pentagon as shown in Figure 1 [9]. Dust explosions, in general are known to cause widespread destruction in powder manufacturing/processing facilities. Some of the common examples of dusts that can ignite are shown in Figure 2 [10]. In some cases, a primary dust explosion is followed by a secondary dust explosion. A secondary dust explosion occurs when the blast wave from a primary explosion travels, causing the settled dust present in the facility to disperse, generating conditions conducive for another dust explosion to occur [9][11]. Some examples where secondary dust explosion increased the

damage and caused great deal of loss are the explosions at the West Pharmaceutical (North Carolina facility) in 2003 and Imperial Sugar (Georgia facility) in 2008 [12].

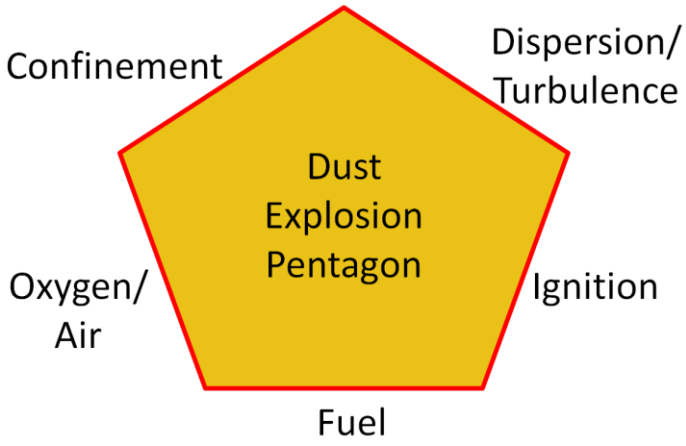

Figure 1 Dust explosion pentagon. Adapted from [13].

Table 2 Dust explosion risk assessment parameters.

Terms	Definition	Standard
Consequence of Dust Explosion		
P_{ex}	Maximum explosion pressure (above the pressure in the vessel at the time of ignition) reached after ignition at specific concentration	ASTM E1226-10
K_{st}	Deflagration Index; $K_{st} = (dP/dt)_{max} * V^{(1/3)}$	ASTM E1226-10
Probability of Dust Explosion		

Table 2 Continued.

Terms	Definition	Standard
Probability of Dust Explosion		
LOC	Oxygen (oxidant) concentration at the limit of flammability for the worst most flammable fuel concentration	ASTM 2931-13
MIE	Energy sufficient to affect ignition of the most easily ignitable concentration of fuel in air	ASTM E2019-03
MEC	Minimum concentration of a combustible dust cloud that is capable of propagating a deflagration	ASTM E1515-07

Figure 2 Example of combustible dusts. Adapted from [10].

In order to evaluate the threat of dust explosion, risk assessment is required. The risk of dust explosion depends on the probability of ignition and the consequence thereafter. The ignition probability or ease of ignition depends on chemical composition of dust, volatile content, particle size distribution, ignition energy, dust cloud concentration, dust cloud turbulence *etc*. The consequence is defined by explosion overpressure, flame speed, rate of pressure rise, radiation signature *etc*. [14]. Several parameters are defined by ASTM International to quantify the ease of ignition and

consequence of dust explosions. These parameters are shown in Table 2. *MEC*, *LOC*, *MIE*, and *AIT* represent the probability of ignition as they control the ease of ignition. P_{ex}, and K_{st} represent the consequence of dust explosions.

To quantify the parameters for dust explosion risk evaluation, several standards have been issued. The standards used to evaluate P_{ex}, K_{st}, *LOC*, and *MEC* include: International Standards Organization (ISO) Method 6184/1; National Fire Protection Association (NFPA) Standard 68; ASTM International Method E1226 and E1515; German Society of Engineers (VDI) Method 3673; British European Standard (BS EN) Methods 14034-1, 14034-2 and 13821 [15][16]. These standards mention the use of 20 L spherical apparatus or 1 m^3 spherical apparatus to measure P_{ex}, K_{st}, *LOC*, and *MEC*. The 20 L dust explosion apparatus consists of a 20 L explosion vessel that has spherical or a cylindrical geometry (length/diameter ratio ~ 1). The dust is stored in a dust container (located outside the explosion vessel). A dispersion nozzle is fixed inside the vessel to facilitate a uniform, turbulent dust cloud inside the spherical explosion vessel. The explosion vessel is initially subjected to a vacuum of approximately 0.3 bar – 0.4 bar (absolute pressure inside the vessel after vacuuming ranges from 0.6 bar – 0.7 bar). The dust container is pressurized with compressed air to approximately 21 bar. The pressure in the container is released which carries the dust from the dust container through the outlet valve and dispersion nozzle into the vessel. This creates a uniform dust cloud in the vessel at ambient pressure (Figure 3) [17][18]. An explosive igniter (1 kJ, 5 kJ, or 10 kJ) at the center of the vessel provides the ignition after a delay of approximately 60 ms. On ignition, the data acquisition system (DAQ) captures the pressure as a function of time as

shown in Figure 4 (a). Figure 4 (b) shows the overpressure profile as a function of dust concentration, generated using a 20 L apparatus to find the optimum concentration for optimum maximum explosion pressure [19]. ISO 1 m^3 apparatus (Figure 5) is similar to the 20 L apparatus but with different dispersion pressure and time delay. In fact, the 20 L dust explosion apparatus is calibrated to yield similar results to that of 1 m^3 apparatus. This is because 1 m^3 apparatus has a larger volume which simulates the industrial scenario and also the generated results in this apparatus are closer to real industrial data [20][21]. There are other apparatus of different volume capacity such as the 36 L dust explosion apparatus (Figure 6) at the Mary Kay O'Connor Process Safety Center (MKOPSC), Texas A&M University, which are calibrated to yield similar results to the standard 20 L and 1 m^3 apparatus [22].

Figure 3 20 L dust explosion apparatus, Fauske & Associates, LLC [23]. Reprinted with permission from "Classification of particle breakage due to dust dispersion" by Bagaria, P., Li, Q., Dastidar, A., & Mashuga, C., 2019. Powder Technology, 342, 204-213. Copyright (2019) by Elsevier.

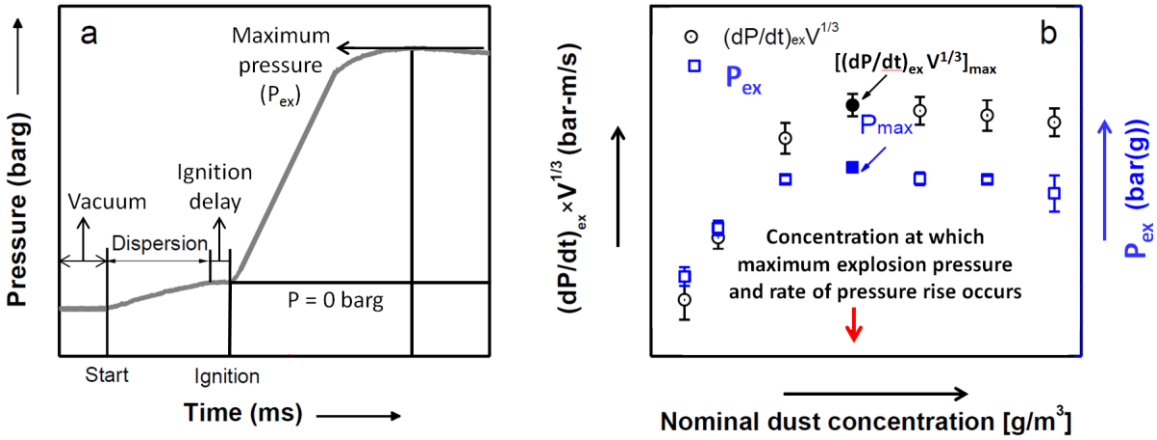

Figure 4 (a) Pressure vs time in a standard 20 L explosion testing at specific concentration; (b) Explosion pressure, explosion pressure rate vs concentration. Adapted from [19].

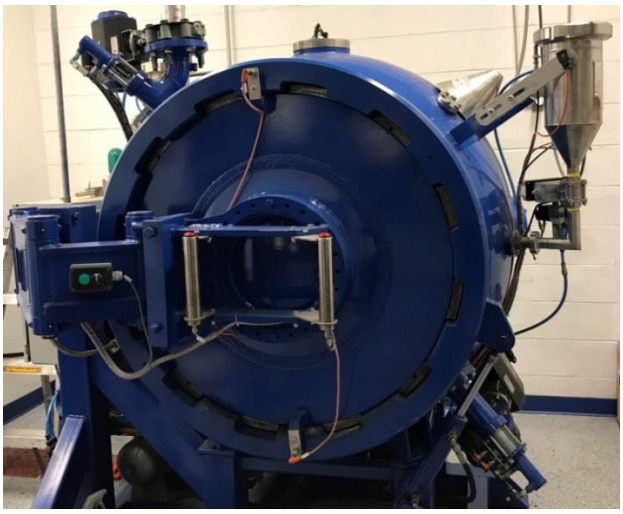

Figure 5 1 m^3 dust explosion apparatus, Fauske & Associates, LLC [23]. Reprinted with permission from "Classification of particle breakage due to dust dispersion" by Bagaria, P., Li, Q., Dastidar, A., & Mashuga, C., 2019. Powder Technology, 342, 204-213. Copyright (2019) by Elsevier.

Figure 6 36 L dust explosion apparatus, Texas A&M University [23]. Reprinted with permission from "Classification of particle breakage due to dust dispersion" by Bagaria, P., Li, Q., Dastidar, A., & Mashuga, C., 2019. Powder Technology, 342, 204-213. Copyright (2019) by Elsevier.

Minimum Ignition Energy (*MIE*) is another important parameter evaluated in accordance with the ASTM E2019-03 (2013), ISO/IEC 80079-20-2, and EN 13821 standards [24]. According to these standards, minimum ignition energy apparatus consists of a 1.2 L cylindrical Hartmann tube and a dispersion nozzle as shown in Figure 7. The dust sample is placed around the mushroom shaped nozzle and the nozzle disperses the dust into the Hartman tube with an air pulse of 7 bar. A capacitive spark triggered between two tungsten electrodes is used to attempt ignition of the dust cloud formed after dispersion. The device allows ignition energy testing in the range of 1 mJ to 1000 mJ at

fixed energy levels of 1, 3, 10, 30, 100, 300 and 1000 mJ. The device permits variable inductance of 0 mH or 1 mH and adjustable ignition delay times of 90, 120, 150 and 180 ms. The dust is tested for ignition / no ignition at concentrations ranging from 125 g/m^3 to 3000 g/m^3. The ignition and no-ignition energy levels are clearly identified while testing. A typical ignition energy (mJ) vs dust weight (mg) relationship is seen in Figure 8. Visual confirmation is required to mark ignition and no ignition. Ten no ignition attempts are required to mark a dust as no ignition at a specific concentration and energy level. From the testing data, the *MIE* is determined statistically based on the equation 1 [25]:

$$MIE = 10^{\frac{(\log E2 - I[E2].(\log E2 - \log E1)}{((NI+I)[E2]+1)}} \quad \text{Eq.1}$$

Where, E_2 is the energy level at which ignition is observed and E_1 is the energy level just below E_2 where no ignition was observed after 10 tests. $I[E_2]$ correspond to the number of tests having ignition at the energy E_2 and $(NI+I)[E_2]$ represent the total number of tests at E_2. For *MIE* calculations, $(NI+I)[E_2]$ should be greater or equal to 5 tests.

Figure 7 Kühner MIKE3 Minimum Ignition Energy (*MIE*) apparatus.

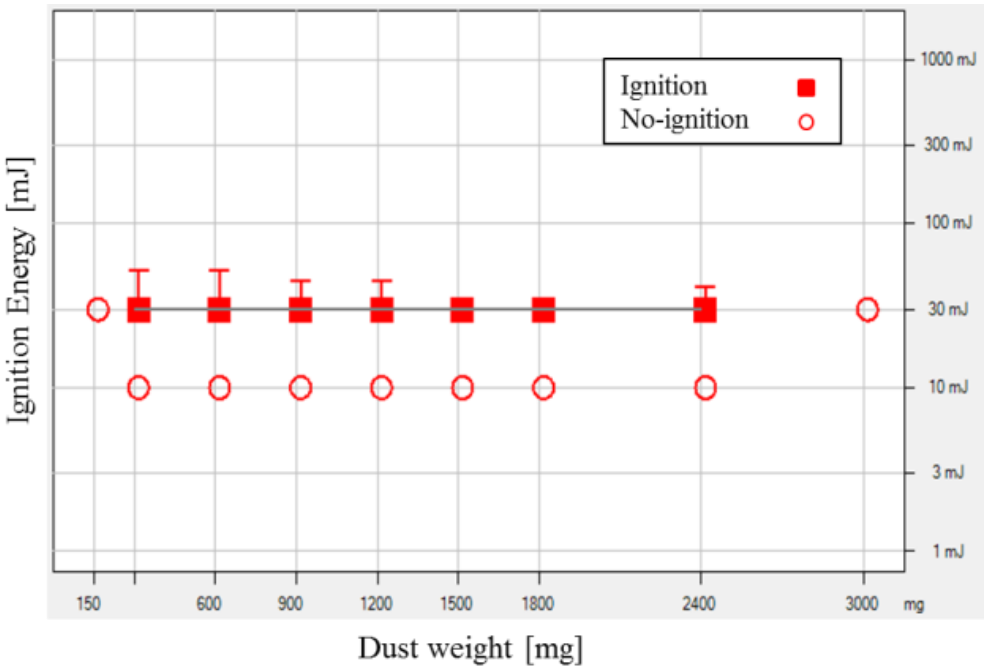

Figure 8 *MIE* test data (ignition energy vs concentration).

With this knowledge of dust explosion, the parameters relevant for dust explosion risk assessment and the equipment used to measure these parameters, the background of this research is described in Chapter II.

CHAPTER II

BACKGROUND

2.1. Synopsis

Dust explosion research has been going on for decades to prevent and mitigate the incidents, yet there are gaping holes in the fundamental understanding and testing of dust explosions. This chapter describes the work (relevant to this research) that has been done in the past and highlights the gaps that exist in the literature. Finally, based on the gaps, the chapter will provide the problem statement and discuss the objectives and significance of this research.

2.2. Literature review and gaps[*]

In Chapter I, the importance of 20 L dust explosion apparatus, 1 m^3 dust explosion apparatus, and the *MIE* apparatus for dust explosion risk assessment was described. During testing, these apparatus disperse the dust uniformly inside the vessel, and then ignite at atmospheric pressure. It is assumed that the dust particle size distribution is unchanged in these apparatus; however, recent studies suggest otherwise

[*] [14] Reprinted with permission from "Effect of dust dispersion on particle breakage and size distribution in the minimum ignition energy apparatus" by Bagaria, P., Zhang, J., & Mashuga, C., 2018. Journal of Loss Prevention in the Process Industries, 56, 518-523, Copyright (2018) by Elsevier.
[18] Reprinted with permission from "Effect of dust dispersion on particle integrity and explosion hazards" by Bagaria, P., Zhang, J., Yang, E., Dastidar, A., & Mashuga, C., 2016. Journal of Loss Prevention in the Process Industries, 44, 424-432. Copyright (2016) by Elsevier.
[23] Reprinted with permission from "Classification of particle breakage due to dust dispersion" by Bagaria, P., Li, Q., Dastidar, A., & Mashuga, C., 2019. Powder Technology, 342, 204-213. Copyright (2019) by Elsevier.

[23]. Kalejaiye et al., [20] investigated the uniformity of the dust cloud formation with three different dusts using a rebound and annular nozzle inside the 20 L explosion vessel with the help of the Pittsburgh Research Laboratory's optical probe which was placed at six different locations. They found the degree of dust dispersion for both nozzles is similar and that good dust dispersion uniformity is achieved by both nozzles based on transmission data at six different locations. However, they noted that the received transmission data was lower than theoretically predicted by Bouguer's law. They investigated this by measuring the particle size for pre and post-dispersion. They showed the particle size reduces to about 50% of its original size and cited the grinding/shearing action from the outlet valve as the main reason with the dispersion nozzle and cloud turbulence having minimal effect on particle breakage. Du et al., [26] used a transparent 20 L spherical chamber along with a high speed camera and an image processing technique to study the behavior of dust dispersion using carbonaceous (wheat flour) dust. Their qualitative analysis based on transmission data and turbulence levels categorized the dust dispersion as three distinct stages: injection stage, stabilization stage and sedimentation stage. They concluded that good dust cloud uniformity is achieved during the stabilization stage. Moreover, they noted that the duration of the stabilization stage varies with dust concentration, thus a variable ignition delay would be required to achieve identical turbulence and record accurate explosion results. They also showed that an increase in dust concentration leads to a plateau in transmission data indicating the dust is not fully dispersed, especially at high concentrations. Sanchirico et al., [27] studied the effect of typical dispersion nozzles (rebound nozzle and annular perforated ring nozzle)

on particle breakage using six different dusts in a 20 L vessel. They found the rebound nozzle has a more prominent role than the annular perforated nozzle in particle breakage. They also showed the effect of dispersion pressure on particle integrity and concluded higher dispersion pressure leads to increased particle breakage. These studies demonstrate that there is significant particle size distribution change in the standard 20 L apparatus on dispersion [18]. Mittal [28] examined the dependence of explosion parameters on dust size distribution. Her work showed as the dust size decreases, both the P_{max} and K_{st} increases to a certain value and thereafter decreases with further decrease in particle size. Thus, there is a prominent dependence of explosion parameters on particle size distribution, and the fact that dispersion in the standard 20 L dust explosion apparatus breaks the dust particles due to shear/grinding from the outlet valve and possibly the nozzle [20][27], thereby altering the particle size distribution can lead to misleading results [18]. This shift in size distribution due to dispersion can increase P_{max}/K_{St}, and lower *MIE* or may decrease P_{max}/K_{St} (Figure 9). Dispersion in the 20 L dust explosion apparatus can cause significant particle breakage in some dusts leading to a significant shift in explosion parameters as shown in Figure 9 (A → B or B → C). Figure 9 also shows slight shift in explosion parameters for dusts undergoing little particle breakage (A → A' or B → B′). Therefore, dispersion in the 20 L dust explosion apparatus can shift size distribution, which can lead to misleading results (overestimation or underestimation of explosion parameters) due to the dependence of explosion parameters on particle size distribution [23].

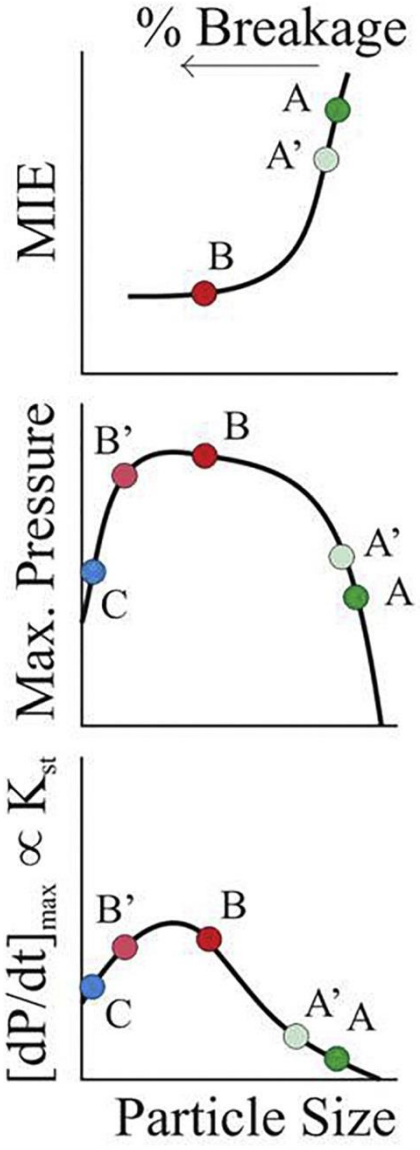

Figure 9 Dust particle size vs explosion parameters [23]. Reprinted with permission from "Classification of particle breakage due to dust dispersion" by Bagaria, P., Li, Q., Dastidar, A., & Mashuga, C., 2019. Powder Technology, 342, 204-213. Copyright (2019) by Elsevier.

Based on the literature, outlet valve (Figure 10) was cited as the main culprit for particle breakage. It was suggested that a novel dust dispersion mechanism that eliminates outlet valve and can help in procuring more representative

explosion/flammability parameters is needed [18][20][27]. Apart from a novel dispersion system that eliminates outlet valve to reduce particle breakage, there exists other gaps that needs to be addressed in order to understand the phenomena of particle breakage due to dispersion in the dust explosion apparatus. These gaps are:

- The effect of the dispersion stages (nozzle, dispersion cloud turbulence) on particle breakage is important but not yet quantified. Studying the effect of nozzle, and dispersion cloud turbulence on dust particle breakage during the dispersion process will draw a complete picture of the role of dispersion stages on particle breakage [18].
- Since different dust concentrations have different dispersion behavior [26], the relation between dust concentration and particle breakage needs to be verified. This study will put *MEC* testing as per the ASTM standard in perspective [18].
- With an increase in industrial scale use of nanomaterials, the behavior of nanomaterial dusts post-dispersion also needs to be analyzed for explosion risk assessment. It is important because dispersion of nanomaterial (mostly in agglomerated form) can lead to de-agglomeration, thereby increasing the explosion risk [18].
- With the studies showing the particle breakage and change in size distribution post-dispersion in the standard 20 L apparatus, which can affect the K_{st}, P_{max}, *MEC*, and *LOC* values, it remains to be seen how dispersion in the *MIE* apparatus affects the size distribution of the dust

sample. It is an important aspect as changes in size distribution of dust post-dispersion in the *MIE* apparatus can lead to erroneous *MIE* values, thus affecting perception of dust explosion risk [14].

- The consequence of particle breakage due to dispersion on the explosion parameters is not yet determined. Dispersion process during testing in the explosion apparatus as well as industrial operations such as cyclone separators, spray drying may result in significant particle breakage which can generate larger surface area available for combustion and increase the explosion hazard.
- Dispersion in the 20 L dust explosion apparatus can shift size distribution, which can lead to misleading results due to the dependence of explosion parameters on particle size distribution. However, it is not reported in literature how the standard 1 m^3 apparatus and the 36 L apparatus compare to the standard 20 L apparatus in terms of particle breakage during dust dispersion. It is important to determine because larger volume apparatus (such as 1 m^3 apparatus) better simulates dispersion cloud in industry and can provide insight into particle breakage due to dispersion in an industrial facility [23].
- It is necessary to quantify particle size reduction in the dust explosion apparatus, while there is also a need to assess the particle breakage behavior of different type of dusts and correlate the size reduction with the material mechanical properties. This will allow the dust explosion testing

community to predict particle breakage based on the material property and thus improve explosion testing. Several studies have identified that the breakage propensity (brittleness) of materials depends on hardness (H) and the fracture toughness (K_c) [[29]-[32]]. These studies define brittleness index (BI) as the ratio of hardness to fracture toughness (H/K_c). Although a wide variety of materials have been studied in literature for brittleness index measurement, there still remain several combustible dusts with brittleness propensity yet to be determined. In addition, the index values have not been correlated with the particle breakage during testing in the dust explosion apparatus, which will help predict particle breakage in the dust explosion apparatus. This approach can help classify dusts into categories based on particle breakage with a brittleness index range associated with each category. It will help the process industries identify dusts that are susceptible to breakage and quantify the breakage based on their brittleness index. It also allows identification of dusts that are prone to give misleading explosion results during dust explosion testing, which can assist in the development of a proper dust explosion risk assessment [23].

The aspect of particle breakage and size distribution on dust explosion is an important area; however, another important parameter that can affect dust explosion parameters is shape/morphology of dust particles. Fuel (dust) is mainly characterized by

its size, polydispersity, chemical composition and morphology (surface area/shape). A lot of studies have focused on size [9][22][28][[33]-[50]], polydispersity [22][44][51][52] and chemical composition [[53]-[59]] as factors affecting dust explosion parameters such as K_{st}, P_{max}, and *MIE*. However, research on morphology/shape as a factor that affects dust explosion parameter is scarce and needs more attention.

A study conducted by Jacobson et al., [60] on explosibility of dusts in the plastics industry revealed that process industries can generate different morphology of plastics and that irregular plastic dusts pose a greater explosion hazard than spherical dust particles. They also tested the explosibility of flaked and atomized aluminum metal powder in another study [61]. It was concluded that flaked powder have more explosion overpressure because of more reaction and less heat loss. However, the dust could have had different polydispersity and size range of particles, also known to affect the dust explosion characteristics [22], which might have led to such results. A module developed by Worsfold et al., [62] reports the effect of morphology on dust terminal settling velocities, which could affect dust explosion characteristics. Russo and Di Benedetto [63] developed a thermo-kinetic model for deflagration index in which particle shape factor was taken into account for cylindrical/flock shaped dusts. Their work categorized the explosion of dust in different classes based on equivalent diameter for cylindrical shaped dust and highlights the need of understanding the shape contribution to dust explosion hazards in a fundamental way. An important work on morphology affecting the dust explosion hazards was done by Thomas et al., [64]. Their work shows that different morphology of lycopodium has different frequency of ignition using Hartmann apparatus.

Different ignition frequency was owed to different surface area per volume, different particle count and settling time at the point of ignition. However, the particle sizes for different morphology lycopodium were different and the size distribution of the samples taken was not shown for polydispersity (an important factor to determine dust explosion properties [22]). Ogle et al., [65] presented a mathematical model to simulate P_{ex}, K_{st} of a dust explosion. The model was compared to the results generated in the 20 L dust explosion apparatus and included particle shape as a factor. They concluded that particle morphology influences radiative conductivity and have an effect on P_{ex}, K_{st} of the dust, which was supported by Kuhl et al., [66]. The work of Matsuda and Yamaguma [67] suggested that particle morphology could be related to particle breakage and that particle shape can influence dust explosion properties. Rowe [67] showed that *MIE* of amorphous shaped and needle shaped chemically identical dust is different. However, the particle sizes of the dusts were different with no mention of the polydispersity. A report by the Aluminum Association [69] shows dust explosion parameters (P_{max}, K_{st}, *MIE*, and *MEC*) of spherical and irregular shaped aluminum dust with similar median (d_{50}). The samples were from various manufacturers with different manufacturing techniques, which could have affected the chemical composition. Also, the report did not mention the particle size distribution and polydispersity of the dust samples, which are important factors in determining dust explosion parameters [22].

Literature shows that particle shape/morphology can be an important factor in influencing dust explosion properties but it is not always evident as the previous studies have not decoupled shape/morphology from size distribution and polydispersity. To

understand the role of particle shape/morphology on explosion parameters, size distribution and polydispersity should be factored out by taking dusts with different shape but same size and polydispersity. It is imperative that effect of particle morphology on dust explosion is taken into account the same way as other fuel characterization parameters (size, polydispersity and chemical composition) for better risk assessment and safe guard. Therefore, a better understanding of the effect of particle shape/morphology on dust explosion parameters is required. This research aims to investigate the role played by particle shape/morphology in affecting the dust explosion parameters, specifically the minimum ignition energy (*MIE*) of the dust. *MIE* of combustible dust is an important dust hazard parameter that describes the ease of ignition of the dust and guides ignition prevention in solids handling facilities. It is one of the first explosion parameters that is measured for risk assessment and remains a critical parameter for dust explosion prevention.

2.3. Problem statement and objectives

The broad aim of this work is to understand the effect of dust dispersion on shift in particle size distribution as well as investigate the role of particle morphology on dust explosion hazard. In section 2.2., several critical gaps pertaining to understanding of dust dispersion on particle breakage and effect of particle morphology on dust explosion hazard were identified. These gaps not only create an incomplete picture for dust explosion parameter measurement but also lead to inaccurate dust explosion risk assessment. Therefore, the purpose of this research is to develop an in-depth

understanding of particle breakage phenomena during dispersion process to improve dust explosion risk assessment. In addition, the understanding of role played by particle shape/morphology on dust minimum ignition energy will be developed to highlight the importance of particle shape/morphology in dust explosion risk assessment and including shape/morphology as a factor in *MIE* prediction models. To address the problem, several objectives were formulated:

1. Effect of dust dispersion on particle integrity **(Chapter III)**. This investigation elucidates the role of dispersion stages (nozzle and dispersion cloud turbulence) and dust concentration on particle breakage. Performance of a novel dispersion mechanism is compared to that of the standard 20 L dust explosion apparatus dispersion mechanism. In addition, the behavior of nanomaterial post-dispersion is studied.
2. Effect of dust dispersion on particle size distribution in the *MIE* apparatus **(Chapter IV)**. This investigation elucidates the particle size distribution shift due to the dispersion process in the *MIE* apparatus. Behavior of electrostatic dusts post-dispersion is emphasized.
3. Classification of particle breakage due to dust dispersion **(Chapter V)**. This investigation compares particle breakage between the standard 20 L dust explosion apparatus, the custom 36 L dust explosion apparatus, and the standard 1 m^3 dust explosion apparatus. Breakage in different type of dust materials is quantified. A correlation between particle breakage due to dispersion and mechanical properties of dust material is established.

4. Consequence of particle size reduction due to dust dispersion on explosion parameter assessment **(Chapter VI)**. This study shows the dust dispersion from processing, upsets or secondary explosions in the process industries (represented by the 1 m^3 apparatus) can lead to reduction in dust particle size distribution making it flammable; thereby affecting the dust explosion risk assessment of the process.
5. Effect of particle morphology on dust explosion hazard **(Chapter VII)**. This investigation elucidates the impact of different particle shape dusts with similar size distribution on the minimum ignition energy. The results are of fundamental importance to improve explosion risk assessment by including particle shape/morphology as a factor.

These objectives will aid in understanding the particle breakage phenomena due to dust dispersion and particle morphology on a more fundamental level and its effects on dust explosion risk assessment.

CHAPTER III

EFFECT OF DUST DISPERSION ON PARTICLE INTEGRITY[*]

3.1. Synopsis

Dust explosion hazards can be described with parameters such as *MIE*, *MEC*, P_{max}, K_{st} *etc.*, which are known to depend on particle size distribution within a dust cloud. Literature has shown the dispersion system (outlet valve, in particular) in a standard 20 L dust explosion apparatus breaks the dust into smaller particles leading to explosion parameters not necessarily corresponding to the original size. This study uses a novel dispersion system in a 36 L dust explosion apparatus to eliminate the mechanical shearing from the outlet valve and investigates its effect on dust particle integrity. The study also aims to observe the role of dispersion stages (nozzle and dispersion cloud turbulence) on particle breakage and compare the performance of our dispersion system to that of a standard 20 L apparatus. In addition, the role of dust dispersion concentration on particle breakage is examined. Anthraquinone, acetaminophen (paracetamol) and ascorbic acid are used to accomplish the goals of the study. Finally, the effect of dispersion on a nanomaterial is investigated using carbon nanofibers (CNFs).

Anthraquinone, acetaminophen and ascorbic acid show that even in the absence of an outlet valve, significant particle breakage occurs. This demonstrates the major role of both the dispersion nozzle and cloud turbulence in particle breakage. In addition, the

[*] [18] Reprinted with permission from "Effect of dust dispersion on particle integrity and explosion hazards" by Bagaria, P., Zhang, J., Yang, E., Dastidar, A., & Mashuga, C., 2016. Journal of Loss Prevention in the Process Industries, 44, 424-432, Copyright (2016) by Elsevier.

experiments revealed dispersion concentration to be an important factor in particle breakage and helped establish the inverse relation between particle breakage and dust dispersion concentration. Nanomaterial experiments with CNFs show significant de-agglomeration in the dispersion cloud followed by re-agglomeration.

3.2. Experiments

3.2.1. Apparatus

Dispersion studies were carried out using a novel dispersion system in a custom 36 L dust explosion apparatus. The apparatus is calibrated to yield results in agreement with a standard 20 L and 1 m^3 apparatus [22]. Our 36 L explosion apparatus and a standard 20 L explosion apparatus are similar not only in terms of generated results but the dispersion pressure, ignition delay and turbulence at ignition. The 36 L explosion vessel consists of seven main parts (see Figure 11): (1) vacuum system, (2) air reservoir, (3) fast acting valve, (4) dust container, (5) rebound dispersion nozzle, (6) igniters, and (7) pressure transducers [70]. The procedure starts with loading the dust into the dust container, and installing the rebound nozzle, igniters and flanged lid. A customized LabVIEW™ program evacuates the vessel to approximately 0.7 bar, then supplies compressed air to the air reservoir to achieve approximately 21 bar. This air is then released via a fast-acting valve actuated for 50 ms. The released compressed air carries the dust from the container through the nozzle into the vessel to make a turbulent dust cloud at 1 bar absolute. 25 ms after valve closure, the igniters are activated [71][72].

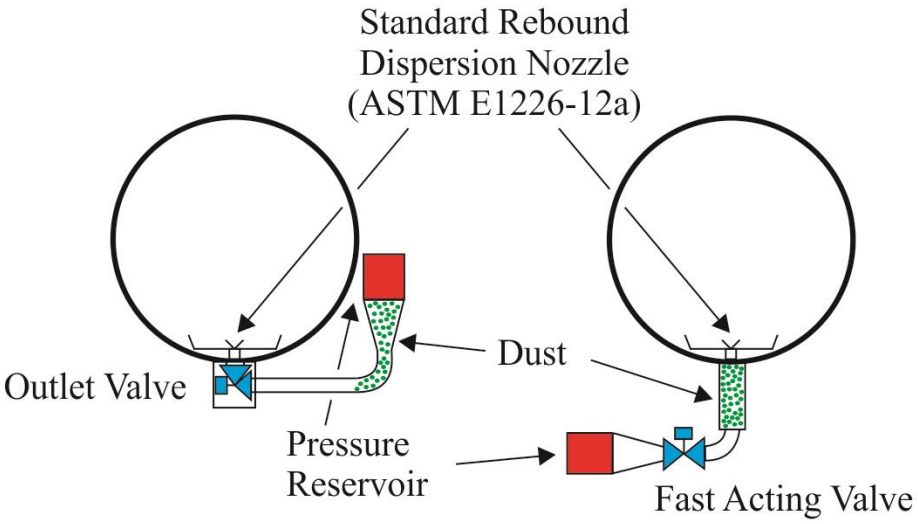

Figure 10 Dust explosion dispersion systems: (a) Standard 20 L; (b) Texas A&M 36 L [18]. Reprinted with permission from "Effect of dust dispersion on particle integrity and explosion hazards" by Bagaria, P., Zhang, J., Yang, E., Dastidar, A., & Mashuga, C., 2016. Journal of Loss Prevention in the Process Industries, 44, 424-432, Copyright (2016) by Elsevier.

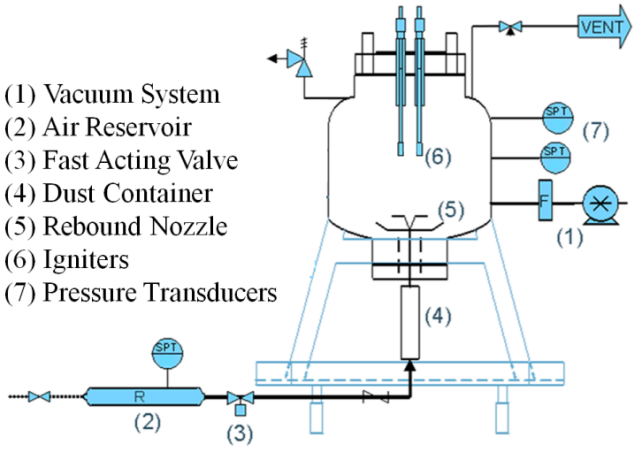

Figure 11 Schematic of 36 L dust explosion apparatus [18]. Adapted from [70]. Reprinted with permission from "Effect of dust dispersion on particle integrity and explosion hazards" by Bagaria, P., Zhang, J., Yang, E., Dastidar, A., & Mashuga, C., 2016. Journal of Loss Prevention in the Process Industries, 44, 424-432, Copyright (2016) by Elsevier.

In this study, the dispersion dynamics of our novel dispersion system and that of a standard 20 L apparatus was investigated without ignition. The difference between our dispersion system in 36 L apparatus and that of a standard 20 L apparatus is shown in Figure 10. In our dispersion system, the dust is stored just below the 36 L vessel and does not pass through the outlet valve (which was reported as the main reason for de-agglomeration by Kalejaiye et al., [20]). This setup enabled us to investigate the particle breakage due to the nozzle, the dispersion cloud, and the combination of both.

3.2.2. Material

For this study, anthraquinone, acetaminophen, and ascorbic acid (samples source-Sigma Aldrich) were selected as study materials because each has a different range of particle breakage based on its mechanical properties, initial particle diameter, and other physical properties such as density [27][73]. In addition, data for particle size reduction due to dispersion in a standard 20 L device is reported in literature for these materials [27]. In this study, these materials were used to investigate the role of nozzle and dispersion cloud turbulence on particle breakage and compare the performance of our novel dispersion system to that of a standard 20 L explosion apparatus, as well as to study the effect of concentration on particle breakage. The effect of dispersion on a nanomaterial was found by examining carbon nanofibers (CNFs, PS grade, density: 20.82 kg/m^3, Pyrograf Products, Inc.) which are used widely in research and industry [74].

Particle size distribution characterization was performed for the as received samples of anthraquinone, ascorbic acid, and acetaminophen (see Figure 12 and Table 3).

The characterization was carried out using a Beckman Coulter LS 13320 single wavelength laser diffraction device. This analysis was not extended to CNFs because it is difficult to characterize the size distribution for such materials using laser diffraction. To characterize the pre-dispersion CNFs, scanning electron microscopy (SEM) imaging was conducted which was also extended to anthraquinone, acetaminophen and ascorbic acid. The pre-dispersion samples of anthraquinone, acetaminophen and ascorbic acid (Figure 13) and carbon nanofibers (Figure 16) were characterized using SEM to visualize the size and morphology changes due to dispersion. The SEM imaging was performed with a JEOL JSM-7500F ultra high resolution field emission scanning electron microscope (FE-SEM).

3.2.3. Methodology

After as received samples characterization, samples were dispersed using the novel dispersion system of our 36 L apparatus. To study the effect our dispersion system has on dust particles and to compare its performance to that of a standard 20 L dispersion system, sample materials were dispersed at a concentration of 500 g/m^3 in both our 36 L apparatus and a standard 20 L apparatus. Sufficient time (~10 min) was given for the dust to settle from suspension followed by post-dispersion sample collection. An additional experimental dimension was added by dispersing the dust at 500 g/m^3 without passing through the nozzle in our 36 L explosion apparatus dispersion system. Dust was placed on top of the nozzle in a uniform manner, so that the compressed air coming from the reservoir through the nozzle sweeps the dust and generates a similar cloud and

turbulence level as generated when passing through the nozzle. This eliminates the forces on the dust from the nozzle and allows quantification of particle breakage due to dust cloud forces. To determine the role of concentration on particle breakage, anthraquinone, acetaminophen and ascorbic acid were dispersed through the nozzle at concentrations of 250, 500 and 1500 g/m^3 in the 36 L explosion apparatus. After settling, the post-dispersion samples were collected for analysis. For studying nanomaterial dispersion, CNFs were dispersed at 250 g/m^3 through the nozzle and the post-dispersion sample was collected by two methods. In method 1, post-dispersion CNFs were collected traditionally after allowing the dust to settle. In method 2, CNFs were captured while in suspension through installed SEM grids. The collected samples were analyzed for particle size distribution using Beckman Coulter LS 13320. SEM imaging was also performed for insights into morphology, and particle size (for CNFs, only SEM was conducted due to inconsistent results from laser diffraction). This data was analyzed to provide a fundamental understanding of the change in particle size distribution pre and post-dispersion and is discussed in section 3.3.

3.3. Results

3.3.1. Particle breakage in a novel 36 L dispersion system vs. a standard 20 L apparatus dispersion system

Anthraquinone, acetaminophen and ascorbic acid (each 500 g/m^3) were dispersed inside both the 36 L apparatus and a standard 20 L apparatus. The post-dispersion sample was collected after the dispersed sample settled, and size distribution and morphology

imaging measurements were conducted for pre and post-dispersion samples using Beckman Coulter LS 13320 and SEM, respectively. The results were compared in order to determine the performance of our dispersion system to that of a standard 20 L apparatus system and can be seen in Figure 12 and Table 3. Figure 13 shows the SEM images of anthraquinone, acetaminophen and ascorbic acid for the as received and post-dispersion samples through the nozzle at a concentration of 500 g/m^3 in the 36 L apparatus. The quantification of particle breakage can be better understood by percent change in mode, median, and *D (3, 2)* of the dispersed sample. Sanchirico et al., [27] used the percent change in mode to represent change in particle size after dispersion in a standard 20 L apparatus. Table 3 shows the % change for some relevant data statistics. Figure 12 and Table 3 show particle breakage occurs even without the outlet valve in the 36 L dispersion system, as evident from decrease in median, mode and *D (3, 2)* post-dispersion. It also reveals the greatest loss in particle size is for ascorbic acid, followed by acetaminophen and anthraquinone respectively. This trend is consistent with the work of Sanchirico et al., [27] in the 20 L apparatus and the experiments performed in the 20 L apparatus in this work. Comparing the change (decrease) of the size distribution median, mode and *D (3, 2)* post-dispersion in 36 L and 20 L systems (Table 3), it is observed that absence of an outlet valve in the dispersion mechanism does not make much of a difference. The particle breaks as much as it did in the presence of the outlet valve. Particle breakage for acetaminophen is 17.7% (median) more in the 20 L dispersion system than the 36 L dispersion system. Anthraquinone breakage is similar in both the systems. Ascorbic acid breaks 9% (median) more in the 36 L system than 20 L system.

The magnitude of particle breakage with the novel dispersion system in the 36 L apparatus is comparable to that of a standard 20 L system and clearly indicates that forces from either nozzle, dispersion cloud, or both plays an important role in particle breakage. This provides a different perspective than Kalejaiye et al., [20], who concluded that the nozzle had a nominal effect on particle breakage. This result directs our focus on the effect of the nozzle and subsequently the dispersion cloud on particle breakage.

3.3.2. Nozzle and dispersion cloud effect on particle breakage

The outlet valve plays a role in particle breakage but its absence confirmed the role of the nozzle, the dispersion cloud, or both on particle breakage in our study. Next, the dispersion stages (nozzle and dispersion cloud) were observed in order to quantify their contribution to particle breakage. Anthraquinone, acetaminophen and ascorbic acid were dispersed in the 36 L apparatus (each 500 g/m^3) through the nozzle and by spreading the dust over the top of the nozzle (see section 3.2.3. Methodology). Dispersing the dust from the top of the nozzle eliminates the nozzle forces. This results in only the cloud dynamics and wall interactions contributing to particle breakage. Figure 12 represents the particle size distribution of the materials as received, after being dispersed through the nozzle and by spreading the material over the nozzle. Table 3 represents the statistics associated with size distribution in Figure 12 and the corresponding percent change in data statistics.

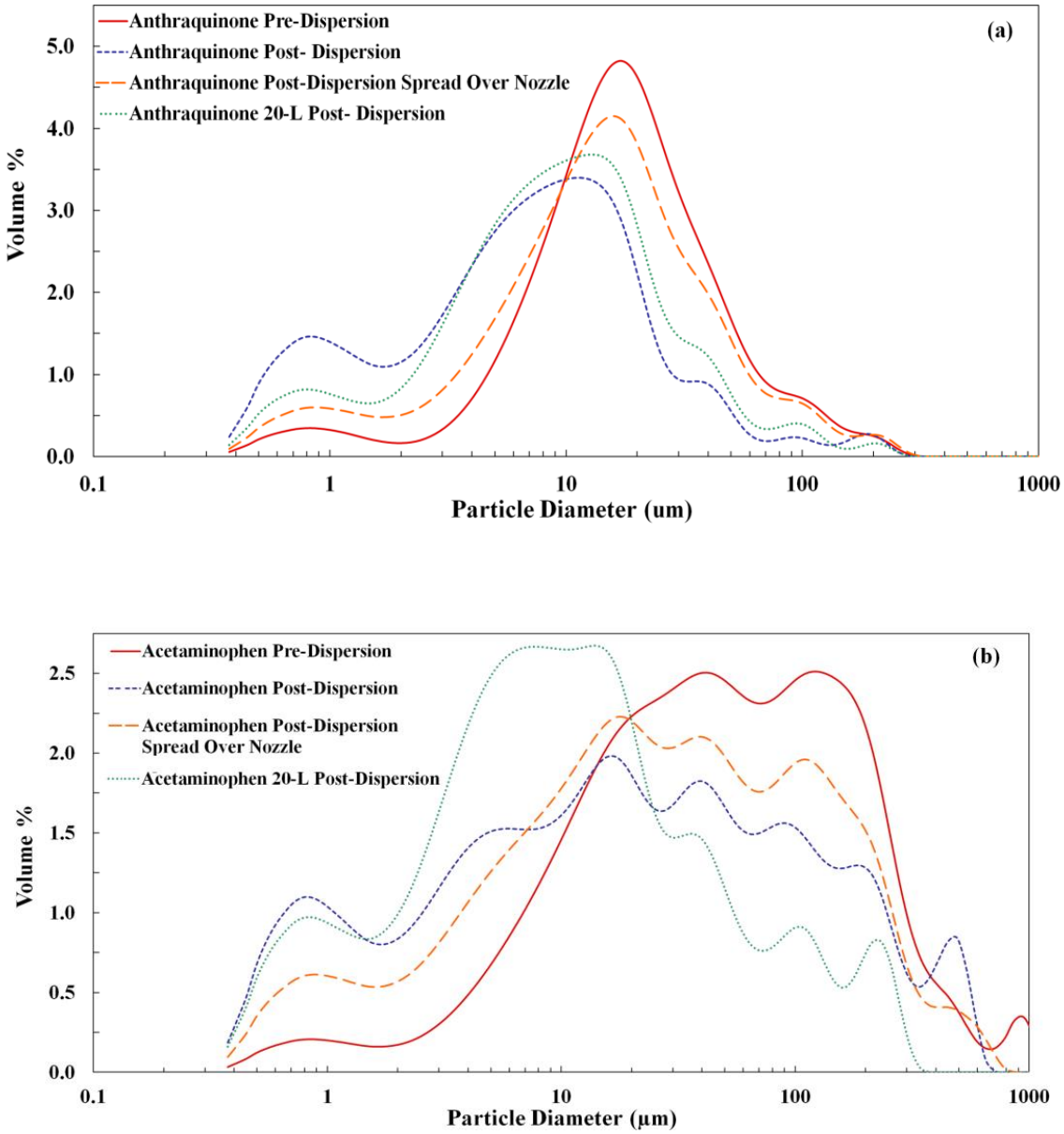

Figure 12 Particle size distributions of pre and post-dispersion 20 L, 36 L (through the nozzle and by spreading dust on top of the nozzle) both at 500 g/m^3: (a) anthraquinone, (b) acetaminophen and (c) ascorbic acid [18]. Reprinted with permission from "Effect of dust dispersion on particle integrity and explosion hazards" by Bagaria, P., Zhang, J., Yang, E., Dastidar, A., & Mashuga, C., 2016. Journal of Loss Prevention in the Process Industries, 44, 424-432, Copyright (2016) by Elsevier.

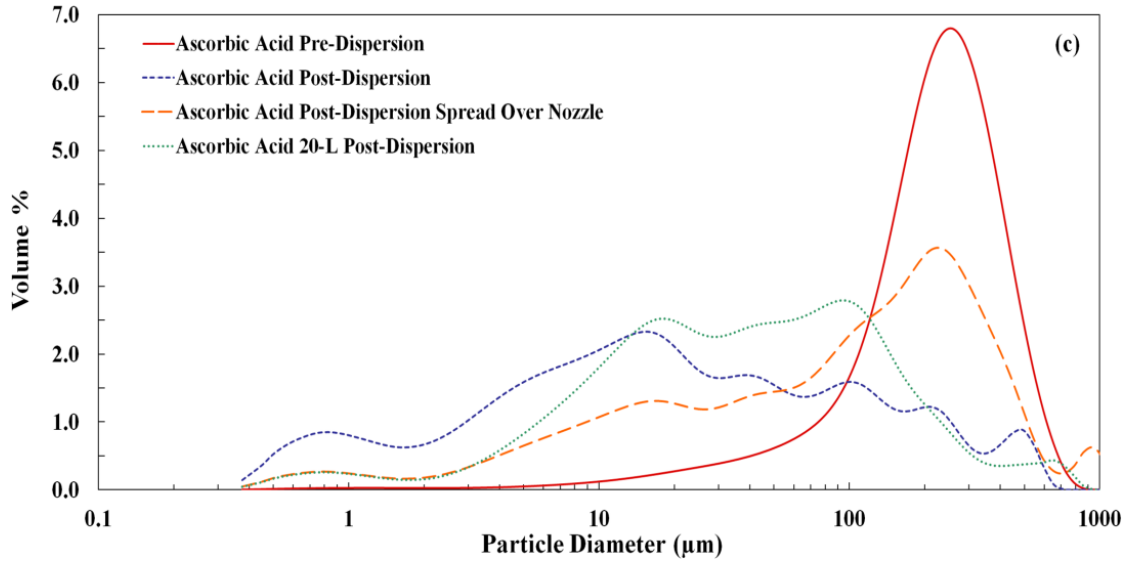

Figure 12 Continued.

The particle size distribution and associated statistics for anthraquinone, acetaminophen and ascorbic acid shows that forces from both the nozzle and dispersion cloud contribute to breakage of the particles. When dust passes through the nozzle in our dispersion system, it breaks more than when it is spread uniformly over the nozzle. For a typical standard dispersion in our system, the dust receives forces from both the nozzle and dispersion cloud (collision with vessel surface, collision between particles etc.) whereas, when the dust is dispersed without passing through the nozzle, the forces from nozzle are eliminated, thus providing less breakage. It clarifies that both the nozzle and dispersion cloud play a significant role in particle breakage, which should be accounted for in dust explosion studies. SEM imaging of the materials as received, for a typical standard dispersion (through nozzle) and dispersion without passing through the nozzle

are shown in Figure 13. These images provide visual evidence of the particle breakage and change in morphology induced by the nozzle and dispersion cloud.

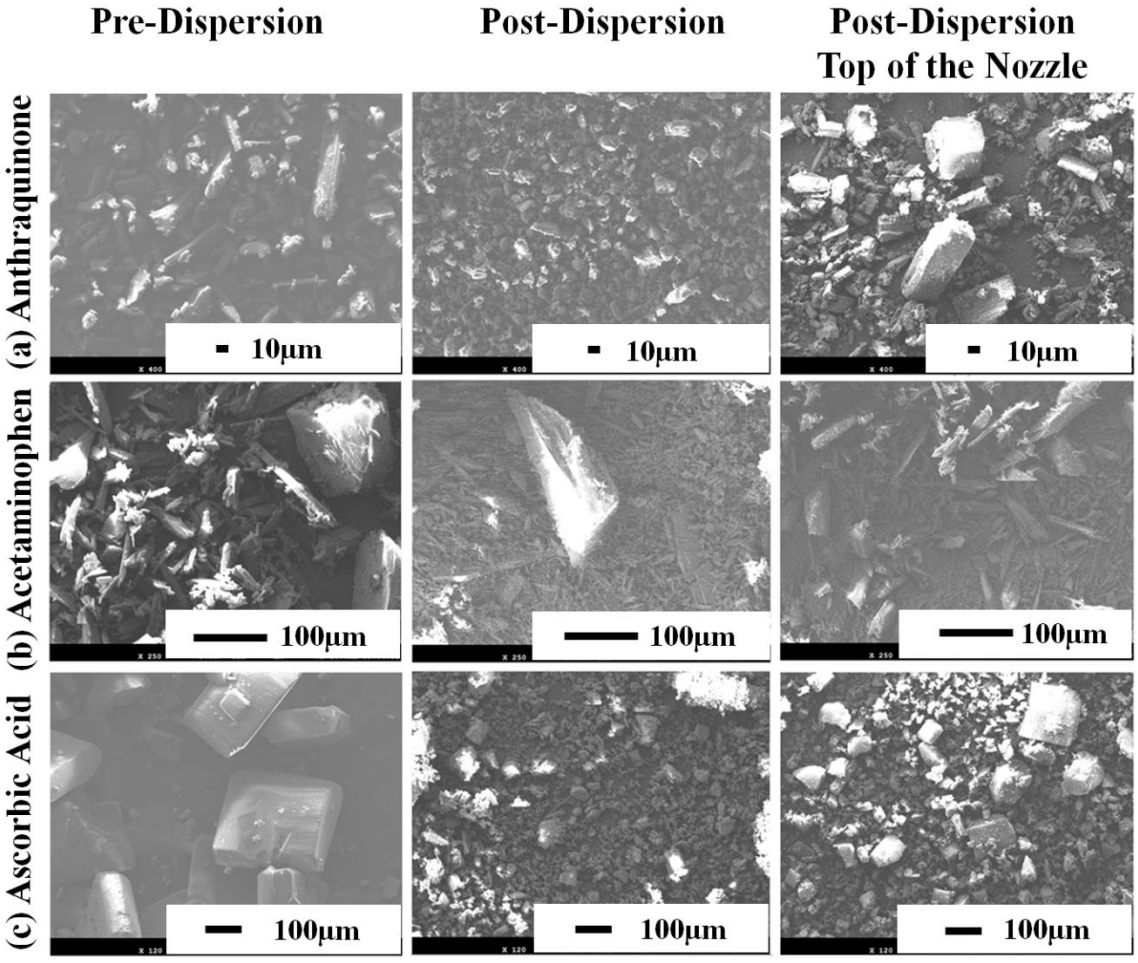

Figure 13 SEM images for pre and post-dispersion (nozzle, top of the nozzle) in the 36 L apparatus at 500 g/m^3: (a) anthraquinone (b) acetaminophen (c) ascorbic acid [18]. Reprinted with permission from "Effect of dust dispersion on particle integrity and explosion hazards" by Bagaria, P., Zhang, J., Yang, E., Dastidar, A., & Mashuga, C., 2016. Journal of Loss Prevention in the Process Industries, 44, 424-432, Copyright (2016) by Elsevier.

Table 3 Size statistics for pre and post-dispersion samples using the novel 36 L and standard 20 L apparatus at 500 g/m^3 [18]. Reprinted with permission from "Effect of dust dispersion on particle integrity and explosion hazards" by Bagaria, P., Zhang, J., Yang, E., Dastidar, A., & Mashuga, C., 2016. Journal of Loss Prevention in the Process Industries, 44, 424-432, Copyright (2016) by Elsevier.

Sample and Statistics (dispersion at 500 g/m^3)		Median/ d_{50} [µm]	% Decrease Median/d_{50}	Mode [µm]	% Decrease Mode	*D (3, 2)* [µm]	% Decrease *D (3, 2)*
Anthraquinone	Pre-dispersion	17.9	-	18	-	8.4	-
	36 L Post-dispersion	7.4	58.3	11.3	37.3	3	64.5
	20 L Post-Dispersion	9.5	46.6	13.6	24.4	4.2	50
	36 L Post-dispersion Spread Over Nozzle	14.7	17.5	16.4	8.9	5.7	33.9
Acetaminophen	Pre-dispersion	48.8	-	127.7	-	13.6	-
	36 L Post-dispersion	18.9	61.4	16.4	87.2	4.1	69.6
	20 L Post-Dispersion	10.2	79.1	14.9	88.3	3.9	71
	36 L Post-dispersion Spread Over Nozzle	27.2	44.4	18	85.9	6.3	53.4
Ascorbic acid	Pre-dispersion	237.8	-	269.2	-	80.5	-
	36 L Post-dispersion	18.6	92.2	16.4	93.9	4.9	93.9
	20 L Post-Dispersion	39.9	83.2	96.5	64.2	11.6	85.6
	36 L Post-dispersion Spread Over Nozzle	111.5	53.1	245.2	8.9	13.3	83.5

D (3, 2): the surface-weighted mean diameter

d_{50}: represent 50 percentile of particles is smaller than tabulated value

% Decrease = [(Original Sample Data-Post Dispersion Data)/Original Sample Data]*100

The effect of the nozzle and cloud forces can be further quantified by examining the size distribution statistics. Table 3 shows the percent change in relevant data after dispersion at 500 g/m^3 with and without nozzle. Significant breakage can be observed from both the dispersion cloud and nozzle even without an outlet valve in our dispersion system. Also, the material breakage trend is the same for dispersion through the nozzle as it is for over the nozzle dispersion. Ascorbic acid breaks the most, followed by acetaminophen and then anthraquinone which is dependent on the materials physical properties and the initial diameter of the pre-dispersed particles. Further insight into this can be provided by the work of Ghadiri and Zhang [73]. Their work describes the dependence of particle breakage (chipping, lateral cracks) on several factors and can be used to quantify the particle breakage through equation 2.

$$\xi = \alpha \frac{\rho V^2 D H}{K_c^2} \qquad \text{Eq. 2}$$

Where, ξ: fractional loss per impact, α: proportionality factor, ρ: particle density, V: impact velocity, D: initial dimension of the particle, H: hardness, K_c: fracture toughness. Equation 2 shows particle breakage is directly related to the initial dimension (diameter) of the particle. In the 20 L apparatus, the outlet valve receives large particles and is a major factor in size reduction. Subsequently, the nozzle receives smaller particles due to grinding from the outlet valve, and it plays its role in particle breakage. It then leads to the dispersion cloud receiving even smaller particles and thus the cloud turbulence offers even lower reduction in size. Thus, in the 20 L device the size reduction action is dominated by the outlet valve and less so from that of the nozzle and dispersion cloud. However, with the novel dispersion mechanism in the 36 L apparatus, in the

absence of an outlet valve, the nozzle receives big particles and thus has a dominant impact on size reduction as compared to the 20 L apparatus. Also, the dispersion cloud may receive larger particles than that of the 20 L and thus lead to a significant amount of size reduction during this stage. Hence, essentially eliminating one stage of the dispersion mechanism does not significantly affect the size reduction because the other two stages receive larger particles and hence cause more attrition comparable to that in a standard 20 L apparatus. Also, it leads to difficulty in predicting the particle breakage due to individual action of the nozzle and dispersion cloud. The data for particle breakage from dispersion cloud and nozzle (when dust passes through the nozzle), and the dispersion cloud (when dust is spread on the nozzle) is available. However, the percent breakage due to the dispersion cloud should not be subtracted from that of the cloud and nozzle to yield percent breakage from just the nozzle. It is because when the dust is dispersed through the nozzle, the nozzle would have reduced the size of the original sample and the particles will be smaller when they reach the dispersion cloud, in comparison to the particles when they are spread over the nozzle. The impact forces due to the dispersion cloud will vary because of different particle size when the particles pass through the nozzle and when it is spread over the nozzle. The effect of the nozzle and dispersion cloud (combined) and dispersion cloud (individual) on particle breakage can be observed and it is significant. Hence, it becomes important to consider particle breakage from the nozzle and dispersion cloud in dust explosion studies to associate explosion results with appropriate size distribution.

3.3.3. Dependence of particle breakage on dust concentration

A study by Du et al., [26] showed dispersions with different dust concentrations had different cloud behavior. This included injection dynamics, stability, settlement period, and that most of the dust does not go into cloud suspensions at higher concentrations. This led to the hypothesis that different concentrations leading to different suspensions and dust cloud behavior results in different breakage rates. Three concentrations, 1500, 500, and 250 g/m^3 of each anthraquinone, acetaminophen, and ascorbic acid, were loaded and dispersed through the nozzle. The particle size distribution and distribution statistics for as received and post-dispersion samples as a function of dispersion concentration are shown in Figure 14 and Table 4, respectively. In Figure 14 and Table 4, it can be seen that as the concentration gets lower, the volume percent of smaller particles increases. This shows that a decrease in dispersion concentration leads to more particle breakage. The post-dispersion SEM imaging for anthraquinone, acetaminophen and ascorbic acid each at 1500 g/m^3, 500 g/m^3, and 250 g/m^3 is shown in Figure 15. These images further show changing the dust concentration affects the particle breakage and they are inversely related.

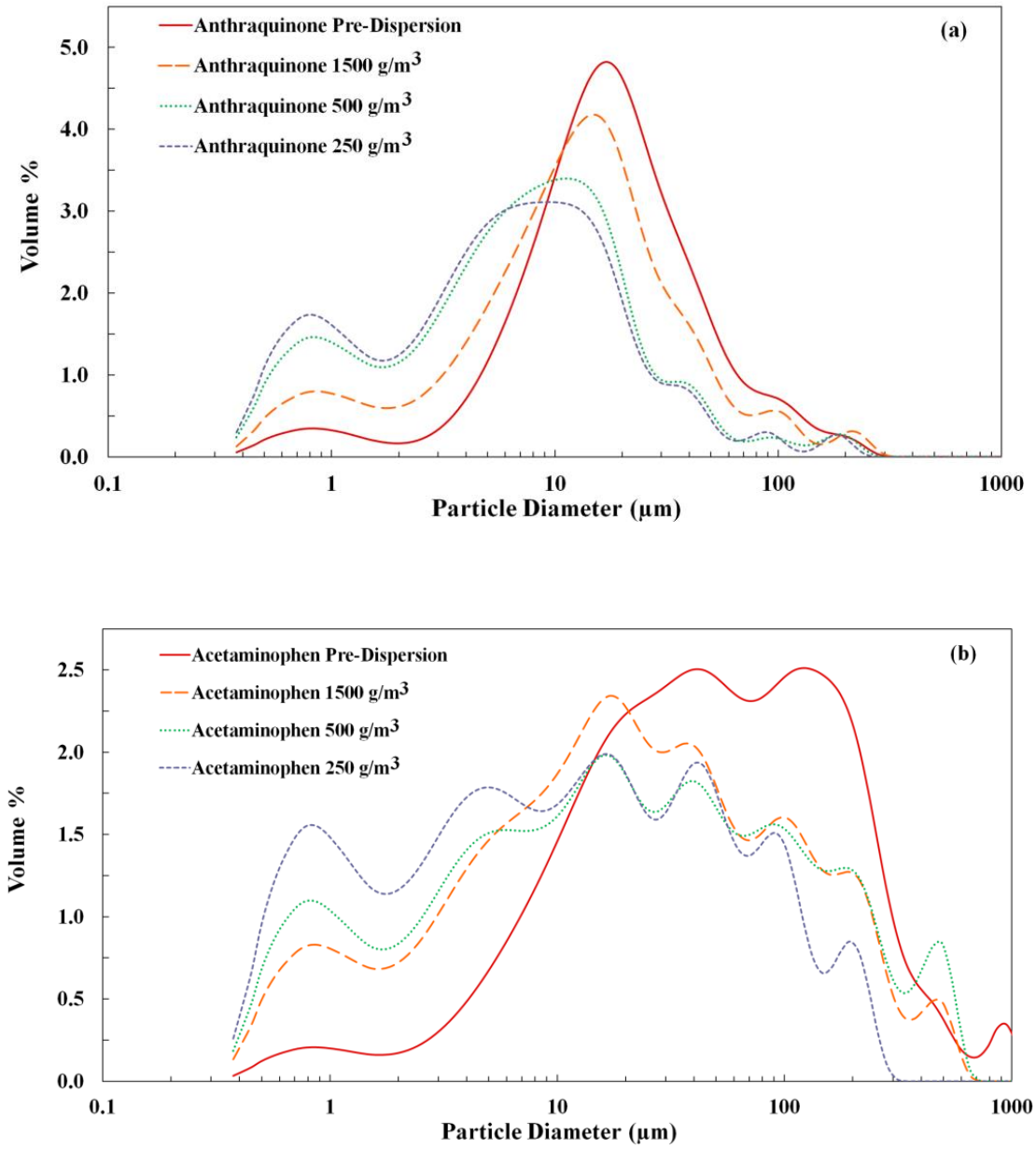

Figure 14 Particle size distribution of pre and post-dispersion samples of: (a) anthraquinone, (b) acetaminophen (c) ascorbic acid at 1500 g/m^3, 500 g/m^3 and 250 g/m^3 in 36 L apparatus [18]. Reprinted with permission from "Effect of dust dispersion on particle integrity and explosion hazards" by Bagaria, P., Zhang, J., Yang, E., Dastidar, A., & Mashuga, C., 2016. Journal of Loss Prevention in the Process Industries, 44, 424-432, Copyright (2016) by Elsevier.

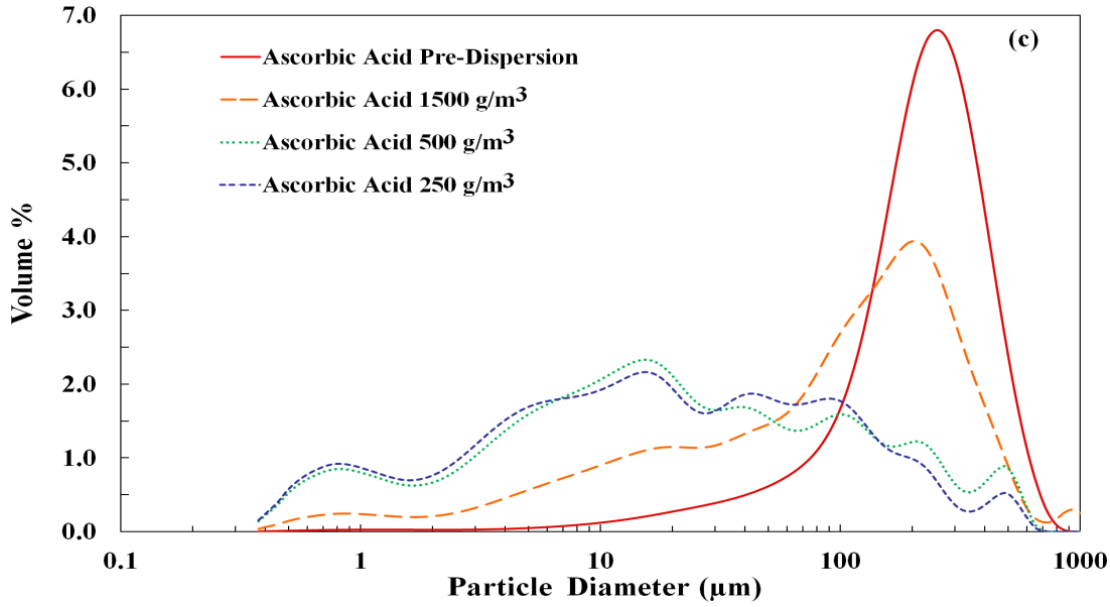

Figure 14 Continued.

This inverse relation between particle breakage and dust dispersion concentration is observed because the energy of the dispersion air is distributed over more particles at higher concentrations leading to lower impact velocities per particle which leads to less breakage. Also at higher concentration, some of the dust does not go into cloud suspension, therefore is not subjected to the cloud dispersion forces, resulting in less particle breakage. The data in Figure 14 and Table 4 suggests that particle breakage depends inversely on concentration; however the dependence is not linear. With an increase in concentration, the percent breakage decreases and then gradually levels off to a particular value after a specific concentration depending on the material. Similarly, there is a limit to breakage percentage increase with a decrease in concentration. A plot of breakage percentage versus inverse concentration should look similar to a sigmoidal

curve with concavity and convexity subject to the nature of the material. This dependence of particle breakage on concentration puts minimum explosible concentration (*MEC*) testing into perspective by generating variable dust cloud size distribution for each concentration.

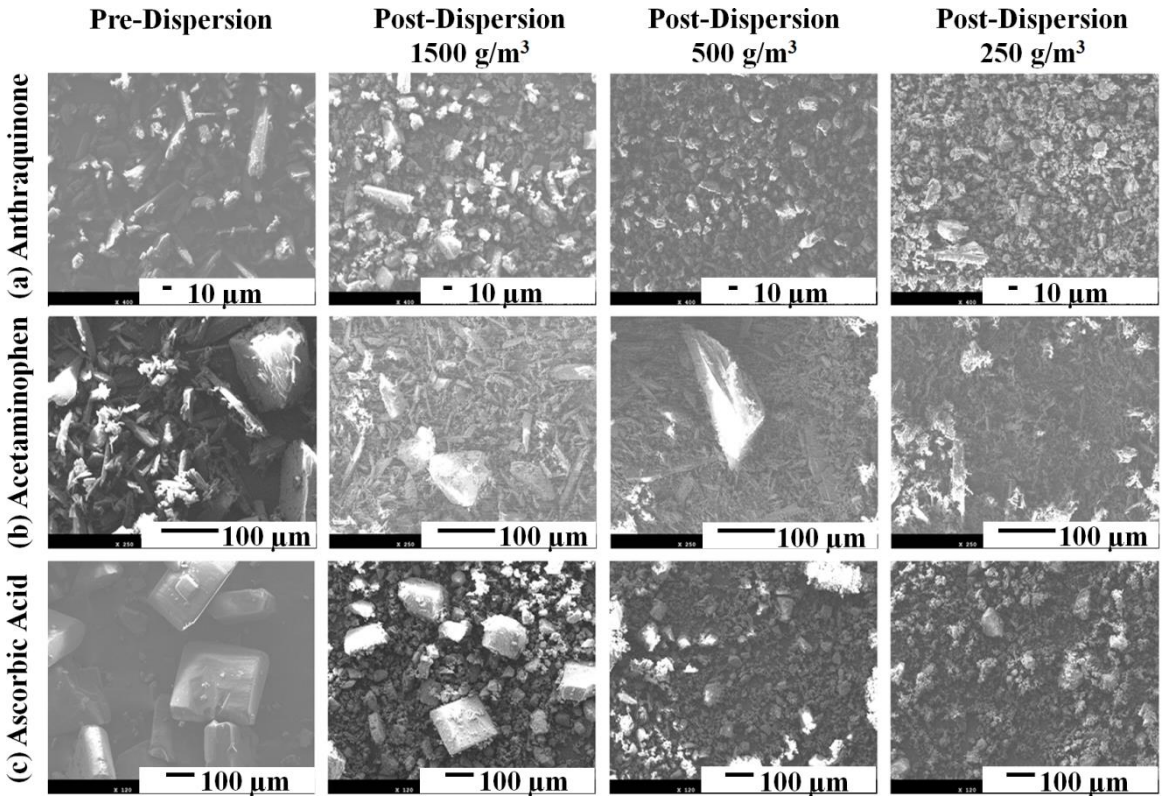

Figure 15 SEM images of pre-dispersion samples, post-dispersion samples at 1500 g/m^3, 500 g/m^3 and 250 g/m^3 for anthraquinone, acetaminophen and ascorbic acid [18]. Reprinted with permission from "Effect of dust dispersion on particle integrity and explosion hazards" by Bagaria, P., Zhang, J., Yang, E., Dastidar, A., & Mashuga, C., 2016. Journal of Loss Prevention in the Process Industries, 44, 424-432, Copyright (2016) by Elsevier.

Table 4 Particle size distribution statistics of pre and post-dispersion samples of anthraquinone, acetaminophen and ascorbic acid at 1500 g/m^3, 500 g/m^3 and 250 g/m^3 in the 36 L apparatus [18]. Reprinted with permission from "Effect of dust dispersion on particle integrity and explosion hazards" by Bagaria, P., Zhang, J., Yang, E., Dastidar, A., & Mashuga, C., 2016. Journal of Loss Prevention in the Process Industries, 44, 424-432, Copyright (2016) by Elsevier.

Sample and Statistics at different concentrations		Median/d_{50} [µm]	% Decrease Median/d_{50}	Mode [µm]	% Decrease Mode	*D (3, 2)* [µm]	% Decrease *D (3, 2)*
Anthraquinone	Pre-dispersion	17.9	-	18.0	-	8.4	-
	1500 g/m^3	12.9	27.7	14.9	17.0	4.8	43.0
	500 g/m^3	7.4	58.3	11.3	37.3	3.0	64.5
	250 g/m^3	6.4	63.9	9.4	47.9	2.6	68.6
Acetaminophen	Pre-dispersion	48.8	-	127.7	-	13.6	-
	1500 g/m^3	20.2	58.6	18.0	85.9	5.0	63.3
	500 g/m^3	18.9	61.4	16.4	87.2	4.1	69.6
	250 g/m^3	11.0	77.5	18.0	85.9	3.1	77.4
Ascorbic acid	Pre-dispersion	237.8	-	269.2	-	80.5	-
	1500 g/m^3	116.3	51.1	223.4	17.0	14.3	82.2
	500 g/m^3	18.6	92.2	16.4	93.9	4.9	93.9
	250 g/m^3	17.6	92.6	16.4	93.9	4.6	94.3

D (3, 2): the surface-weighted mean diameter

d_{50}: represent 50 percentile of particles is smaller than tabulated value

% Decrease = [(Original Sample Data-Post Dispersion Data)/Original Sample Data]*100

3.3.4. Nanomaterial dispersion behavior

Having observed the dispersion behavior of anthraquinone, acetaminophen and ascorbic acid (micron size regime), it became important to study the behavior of nanomaterials after dispersion because nanomaterials often tend to agglomerate and can generate large surface areas for combustion if they de-agglomerate. Considering the growth in the nanomaterial industry, the consequences of this could be devastating. Carbon nanofibers (CNFs) were used to study the behavior of nanomaterials after dispersion using two methods, particles collected in the cloud and post-settling (see section 3.2.3. Methodology). SEM comparison of original sample and samples by the two collection methods can be seen in Figure 16.

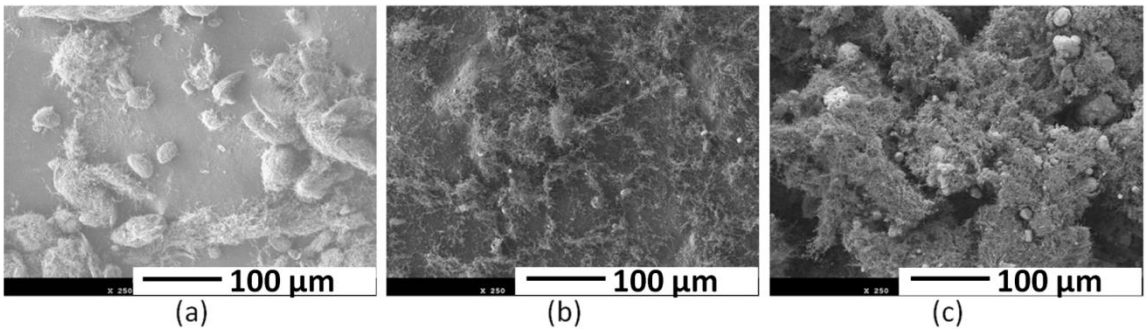

Figure 16 SEM images of (a) pre-dispersion samples of CNFs; (b) CNFs captured in dust cloud; (c) CNFs collected post-settling [18]. Reprinted with permission from "Effect of dust dispersion on particle integrity and explosion hazards" by Bagaria, P., Zhang, J., Yang, E., Dastidar, A., & Mashuga, C., 2016. Journal of Loss Prevention in the Process Industries, 44, 424-432, Copyright (2016) by Elsevier.

The images show that the dispersion of CNFs results in breaking of the agglomerates which is evident by Figure 16 (b). CNF clusters (agglomerates) break and are dispersed into thin fibers due to forces from the nozzle and dispersion cloud. However, if allowed sufficient time, the fibers have an inherent tendency to re-agglomerate and form clusters (Figure 16 (c)). The re-formed clusters have a different morphology than that of the original sample. This is significant because at the time of ignition after dispersion, CNFs would likely exist as thin fibers in the cloud and would yield explosion parameters corresponding to surface area of dispersed thin fibers. The explosion consequence parameters (P_{max}, K_{st}) would be higher because of the larger surface area and the material would be easier to ignite. People should be aware of such behavior of nanomaterials for proper safeguarding against dust explosions.

3.4. Conclusions

This research studied the effect of dispersion on combustible dust particle breakage using our novel dispersion system in a 36 L explosion apparatus. Our dispersion system does not use an outlet valve in an attempt to reduce mechanical shearing and allows us to study the effect of the nozzle and dispersion cloud on particle breakage. Anthraquinone, acetaminophen and ascorbic acid were used for dispersion experiments, to evaluate the role of the nozzle, dispersion cloud turbulence, and concentration on particle integrity and to compare the performance of our dispersion system to that of a standard 20 L explosion apparatus. Particle size characterization and distribution were measured using laser diffraction (Beckman Coulter LS 13320) and SEM imaging.

Dispersion experiments at 500 g/m^3 were performed with samples dispersed through the nozzle and by spreading it uniformly over the nozzle to quantify the role of the nozzle and dispersion cloud on particle breakage. Further experiments were conducted by passing the dust through the nozzle with different concentrations (1500, 500, 250 g/m^3) to determine the role of concentration on particle breakage. The post-dispersion samples were analyzed using laser diffraction and SEM imaging and were compared to as received samples. Variations in particle size distribution were quantified using percent change values. This research also investigated the effect of dispersion on nanomaterials using CNFs as material of study. SEM characterization was done for the as received sample, from the dispersion cloud and from the post-dispersion sample after settling. Based on results from these studies, the following can be concluded:

- Significant particle breakage occurs even without an outlet valve in our dispersion system suggesting the dispersion nozzle, dispersion cloud turbulence, or both have a major role in particle breakage. This is contradictory to work of Kalejaiye et al., [20] that concluded the nozzle and dispersion cloud turbulence have nominal effect on particle breakage.
- Particles break when dispersed by spreading them over the nozzle; however there is more breakage if they are dispersed through the nozzle, implying that both nozzle and dispersion cloud turbulence have a major role in the loss of particle integrity. Ghadiri and Zhang [73] provided an equation for particle breakage which states a directly proportional relationship between initial diameter of the particle and particle breakage in each stage of dispersion. In the standard 20 L

device, the outlet valve receives larger particles than the nozzle and resulting dispersion cloud. Thus, it has a prominent role in particle breakage. Our 36 L explosion apparatus with novel dispersion system delivers large particles to the nozzle due to the absence of an outlet valve; thus it has a major role in particle breakage. However, the effect of the other stages of dispersion (nozzle and cloud in 20 L and cloud in 36 L) on particle breakage is also very significant and should not be ignored. Eliminating one stage of the dispersion mechanism would not affect the size reduction significantly because the other stages will receive larger particles and hence cause a similar amount of attrition.

- Dust dispersion concentration and particle breakage are inversely related due to lowering of the impact energy per particle as well as some of the dust not undergoing suspension turbulence at higher concentration. However, the trend of reduced particle breakage with respect to concentration is not linear, but rather some function of concentration which remains to be determined.
- CNFs de-agglomerate into thin fibers post-dispersion. However, after the dust cloud settles, this nanomaterial re-agglomerates into a different morphology and size distribution than pre-dispersed or that in the cloud. Hence, more study is required to observe the size distribution and morphology of different nanomaterials after dispersion and at the time of ignition. This is crucial as nanomaterial breakage can yield large surface areas which may make them more combustible with larger consequences and may lead to misleading experimental results.

CHAPTER IV

EFFECT OF DUST DISPERSION ON PARTICLE SIZE DISTRIBUTION IN THE *MIE* APPARATUS[*]

4.1. Synopsis

For dust explosion studies, some of the standard parameters are the maximum overpressure (P_{max}) and deflagration index (K_{st}). These parameters are typically measured with a 20 L dust explosion apparatus in accordance with ASTM standard (ASTM E 1226 [19]). Another important parameter is the minimum ignition energy (*MIE*), which is found using the MIKE3 *MIE* apparatus, according to the ASTM E2019-03 (2013) standard [75]. Recent studies have shown that the dispersion system for the required dust cloud formation in the standard 20 L apparatus induces significant mechanical shear, resulting in breakage of dust particles. Therefore, the explosion parameters obtained (P_{max} and K_{st}) are not representative of the original dust size distribution prior to testing. In this work, the influence of dust dispersion on particle size distribution and particle breakage in a standard minimum ignition energy apparatus (Kühner MIKE3) is presented and compared to a 36 L dust explosion apparatus. The 36 L dust explosion apparatus was developed at the Mary Kay O'Connor Process Safety Center, Texas A&M University to give similar P_{max}, K_{st} results to that of a standard 20 L apparatus. Previous work (Chapter III) has shown that similar particle breakage occurs in 36 L and 20 L apparatus.

---

[*] [14] Reprinted with permission from "Effect of dust dispersion on particle breakage and size distribution in the minimum ignition energy apparatus" by Bagaria, P., Zhang, J., & Mashuga, C., 2018. Journal of Loss Prevention in the Process Industries, 56, 518-523, Copyright (2018) by Elsevier.

Anthraquinone, ascorbic acid, and acetaminophen (paracetamol) were used to achieve the goals of this study. The results show particle breakage due to dispersion does not occur in the MIKE3 *MIE* apparatus. However, a minor portion of smaller particles can escape the Hartmann tube through the top lid, stick to the Hartmann tube and become trapped in the crevasses around and under the electrode. Additionally, it was found that for electrostatic materials such as acetaminophen, the particle size distribution shifts significantly as the particles stick to the Hartmann tube. Thus, these particles are not part of the dust cloud, which can lead to erroneous minimum ignition energy results.

4.2. Experiments

4.2.1. Apparatus

Kühner MIKE3 Minimum Ignition Energy (*MIE*) apparatus (Figure 7) was used to study the effect of dust dispersion on particle breakage and size distribution changes. This apparatus is commonly used worldwide to investigate the minimum ignition energy values of dust cloud in air. The detail about the apparatus and testing procedure is previously described in Chapter I, section 1.2. (Figure 7 and Figure 8).

4.2.2. Materials

Anthraquinone, ascorbic acid, and acetaminophen (paracetamol) were chosen to study the effect of dust dispersion in the *MIE* apparatus. Anthraquinone (assay: 97%, A90004 ALDRICH) is a light-yellow, crystalline powder used in dyes, drugs, and manufacturing bleaching agents. Ascorbic acid (L-Ascorbic acid, assay: 99%, A92902

ALDRICH) is an organic powder known for its antioxidant properties, and used as a drug to treat lack of Vitamin C and scurvy. The crystals are white in color. Acetaminophen (paracetamol, assay: 98–102%, A5000 ALDRICH) is an aromatic organic powder used as a drug for cold, pain relief, and fever. It is a mild analgesic and a white powder with good electrostatic property.

Besides these materials falling into different ranges of particle breakage based on their properties [27], the available data for particle size distribution change due to dispersion in the standard 20 L and 36 L apparatus [18] made these materials of interest. These materials can provide an insight to particle breakage in the *MIE* apparatus compared to other dust explosion apparatus such as the 20 L and 36 L. Figure 17 shows the SEM imaging of the as received (pre-dispersion) samples of anthraquinone, ascorbic acid, and acetaminophen. Figure 18, Figure 19, and Figure 20 shows the particle size distribution of the as received samples of anthraquinone, ascorbic acid, and acetaminophen, respectively.

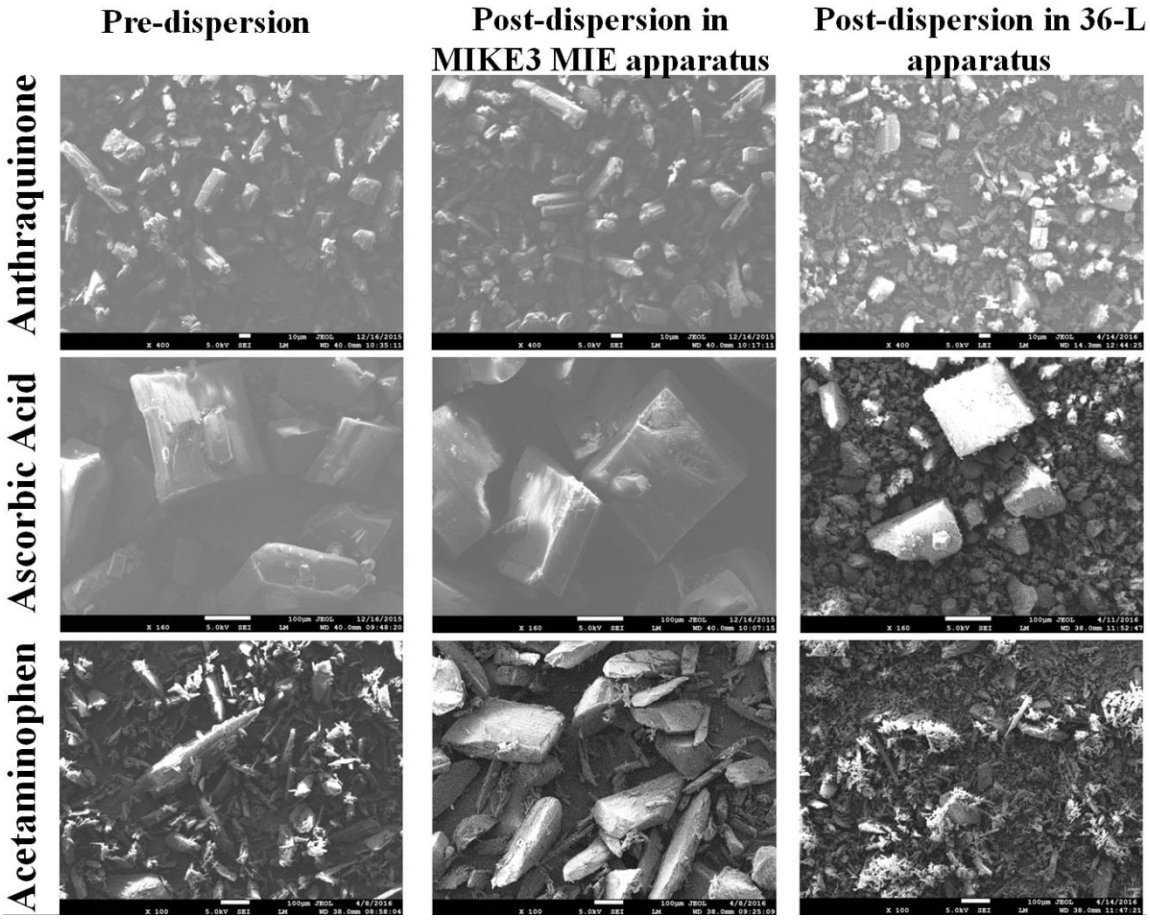

Figure 17 SEM images for pre-dispersion, post-dispersion in the MIKE3 *MIE* apparatus at 3000 g/m^3, and post-dispersion in the 36 L apparatus at 1500 g/m^3 for samples of anthraquinone, ascorbic acid, and acetaminophen [14]. Reprinted with permission from "Effect of dust dispersion on particle breakage and size distribution in the minimum ignition energy apparatus" by Bagaria, P., Zhang, J., & Mashuga, C., 2018. Journal of Loss Prevention in the Process Industries, 56, 518-523, Copyright (2018) by Elsevier.

4.2.3. Methodology

The as received samples of anthraquinone, ascorbic acid and acetaminophen from Aldrich were characterized by their size distribution and morphology using Beckman Coulter Laser Diffraction Particle Size Analyzer LS 13320 and JEOL JSM-7500F Ultra

High Resolution Field Emission Scanning Electron Microscope (FE-SEM), respectively. After characterizing the as received samples, they were dispersed to study the effect of *MIE* apparatus dispersion on size distribution changes and particle breakage. Anthraquinone, ascorbic acid, and acetaminophen were loaded in the dust container individually, each at 3000 g/m^3 (3600 mg). The loaded samples were dispersed at 7 bars in the Hartmann tube. Each material was dispersed ten times and the ignition energy was kept low enough (1 mJ for anthraquinone and 3 mJ for acetaminophen and ascorbic acid) to avoid ignition. The dust was dispersed ten times because it requires ten tries to conclude if the dust can be ignited at that particular energy and concentration level. The post-dispersion materials were collected for size distribution (Beckman Coulter Laser Diffraction Particle Size Analyzer LS 13320) and morphology (JEOL JSM-7500F FE-SEM) analysis. The resulting data was analyzed to gain fundamental insight to the change in particle size distribution post-dispersion in the *MIE* apparatus and also was compared to the 36 L apparatus dispersion results.

4.3. Results

Anthraquinone, ascorbic acid, and acetaminophen (each at 3000 g/m^3) were dispersed ten times in the MIKE3 *MIE* apparatus. The post-dispersion sample was collected after the process. The collected sample was further analyzed for particle size distribution and morphology using Beckman Coulter Laser Diffraction LS 13320 and JEOL JSM-7500F FE-SEM, respectively. The obtained results were then compared to the

size distribution and morphology of pre-dispersion samples to analyze and quantify the change in these parameters due to dispersion.

Figure 17 shows the morphology and particle size of pre-dispersion and post-dispersion samples of anthraquinone, ascorbic acid, and acetaminophen in the MIKE3 *MIE* apparatus using SEM imaging. It also captures the particle breakage due to dispersion in the 36 L apparatus. Unlike in the 36 L apparatus, dispersion in the MIKE3 *MIE* apparatus does not cause the dust particles to break, as seen in the SEM image. The dispersion pressure for the 36 L apparatus is approximately 21 bar, which creates enough force to break the particles. However, in the MIKE3 *MIE* apparatus, the dispersion pressure is 7 bar, which is not enough to break the particles. In addition, it shows that for acetaminophen, the pre-dispersion sample had more fine particles than post-dispersion in the MIKE3 *MIE* apparatus. This SEM image provides a qualitative insight to the size distribution change and particle breakage. More detailed and quantitative analysis for pre and post-dispersion samples in the MIKE3 *MIE* apparatus are provided in Figure 18, Figure 19, Figure 20 and Table 5.

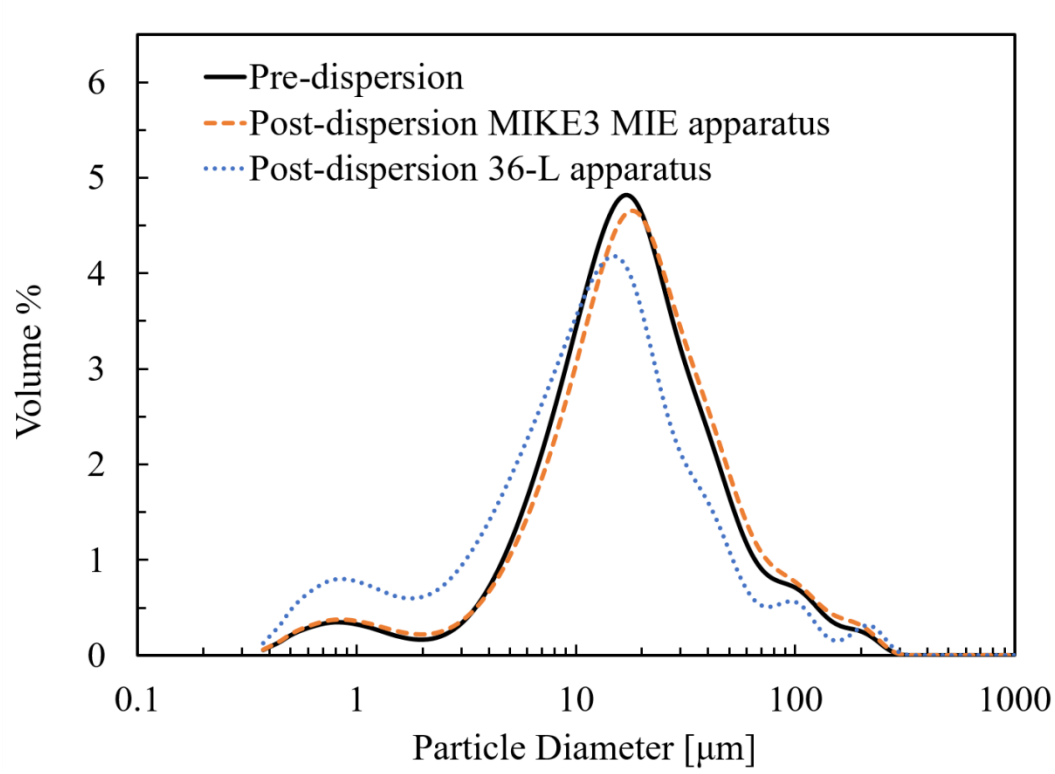

Figure 18 Anthraquinone particle size distributions for pre-dispersion, post-dispersion in the MIKE3 *MIE* apparatus at 3000 g/m^3, and post-dispersion in the 36 L apparatus at 1500 g/m^3 [14]. Reprinted with permission from "Effect of dust dispersion on particle breakage and size distribution in the minimum ignition energy apparatus" by Bagaria, P., Zhang, J., & Mashuga, C., 2018. Journal of Loss Prevention in the Process Industries, 56, 518-523, Copyright (2018) by Elsevier.

Table 5 Particle size distribution statistics for pre-dispersion, post-dispersion in the MIKE3 *MIE* apparatus at 3600 mg, and post-dispersion in the 36 L apparatus at 1500 g/m^3 [18] samples of anthraquinone, ascorbic acid and acetaminophen [14]. Reprinted with permission from "Effect of dust dispersion on particle breakage and size distribution in the minimum ignition energy apparatus" by Bagaria, P., Zhang, J., & Mashuga, C., 2018. Journal of Loss Prevention in the Process Industries, 56, 518-523, Copyright (2018) by Elsevier.

Sample and Statistics (dispersion at 500 g/m^3)		Median/d_{50} [µm]	% Change Median/d_{50}	Mode [µm]	% Change Mode
Anthraquinone	Pre-dispersion	17.9	-	18	-
	Post-dispersion MIKE3 *MIE* apparatus	19.1	6.9 (I)	19.8	9.8 (I)
	Post-dispersion 36 L apparatus	12.9	27.7 (D)	14.9	17.0 (D)
Acetaminophen	Pre-dispersion	48.8	-	127.7	-
	Post-dispersion MIKE3 *MIE* apparatus	79.7	63.2 (I)	168.9	32.3 (I)
	Post-dispersion 36 L apparatus	20.2	58.6 (D)	18.0	85.9 (D)
Ascorbic acid	Pre-dispersion	237.8	-	269.2	-
	Post-dispersion MIKE3 *MIE* apparatus	255.4	7.4 (I)	269.2	0
	Post-dispersion 36 L apparatus	116.3	51.1 (D)	223.4	17.0 (D)

d_{50}: represent 50 percentile of particles is smaller than tabulated value
% Change = [(|Original Sample Data-Post Dispersion Data|)/Original Sample Data]*100
(I): Increase in statistics
(D): Decrease in statistics

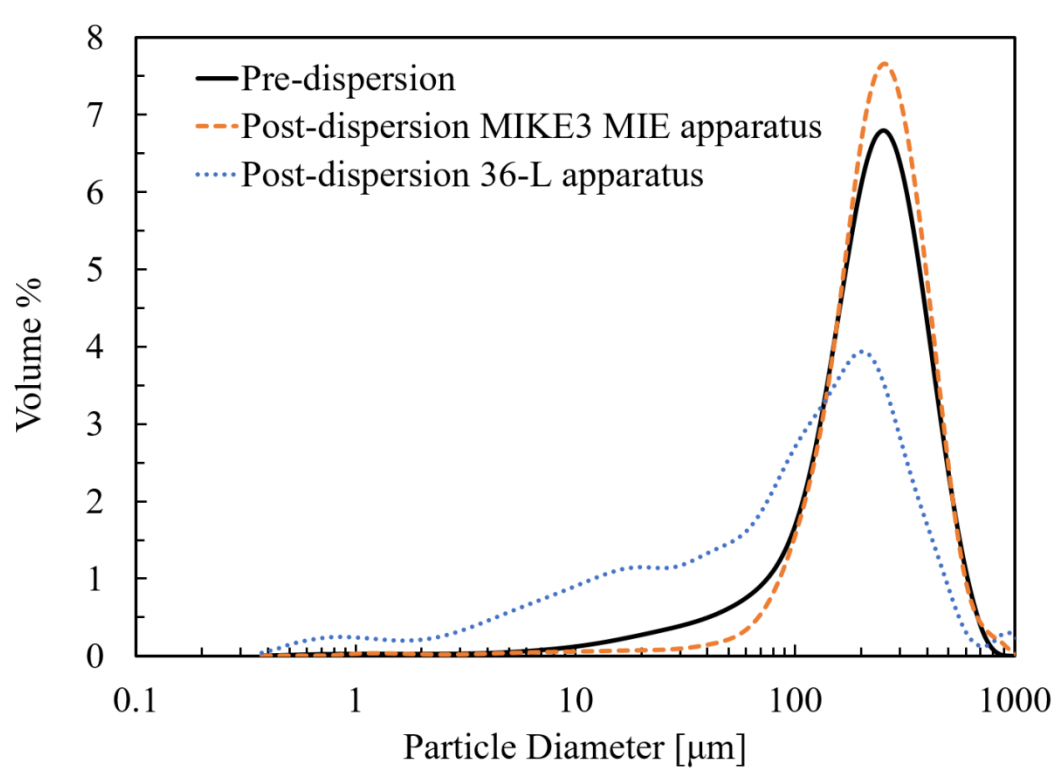

Figure 19 Ascorbic acid particle size distributions for pre-dispersion, post-dispersion in the MIKE3 *MIE* apparatus at 3000 g/m^3, and post-dispersion in the 36 L apparatus at 1500 g/m^3 [14]. Reprinted with permission from "Effect of dust dispersion on particle breakage and size distribution in the minimum ignition energy apparatus" by Bagaria, P., Zhang, J., & Mashuga, C., 2018. Journal of Loss Prevention in the Process Industries, 56, 518-523, Copyright (2018) by Elsevier.

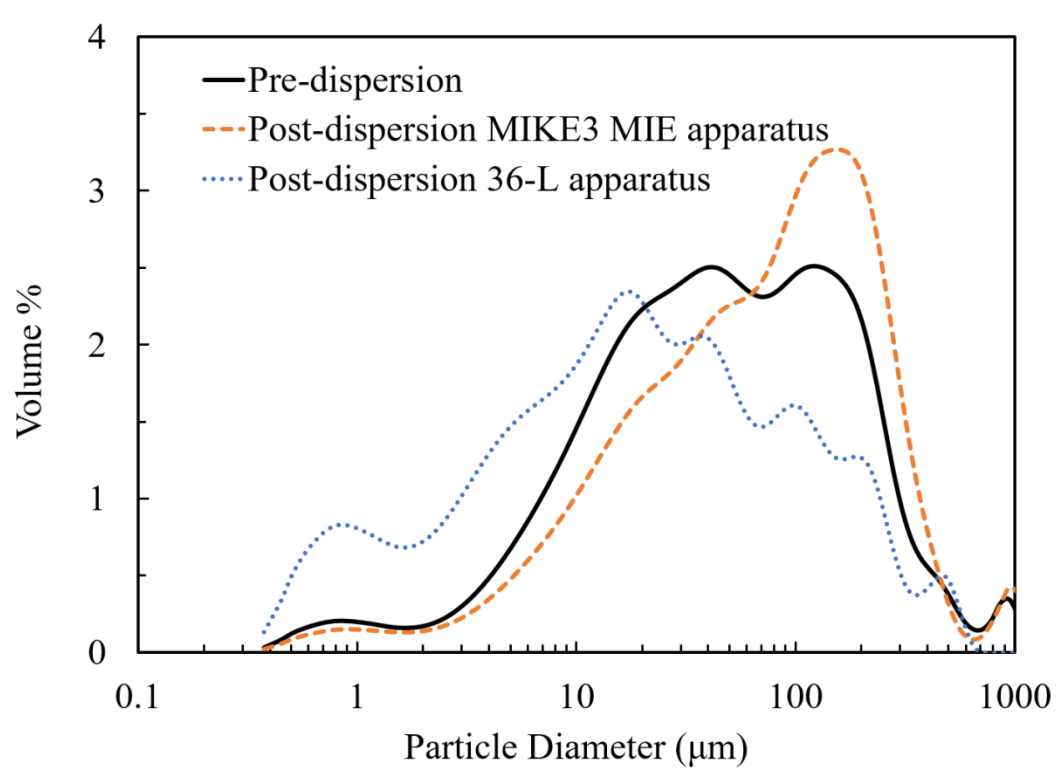

Figure 20 Acetaminophen particle size distributions for pre-dispersion, post-dispersion in the MIKE3 *MIE* apparatus at 3000 g/m^3, and post-dispersion in the 36 L apparatus at 1500 g/m^3 [14]. Reprinted with permission from "Effect of dust dispersion on particle breakage and size distribution in the minimum ignition energy apparatus" by Bagaria, P., Zhang, J., & Mashuga, C., 2018. Journal of Loss Prevention in the Process Industries, 56, 518-523, Copyright (2018) by Elsevier.

Figure 18, Figure 19, and Figure 20 shows the particle size distribution of anthraquinone, ascorbic acid, and acetaminophen, respectively. It can be seen that pre and post-dispersion size distribution for anthraquinone and ascorbic acid are very similar, indicating that the particles do not break due to dispersion in the MIKE3 apparatus, unlike in the 36 L apparatus. The dispersion pressure in the MIKE3 *MIE* apparatus is 7 bar, which does not generate enough force for particle breakage. Also, for anthraquinone

(Figure 18) and ascorbic acid (Figure 19), it can be seen that there is slightly less percentage of small particles post-dispersion in the MIKE3 *MIE* apparatus, hinting that a minor fraction of particles with smaller diameter are removed from the dust cloud due to the dispersion process. These particles can escape the Hartmann tube through the top lid, stick to the Hartmann tube and become trapped in the crevasses around and under the electrode. Because of this, these particles do not participate in the dust cloud formation. However, it is not significant to cause an evident shift in the size distribution. For acetaminophen, although the SEM imaging (Figure 17) shows that it does not break due to dispersion in the MIKE3 *MIE* apparatus, there is a significant shift in particle size distribution (Figure 20). This is an interesting observation and can be explained by the fact that acetaminophen is electrostatic and some of the particles stick to the Hartmann glass tube when dispersed, enough to change the size distribution in a significant manner. The particles that stick to the glass on dispersion are not part of the ignited dust cloud during minimum ignition energy measurement testing. Table 5 provides quantitative statistics for Figure 18, Figure 19, and Figure 20. It shows that for anthraquinone and ascorbic acid, the median and mode values increase post-dispersion in the MIKE3 *MIE* apparatus, indicating that smaller particles are removed from the dust cloud during the dispersion process. This increase also indicates that there is no particle breakage in MIKE3 *MIE* apparatus for these materials, unlike the 36 L apparatus. Also for acetaminophen, median, and mode values are significantly higher post-dispersion in MIKE3 *MIE* apparatus owing to the fact that particles stick to the Hartmann tube due to their electrostatic nature and thus are absent from the cloud. This means that for

electrostatic dusts, the size distribution of the cloud is significantly different from the size distribution of the pre-dispersion sample and the obtained minimum ignition energy values do not necessarily correspond to the intended original sample. This significant shift in particle size distribution for electrostatic dusts can lead to an incorrect, non-conservative assessment of the ignition risk in the process industries. The results of the acetaminophen dispersion are used to quantify the impact of a shift in particle size distribution on the *MIE* values. Studies [42][76] have shown that *MIE* is directly proportional to the cube of diameter ($MIE \propto d^3$). The median/d_{50} values for pre and post-dispersion of acetaminophen (Table 5) are used to determine the potential *MIE* change. The other parameters inherent to the dust and the dispersion gas are constant for acetaminophen. Equation 3 shows the ratio of MIE_1 to MIE_2. This is the ratio of acetaminophen *MIE* with shifted size distribution to the original size distribution. d_1 is the post-dispersion d_{50} of acetaminophen when the size distribution has changed and d_2 is the d_{50} of the original size specification (Table 5).

$$\frac{MIE_1}{MIE_2} = \frac{{d_1}^3}{{d_2}^3} = \frac{79.7^3}{48.8^3} = 4.35 \qquad \text{Eq. 3}$$

The calculation from equation 3 suggests that the *MIE* for electrostatic dusts (acetaminophen, in our case) may almost quadruple due to the shift in particle size distribution during dispersion. This means the *MIE* value for acetaminophen can be more than 4 times higher than what we may have obtained. Although the correlation in the studies ($MIE \propto d^3$) has made several assumptions [42][76], the calculation in equation 3 demonstrates the potential for a serious underassessment of ignition probability for

electrostatic dusts and can undermine the risk of a dust explosion. Thus, minimum ignition energy testing for electrostatic materials needs to be improved in order to obtain accurate values that match the credible scenarios in a given process.

4.4. Conclusions

This research studied the effect of dispersion in the MIKE3 *MIE* apparatus on combustible dust particle size distribution and particle breakage. Anthraquinone, ascorbic acid, and acetaminophen were used for evaluating the dispersion effect on particle size distribution change in the MIKE3 apparatus. For each material, dispersion was conducted ten times as ten tries and no ignition at a particular energy and concentration level is required to determine a dust is non-ignitable at that energy and concentration. The dispersion pressure was 7 bar and the dispersion concentration was 3000 g/m^3. Particle characterization and size distribution was conducted for pre and post-dispersion samples using SEM imaging (JEOL JSM-7500F FE-SEM) and laser diffraction (Beckman Coulter LS 13320), respectively. The results were compared to observe particle breakage and size distribution change in the MIKE3 apparatus, and then compared to results from the 36 L apparatus [18]. Based on the obtained results and comparisons, the following can be concluded:

- Particle breakage does not occur in the MIKE3 *MIE* apparatus due to dispersion, unlike the 36 L apparatus. This might be because the dispersion pressure is 7 bar and does not generate enough force to break the particles. In the 36 L apparatus,

the dispersion pressure is 21 bar, which generates enough force to break the particles.

- For anthraquinone and ascorbic acid, particle size distribution slightly shifts towards larger diameter particles post-dispersion in the MIKE3 *MIE* apparatus, suggesting that some smaller particles are removed from the dust cloud by escaping the Hartmann tube, sticking to its walls and becoming trapped in the crevasses around and under the electrodes. The dust cloud ignited for minimum ignition energy measurement testing does not contain these smaller particles, and this can slightly influence the minimum ignition energy values for these dusts.
- There is a significant shift in the post-dispersion size distribution for acetaminophen in the MIKE3 *MIE* apparatus. This is due to the electrostatic nature of acetaminophen, promoting many of the smaller particles to stick to the Hartmann tube, leading to the significant shift in size distribution. This significant shift in particle size distribution can change the *MIE* values significantly and lead to minimum ignition energy values that do not correspond to the original pre-dispersion sample. Studies [42][76] have shown the minimum ignition energy is directly proportional to the particle diameter cubed. This shows how significant the dependence of minimum ignition energy on particle size is and supports our hypothesis that the change in particle size and its distribution due to dispersion in *MIE* apparatus for electrostatic dust can significantly affect the minimum ignition energy.

- Analyzing post-dispersion dust is a good way to quantify the shift in particle size distribution due to the dispersion process in the MIKE3 *MIE* apparatus. A more comprehensive way to analyze this effect is through real time optical monitoring using laser techniques (Malvern etc.). Additionally, dust cloud concentration as a function of cloud position can also be resolved. Application of laser technology in the *MIE* apparatus for laser ignition, flame speed, thermal gradient, and concentration gradient measurements have been investigated [[77]-[80]]. The application of real time particle size distribution and concertation monitoring would result in a more comprehensive understanding of the cloud dynamics. This enhanced understanding can only help result in a better assessment of the ignition energy and ignition risk assessment.

CHAPTER V

CLASSIFICATION OF PARTICLE BREAKAGE DUE TO DUST DISPERSION[*]

5.1. Synopsis

Recent studies have found that dust particle size distribution can significantly reduce upon dispersion in the standard 20 L and 36 L apparatus, which can affect the explosion parameters. The reduction in particle size distribution due to the dispersion process depends on the dust and explosion apparatus. Therefore, it is necessary to quantify the particle size reduction of different dusts due to dispersion in various explosion apparatuses (20 L, 36 L and 1 m^3) and correlate it to the dust properties that influence particle breakage (*i.e.*, hardness and fracture toughness).

This investigation aims to study post-dispersion particle size reduction in the 20 L, 36 L and 1 m^3 dust explosion apparatus and classify dusts into particle breakage categories, with a range of brittleness index associated with each category. It will help the process industries identify dusts that are susceptible to breakage (based on their brittleness index) and prone to give misleading explosion results during dust explosion testing, permitting a proper dust explosion risk assessment. Ascorbic acid, acetaminophen (paracetamol), anthraquinone, active charcoal, Pittsburgh pulverized coal (PPC), cornstarch, lycopodium clavatum, and polyethylene were used in this study. These materials were dispersed in the 20 L, 36 L and 1 m^3 apparatus at a concentration of

[*] [23] Reprinted with permission from "Classification of particle breakage due to dust dispersion" by Bagaria, P., Li, Q., Dastidar, A., & Mashuga, C., 2019. Powder Technology, 342, 204-213, Copyright (2019) by Elsevier.

500 g/m^3 and post-dispersion samples were analyzed for particle size distribution changes. The mechanical properties (hardness and fracture toughness) of these materials were measured using Nanoindentation. The dispersion-induced change in size distribution was correlated to the measured mechanical properties of the dusts.

Dispersion results show the 20 L and 36 L dust explosion apparatus cause significantly more particle breakage than the 1 m^3 apparatus. Particle breakage is highest in ascorbic acid followed by acetaminophen, anthraquinone, active charcoal, and Pittsburgh pulverized coal, respectively. Cornstarch, lycopodium clavatum and polyethylene did not undergo particle size reduction due to dispersion. In addition, the 1 m^3 apparatus caused particle breakage only in ascorbic acid, acetaminophen and anthraquinone. Nanoindentation results show ascorbic acid has the highest brittleness index value followed by acetaminophen, anthraquinone, active charcoal, and Pittsburgh pulverized coal, respectively. The brittleness index correlates directly to the particle breakage trend. Based on the results, ascorbic acid, acetaminophen and anthraquinone were classified into class I breakage category (high breakage). These materials are most susceptible to giving misleading explosion results because of altered particle size distributions. Active charcoal and Pittsburgh pulverized coal were classified into class II breakage category (medium breakage), while cornstarch, lycopodium clavatum and polyethylene were placed into class III breakage category (little or no breakage).

5.2. Experiments

5.2.1. Apparatus

The study of particle breakage due to dispersion is carried out in the standard 20 L dust explosion apparatus, 36 L dust explosion apparatus and the standard 1 m^3 dust explosion apparatus. Quantification of dust particle hardness and fracture toughness is conducted using a Nanoindenter.

The details about the standard 20 L dust explosion apparatus which is widely used to measure the explosion properties of combustible dust is provided in Chapter I, section 1.2 [Figure 3, Figure 4]. 36 L dust explosion apparatus, custom built at the Mary Kay O'Connor Process Safety Center, is calibrated to give similar results to that of the standard 20 L and the standard 1 m^3 apparatus and is described in detail in Chapter III, section 3.2.1. [Figure 10, Figure 11]. Both, standard 20 L dust explosion apparatus and the custom 36 L dust explosion apparatus are calibrated to replicate the results produced by the 1 m^3 apparatus. The 1 m^3 dust explosion apparatus is described as the gold standard of dust explosion testing because the 1 m^3 apparatus has a larger volume, which better simulates an actual process, resulting in more realistic data [20][21]. The 1 m^3 chamber (Figure 5) is equipped with two air nozzles and reservoirs to disperse the dust, and two electrodes for connecting igniters to a voltage source. The chamber is equipped with two pressure transducers to measure the pressure output of an explosion. The pressure-time data is collected by a high-speed data acquisition system. The test is automated and computer controlled. For each test, a known amount of material is weighed and then placed in the dust dispersion chamber (or the dust quantity is split in

half and placed equally inside each of the two dispersion chambers if there is too much dust to fit in a single dispersion chamber). The ignition source is then attached to the electrode in the center of the chamber. The chamber is sealed and all valves are closed. Then, the chamber is partially evacuated so after dispersing air, the desired nominal pressure in the test chamber is 1 bar (a). Then the automated test sequence is initiated using the computer control software. The dust dispersion chamber(s) are pressurized to 21 bar (a). The dispersion valves are opened releasing the dust into the 1 m^3 chamber and raising the chamber pressure to 1 bar (a). After a computer controlled delay time of 550 ms, the chemical squib igniters are initiated. The resulting pressure rise is measured by two piezoelectric pressure transducers. The pressure-time history data is then reviewed and the maximum explosion pressure and rate of pressure rise is determined.

Nanoindentation was carried out using the Hysitron TI 950 Triboindenter (Figure 21) to measure the hardness and fracture toughness of the dust samples. The testing is based on the ASTM standard E2546 [81]. In this apparatus, the indents are made using a Berkovich tip, which is a three-sided pyramidal tip (approximate radius 100 nm). Built-in scanning probe microscope (SPM) helps to identify the flat and smooth crystals for indentation. During the indentation process, the apparatus applies a normal force on a material using the Berkovich tip. The material is displaced and applies a force back to the apparatus. On reaching the pre-set value of force, the normal force by the apparatus is slowly reduced until there is complete relaxation of the material. A transducer quantifies the responding force of the material and generates a force load-displacement curve. Established models are then used to assess elasticity, hardness, fracture toughness, *etc.*

[82]. The force application by the apparatus ranges from ≤30 nN to 10 N. The transducer load resolution is <1 nN. Additional specifications can be found in the TI 950 Triboindenter user manual.

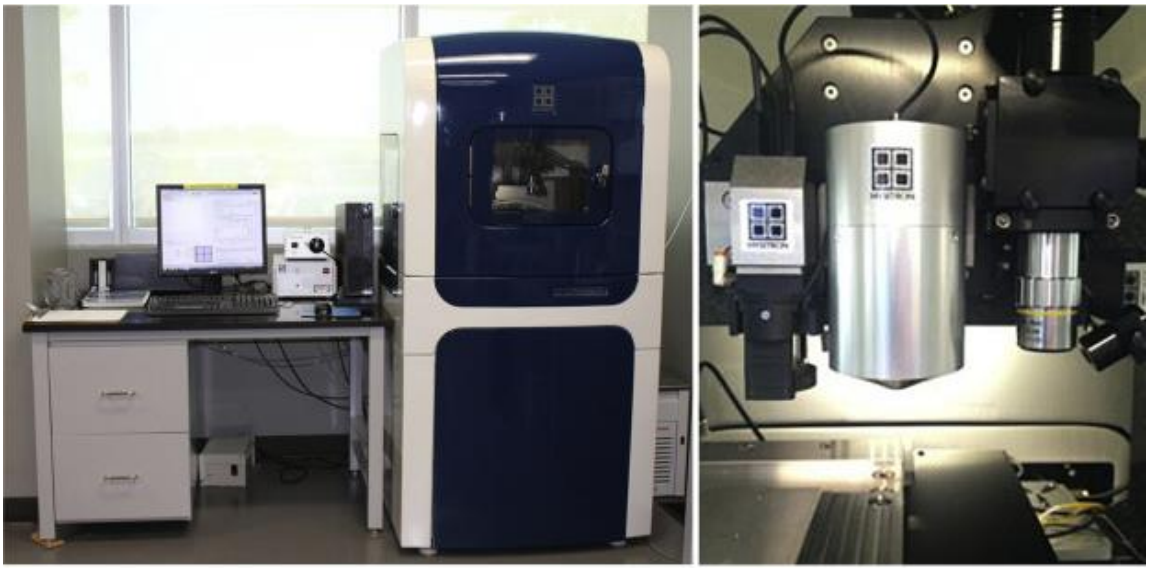

Figure 21 Hysitron TI 950 Triboindenter and Indenter Transducer [23]. Adapted from [83]. Reprinted with permission from "Classification of particle breakage due to dust dispersion" by Bagaria, P., Li, Q., Dastidar, A., & Mashuga, C., 2019. Powder Technology, 342, 204-213, Copyright (2019) by Elsevier.

5.2.2. Materials

Ascorbic acid, acetaminophen (paracetamol), anthraquinone, active charcoal, Pittsburgh pulverized coal (PPC), cornstarch, lycopodium clavatum, and polyethylene were used in the study. These materials were selected for two reasons. First, these materials represent dusts from various industries such as pharmaceutical, mining, food

processing, and chemical. Second, these dusts represent a wide range of post-dispersion particle breakage. For example, ascorbic acid undergoes ~ 80%–90% reduction in the median size distribution [18][27] while, lycopodium clavatum particles do not break [27]. The dusts selected are distributed uniformly in the particle breakage range [18][20][27]. Pre-dispersion particle size distribution of these materials (Table 6, Figure 22) was characterized using the Beckman Coulter LS 13320 single wavelength laser diffraction apparatus.

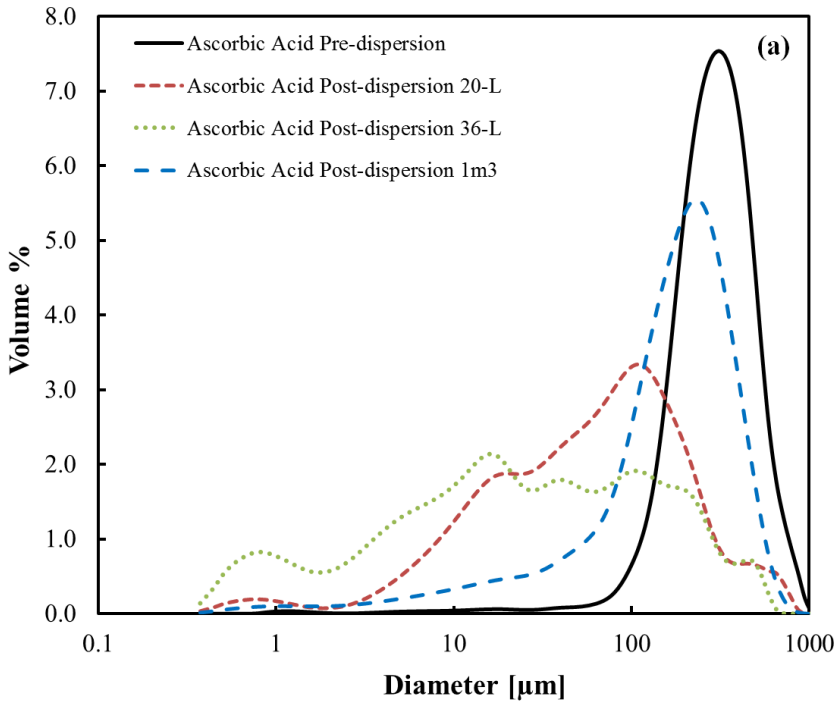

Figure 22 Particle size distributions of pre-dispersion and post dispersion dusts at 500 g/m3: (a) ascorbic acid (b) acetaminophen; (c) anthraquinone; (d) active charcoal; (e) Pittsburgh pulverized coal; (f) cornstarch; (g) lycopodium; (h) polyethylene [23]. Reprinted with permission from "Classification of particle breakage due to dust dispersion" by Bagaria, P., Li, Q., Dastidar, A., & Mashuga, C., 2019. Powder Technology, 342, 204-213, Copyright (2019) by Elsevier.

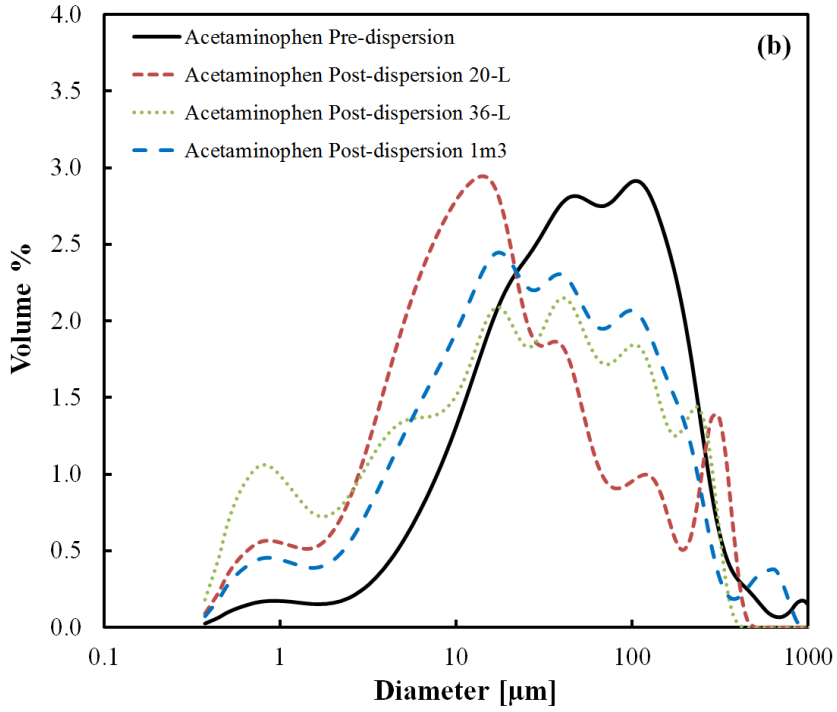

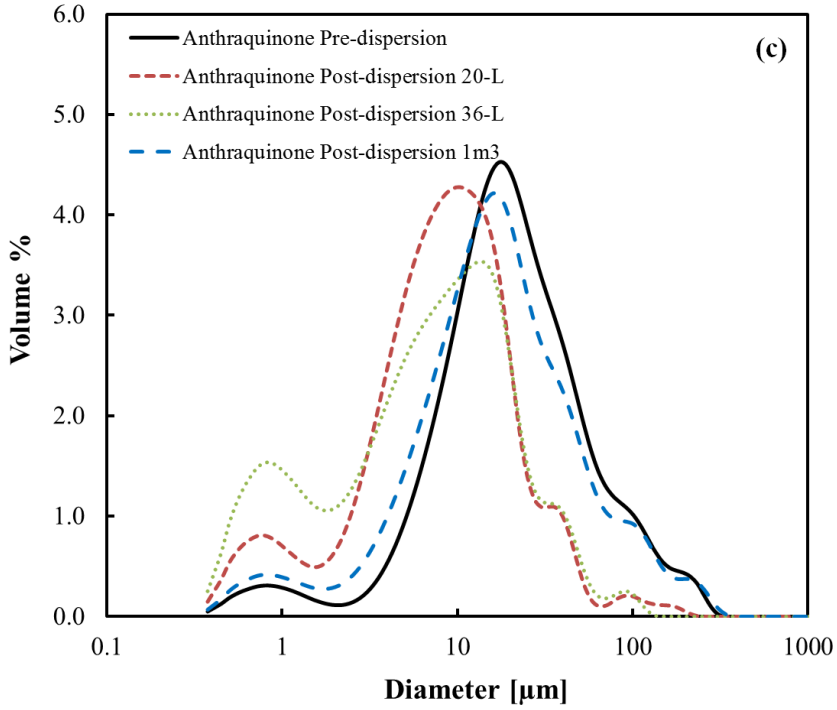

Figure 22 Continued.

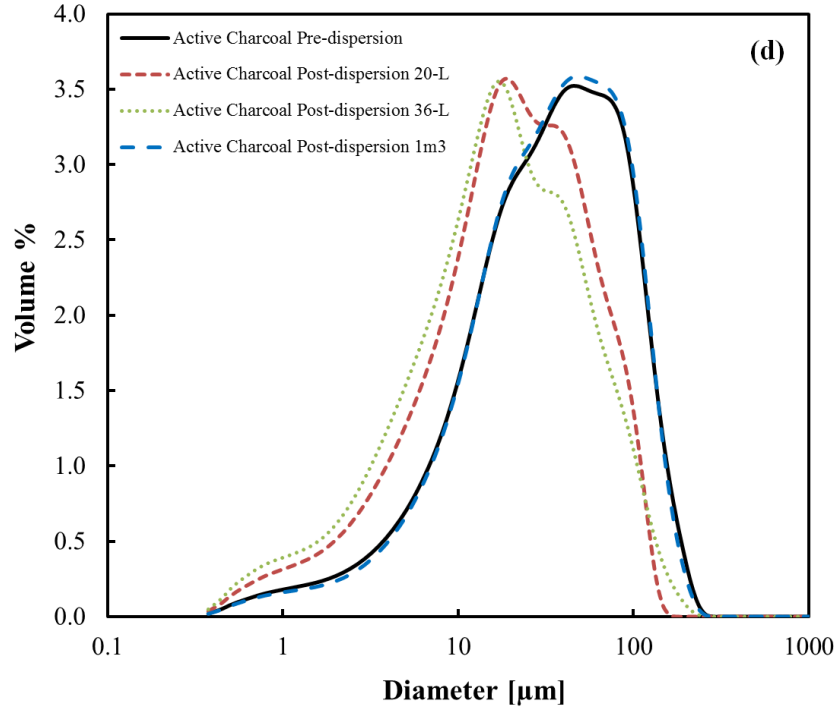

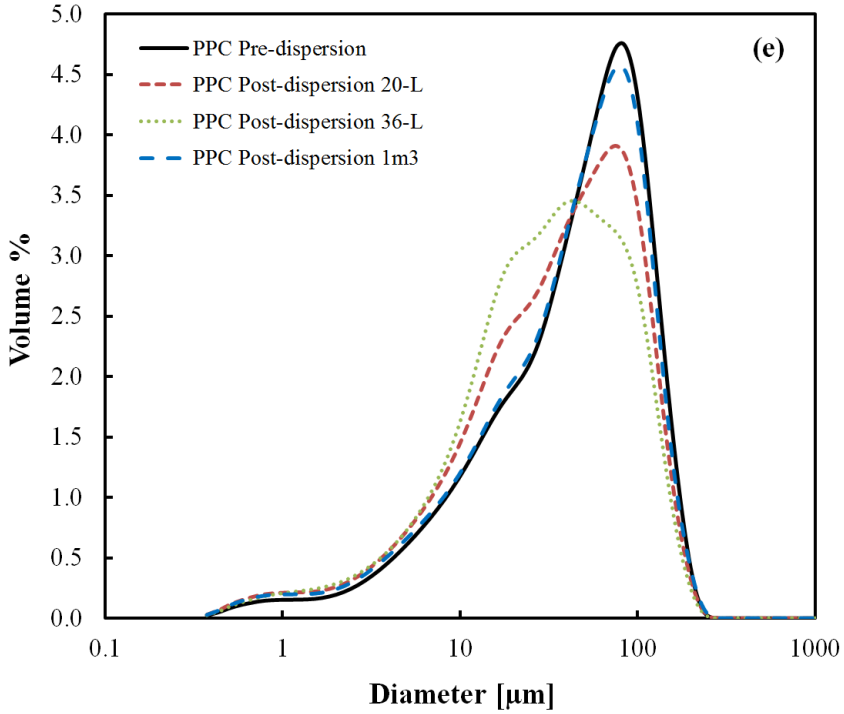

Figure 22 Continued.

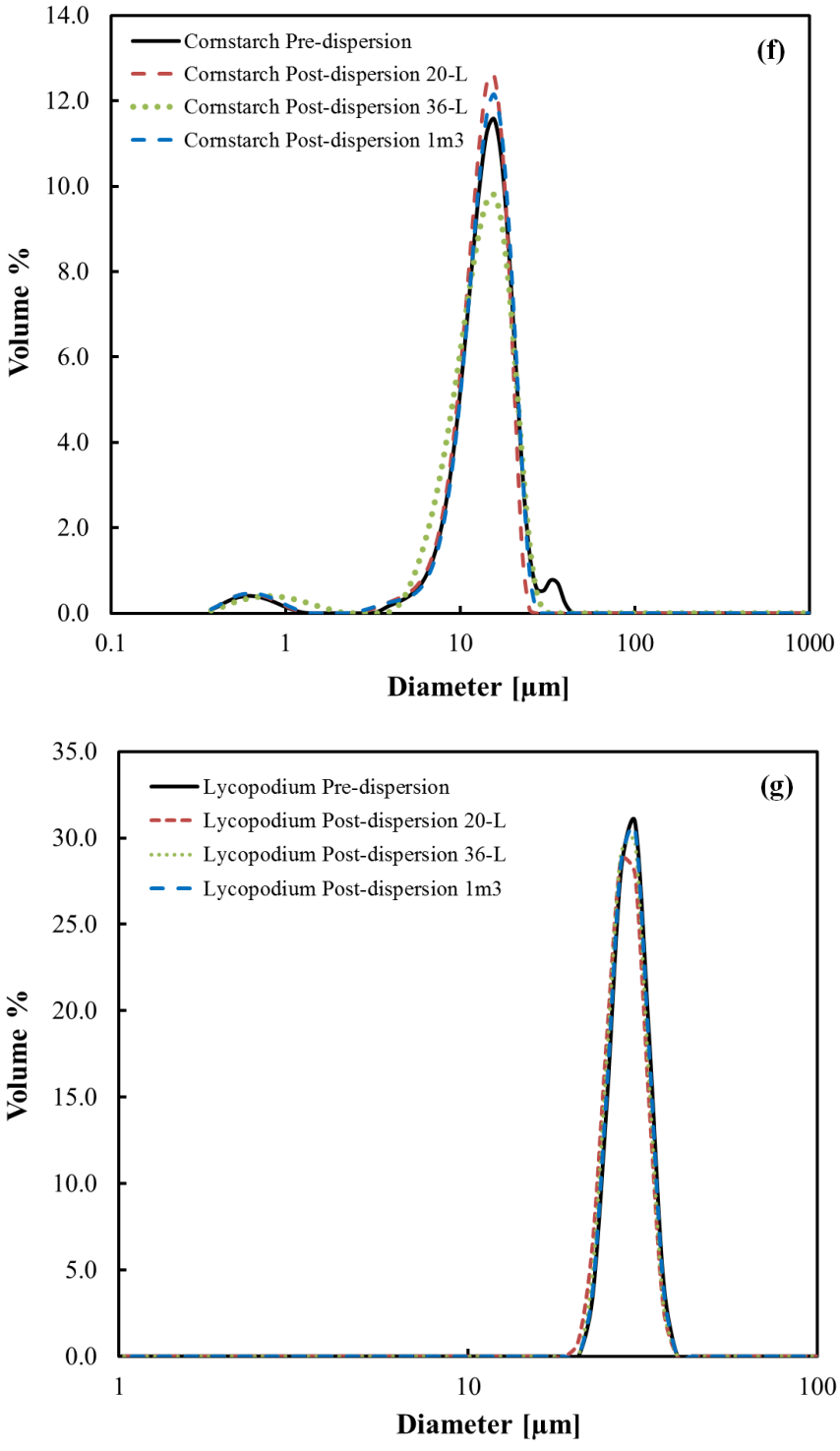

Figure 22 Continued.

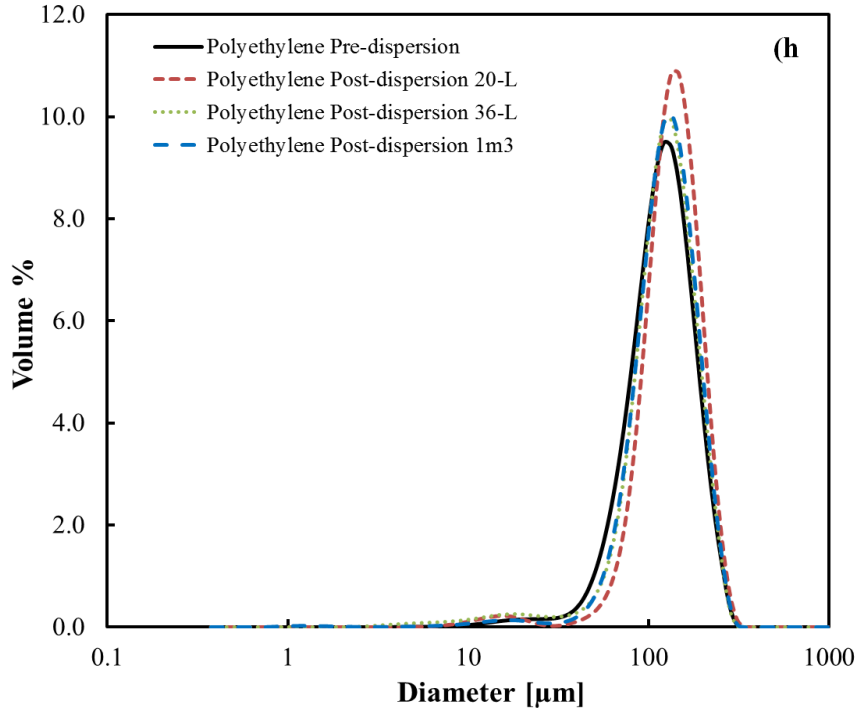

Figure 22 Continued.

5.2.3. Methodology

After pre-dispersion particle size distribution characterization of the dusts, each material was dispersed in the standard 20 L apparatus, 36 L apparatus and 1 m^3 apparatus at a concentration of 500 g/m^3. The dispersed cloud was allowed to settle for a sufficient time (10 min) and the post-dispersion sample was collected for particle size distribution. The pre-dispersion and post-dispersion size distribution data were compared to quantify the particle breakage (Table 6, Figure 22). Also, variation in the particle breakage for different materials was compared.

For the measurement of hardness and fracture toughness using Nanoindentation, the dust samples were prepared by embedding the dust in epoxy. The epoxy embedded dust samples were cut and polished using a Microtome to generate a smooth surface with dust particles on the epoxy surface. This approach was followed for all eight materials. Figure 23 shows an image of epoxy embedded dust sample for ascorbic acid. The Nanoindentation apparatus (Figure 21) was then used to create indents on the surface of the dust particles to determine the hardness and fracture toughness of the selected materials. Indents were made in several locations on a single particle, and several particles were indented for each sample. For the hardness measurement, the Berkovich tip was used and the force load for indentation was set as 80 μN for anthraquinone, PPC, cornstarch, lycopodium clavatum, and polyethylene, 150 μN for ascorbic acid, and 2000 μN for acetaminophen and active charcoal. The force load was set to achieve a minimum displacement of 50 μm, which is required to achieve reliable data [82]. The apparatus captures the force load-displacement response of the material to evaluate the hardness. For fracture toughness measurements, a cube-corner tip was used and the force load was set at 10,000 μN for all materials. After the indentations, the crack length on the particle surface was measured for the materials to evaluate fracture toughness.

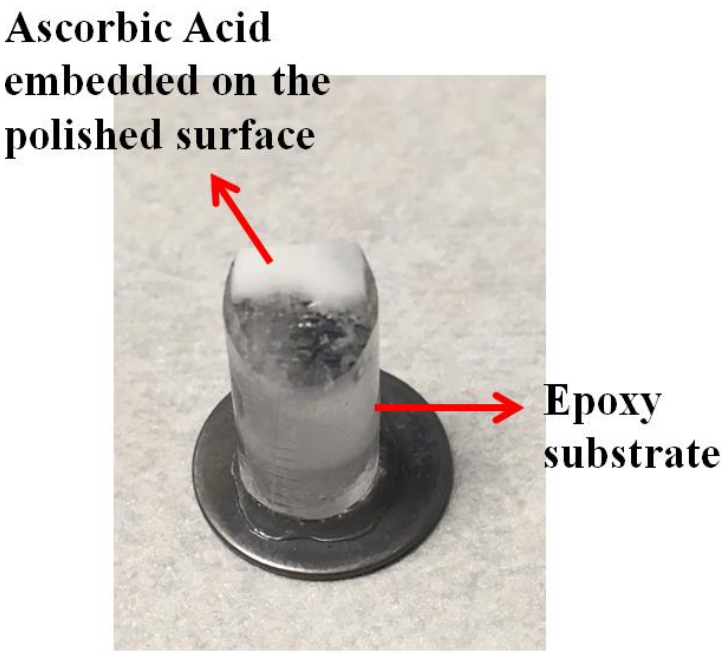

Figure 23 Ascorbic acid dust-embedded in epoxy substrate [23]. Reprinted with permission from "Classification of particle breakage due to dust dispersion" by Bagaria, P., Li, Q., Dastidar, A., & Mashuga, C., 2019. Powder Technology, 342, 204-213, Copyright (2019) by Elsevier.

5.3. Results

5.3.1. Dispersion experiments (20 L, 36 L, 1 m^3)

Eight materials (ascorbic acid, acetaminophen (paracetamol), anthraquinone, active charcoal, Pittsburgh pulverized coal (PPC), cornstarch, lycopodium clavatum, and polyethylene) were used to quantify the post-dispersion particle breakage in 20 L, 36 L and 1 m^3 apparatus. The pre and post-dispersion particle size distribution curves for these materials dispersed in the 20 L, 36 L and 1 m^3 apparatus are shown in Figure 22 and the statistics (mean, median, *D (3, 2)*) are shown in Table 6. Additionally, Table 6 also shows the percent decrease in the mean, median, and *D (3, 2)* values post-dispersion.

Table 6 Size statistics for pre and post-dispersion samples using the standard 20 L apparatus, 36 L apparatus and the standard 1 m^3 apparatus at 500 g/m^3 [23]. Reprinted with permission from "Classification of particle breakage due to dust dispersion" by Bagaria, P., Li, Q., Dastidar, A., & Mashuga, C., 2019. Powder Technology, 342, 204-213, Copyright (2019) by Elsevier.

Sample and Statistics (dispersion at 500 g/m^3)		Median/d_{50} [µm]	% Decrease Median/d_{50}	Mean [µm]	% Decrease Mean	*D (3, 2)* [µm]	% Decrease *D (3, 2)*
Anthraquinone	Pre-dispersion	20.3	-	33.5	-	9.4	-
	Post-dispersion 20 L	8.9	56.0	13.4	60.0	4.2	55.5
	Post-dispersion 36 L	7.8	61.6	12.1	63.9	2.9	68.9
	Post-dispersion 1m^3	17.1	15.8	30.5	9.0	7.3	22.7
Ascorbic acid	Pre-dispersion	309.0	-	336.0	-	151.0	-
	Post-dispersion 20 L	67.0	78.3	109.2	67.5	16.0	89.4
	Post-dispersion 36 L	25.9	91.6	76.0	77.4	5.3	96.5
	Post-dispersion 1m^3	192.0	37.9	211.0	37.2	32.5	78.5
Acetaminophen	Pre-dispersion	50.9	-	87.0	-	15.2	-
	Post-dispersion 20 L	15.2	70.2	48.9	43.8	5.8	62.1
	Post-dispersion 36 L	21.8	57.2	54.5	37.4	4.3	71.5
	Post-dispersion 1m^3	27.9	45.2	68.2	21.6	7.5	50.5
PPC	Pre-dispersion	52.4	-	60.5	-	15.5	-
	Post-dispersion 20 L	40.9	21.9	52.3	13.6	12.5	19.4
	Post-dispersion 36 L	34.1	34.9	46.9	22.5	12.3	20.8
	Post-dispersion 1m^3	49.4	5.7	58.0	4.1	13.6	12.3
Active charcoal	Pre-dispersion	36.1	-	48.8	-	13.2	-
	Post-dispersion 20 L	21.2	41.3	30.5	37.5	8.5	35.8
	Post-dispersion 36 L	18.1	49.9	28.9	40.8	7.2	45.2
	Post-dispersion 1m^3	36.6	-1.4	48.7	0.2	13.9	-5.3

Table 6 Continued.

Sample and Statistics (dispersion at 500 g/m^3)		**Median/d_{50} [µm]**	**% Decrease Median/d_{50}**	**Mean [µm]**	**% Decrease Mean**	***D (3, 2)* [µm]**	**% Decrease *D (3, 2)***
Cornstarch	Pre-dispersion	15.0	-	15.2	-	8.3	-
	Post-dispersion 20 L	14.4	4.0	14.0	7.9	7.6	8.1
	Post-dispersion 36 L	14.0	6.7	14.0	7.9	7.6	8.5
	Post-dispersion 1m^3	14.9	0.7	14.6	3.9	7.6	7.6
Polyethylene	Pre-dispersion	126.0	-	131.0	-	104.0	-
	Post-dispersion 20 L	143.0	-13.5	147.0	-12.2	114.0	-9.6
	Post-dispersion 36 L	130.0	-3.2	134.0	-2.3	88.2	15.2
	Post-dispersion 1m^3	132.0	-4.8	137.0	-4.6	93.5	10.1
Lycopodium	Pre-dispersion	30.4	-	30.5	-	30.2	-
	Post-dispersion 20 L	29.6	2.6	29.8	2.3	29.4	2.6
	Post-dispersion 36 L	30.0	1.3	30.1	1.3	29.7	1.7
	Post-dispersion 1m^3	30.3	0.3	30.4	0.3	30.0	0.7

D (3, 2): the surface-weighted mean diameter

d_{50}: represent 50 percentile of particles is smaller than tabulated value

% Decrease = [(Original Sample Data-Post Dispersion Data)/Original Sample Data]*100

Figure 22 and Table 6 show a more substantial reduction in particle size for the materials dispersed in the 20 L and 36 L apparatus as compared to the 1 m^3 apparatus. This implies the dispersion process in 20 L and 36 L apparatus causes significantly more particle breakage than in 1 m^3 apparatus. The results also show that the 1 m^3 apparatus causes significant breakage in only a few dusts, which are ascorbic acid, acetaminophen and anthraquinone. These dusts have a tendency to break, as the particle breakage is more in these dusts compared to others when dispersed in 20 L and 36 L apparatus. The reason that the 1 m^3 apparatus leads to less particle size reduction compared to 20 L and 36 L apparatus can be due to reduced force generated during the dispersion process in the 1 m^3 apparatus. The dust in the 1 m^3 chamber passes through a smooth ball valve and the dust flow path has no sharp turns. Also, it has been shown in literature [27][84] that the rebound nozzle used in experiments with the 20 L and 36 L affects fluid flow by generating significantly high turbulent kinetic energy, which can lead to higher shear and impact force. This can cause more particle breakage in the 20 L and 36 L apparatus compared to 1 m^3 apparatus which typically uses an air nozzle. In addition, there is less particle impact force through interaction with the vessel wall due to the 1 m^3 apparatus larger volume. The 20 L and the 36 L apparatus provide sufficient force to induce particle breakage through frictional and impact forces via outlet valve, dispersion nozzle and the equipment vessel. The force generated in 1 m^3 apparatus is sufficient enough to cause size reduction in materials with high breakage tendency but it does not affect the particle size distribution of other dusts, unlike the 20 L and 36 L apparatus. This adds to the credibility of 1 m^3 apparatus since the explosion parameters generated in this apparatus

correspond to the pre-dispersion dust distribution, which leads to a more proper dust explosion risk assessment.

Figure 22 and Table 6 also show the particle breakage behavior of different materials post-dispersion in 20 L, 36 L and 1 m^3 apparatus. The results show the breakage trend as ascorbic acid > acetaminophen > anthraquinone > active charcoal > Pittsburgh pulverized coal in the 20 L apparatus. A similar trend is observed in the 36 L apparatus as well. Cornstarch, lycopodium clavatum and polyethylene particles didn't undergo reduction on dispersion in the 20 L and 36 L apparatus. This is because of different breakage propensity/brittleness, which depends on the mechanical properties (hardness and fracture toughness) of materials. Ascorbic acid has properties that make it the most brittle out of the dust samples being tested; while cornstarch, lycopodium clavatum and polyethylene have properties that make them least brittle/not brittle. Also, 1 m^3 apparatus only caused particle size reduction in ascorbic acid, anthraquinone, and acetaminophen. The other materials did not break in the 1 m^3 apparatus. This particle breakage behavior is dependent on the mechanical properties of the materials.

The results in Figure 22 and Table 6 demonstrate that the 20 L and 36 L apparatus cause more particle breakage than the 1 m^3 apparatus. This highlights the point that 20 L apparatus is calibrated to yield similar results to the 1 m^3 apparatus with potentially different post-dispersion particle size distribution. This can be attributed to the fact that there are many materials (including calibration materials, such as cornstarch, lycopodium, etc.) which do not break post-dispersion (low brittleness) in the 20 L and 1 m^3 apparatus. The post-dispersion particle size distribution remains the same for these

materials in the 20 L and 1 m^3 apparatus, generating similar explosion parameters. Some materials undergo variable particle breakage in the 20 L and 1 m^3 apparatus, yet still yield similar explosion parameters. One explanation is the lumped turbulence-ignition delay tuning of the 20 L apparatus to match the 1 m^3 apparatus explosion parameters. This provides a sense that the 20 L and 1 m^3 apparatus yield similar explosion parameters. However, there are cases for several materials when the 20 L explosion results differ from 1 m^3 apparatus [21][85]. This difference is often caused by overdriving, under driving, and perhaps differences in post-dispersion particle size distribution. For further insight into this, a more in-depth subsequent study is required.

Since, the particle breakage behavior is dependent on material's mechanical properties; these properties can be measured by indentation tests and can be correlated to particle breakage post-dispersion in the dust explosion apparatus. This correlation can be used to classify dusts prone to breakage and misleading dust explosion testing results so that proper dust explosion risk assessments can be made.

5.3.2. Nanoindentation results

Nanoindentation was used to measure hardness and fracture toughness of the prepared dust samples in order to measure their respective brittleness index. The indentations were carried out at the Materials Characterization Facility (MCF), Texas A&M University, College Station. Figure 24 shows an image of the indented ascorbic acid surface with cracks at a 10,000 μN force load.

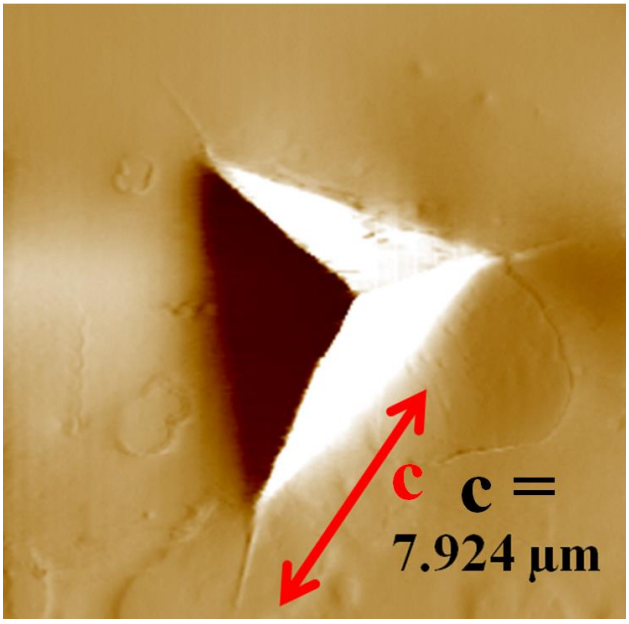

Figure 24 Indented surface image of ascorbic acid sample; c is the crack length due to indentation [23]. Reprinted with permission from "Classification of particle breakage due to dust dispersion" by Bagaria, P., Li, Q., Dastidar, A., & Mashuga, C., 2019. Powder Technology, 342, 204-213, Copyright (2019) by Elsevier.

Hardness was calculated based on the force load and projected contact area of each material using equation 4 [86]:

$$H = P/A_c \qquad \text{Eq. 4}$$

Where, H is the hardness (Pa); P is the set force load (N); A_c is the projected contact area (m^2). A_c is calculated using the contact depth (h_c). Contact depth is measured from the force load-displacement curve of the material [86]. Table 8 shows the measured hardness values of the materials. Ascorbic acid has the highest hardness value among the tested materials followed by acetaminophen, anthraquinone, active charcoal, PPC, cornstarch, lycopodium clavatum, and polyethylene respectively.

Calculation of the fracture toughness requires the hardness value, elastic modulus of the dust, and indention crack length and can be found with equation 5 [86]:

$$Kc = \alpha * (E / H)^{1/2} * (P_{set} / (c^{3/2})) \quad \text{Eq. 5}$$

Where, K_c is the fracture toughness; α is an empirical constant (0.032 for cube-corner tip); E is the Young's modulus; H is the hardness; P_{set} is the set force load (10,000 μN for fracture toughness test); c is the crack length due to indentation as shown in Figure 24 for ascorbic acid. Young's modulus (E) can be calculated from Reduced modulus (E_r), Young's modulus and Poisson's ratio of indenter, and Poisson's ratio of sample as shown in equation 6 [86]:

$$(1/E_r) = ((1 - \nu^2) / E) + ((1 - \nu_i^2) / E_i) \quad \text{Eq. 6}$$

Where, E_r is the Reduced modulus, ν is the Poisson's ratio of the sample, E is the Young's modulus of the sample, ν_i is the Poisson's ratio of the indenter and E_i is the Young's modulus of the indenter. For the cube corner tip (made with diamond), the value for ν_i and E_i are 0.07 and 1140 GPa, respectively. E_r is calculated from the force load-displacement curves of the samples when indentions were performed for hardness measurement. Table 7 shows the values for E_r, ν, E and the crack length (c).

Table 7 Reduced modulus, Poisson's ratio [[87]-[94]], Young's modulus and observed crack length for the materials [23]. Reprinted with permission from "Classification of particle breakage due to dust dispersion" by Bagaria, P., Li, Q., Dastidar, A., & Mashuga, C., 2019. Powder Technology, 342, 204-213, Copyright (2019) by Elsevier.

Materials	Reduced Modulus [E_r], GPa	Poisson's Ratio of the Sample [v]	Calculated Young's Modulus of the Sample [E], GPa	Observed Crack Length [c], µm
Ascorbic acid	42.7	0.30	40.36	7.924
Acetaminophen	11.83	0.29	10.95	4.254
Anthraquinone	13.83	0.24	13.19	4.907
Active charcoal	4.773	0.19	4.62	4.072
Pittsburgh pulverized coal	6.62	0.35	5.84	2.482
Cornstarch	9.15	0.30	8.39	-
Lycopodium	3.06	0.50	2.30	-
Polyethylene	2.52	0.46	1.99	-

The information from Table 7 was used to calculate fracture toughness using equation 5. Table 8 shows the calculated fracture toughness values. Hardness and fracture toughness values in Table 8 were used to measure the brittleness index (*BI*) of each material through equation 7 [29]:

$$BI = H / K_c \qquad \text{Eq. 7}$$

Where, H is the hardness found from equation 4, and K_c is the fracture toughness from equation 5. The results show that ascorbic acid has the highest brittleness index while PPC has the lowest among the materials that were tested and underwent particle breakage. The observed trend of the brittleness index was ascorbic acid > acetaminophen > anthraquinone > active charcoal > PPC. Cornstarch, lycopodium clavatum and

polyethylene did not undergo breakage on dispersion and no cracks were observed on indenting these materials. This represents the respective order of the material's susceptibility to breakage. Based on Table 6 and Table 8, significant particle breakage is observed for materials having higher brittleness index. The trend of brittleness index was correlated with the trend of particle breakage post-dispersion in the 20 L apparatus (most common apparatus for dust explosion testing) (Table 8, Figure 25). As expected, a correlation between brittleness index and the post-dispersion particle breakage in the dust explosion apparatus was observed. Figure 25 shows the relation between percent decrease in the post-dispersion median size (d_{50}) in the 20 L apparatus and the brittleness index for the materials. The relationship between breakage and the brittleness index is sigmoidal with an R^2 value of 0.987 as shown in equation 8. The equation only applies to particle breakage corresponding to 500 g/m^3 concentration as different concentrations will lead to different % breakage [18] and hence alter the coefficients of the sigmoid. Also, the upper limit of this sigmoidal (equation 8) is around 77% and the lower limit is around 21%. For a more accurate correlation between % breakage and brittleness index, an in-depth study with more data points over a wider spectrum of brittleness index is required.

$$\% \text{ Breakage} = 76.37 + (21.57\text{-}76.37) / (1 + (BI/3.89)^{7.32}) \qquad \text{Eq. 8}$$

Table 8 Hardness, fracture toughness, brittleness index, % particle breakage post-dispersion in the 20 L apparatus, breakage class for the combustible dust materials [23]. Reprinted with permission from "Classification of particle breakage due to dust dispersion" by Bagaria, P., Li, Q., Dastidar, A., & Mashuga, C., 2019. Powder Technology, 342, 204-213, Copyright (2019) by Elsevier.

Material	Hardness (GPa), H	Fracture Toughness (MPa*m$^{0.5}$), K_c	Brittleness Index (H/K_c)*10^3, m$^{-0.5}$	%Particle Breakage Post-dispersion (d_{50} decrease in 20 L apparatus)	Breakage Class
Ascorbic acid	0.963	0.093	10.365	78.3	I
Acetaminophen	0.777	0.137	5.674	70.2	I
Anthraquinone	0.573	0.141	4.055	56.0	I
Active charcoal	0.457	0.124	3.689	41.3	II
Pittsburgh pulverized coal	0.406	0.310	1.307	21.9	II
Cornstarch	0.340	-	-	4.0	III
Lycopodium	0.123	-	-	2.6	III
Polyethylene	0.095	-	-	-13.5	III

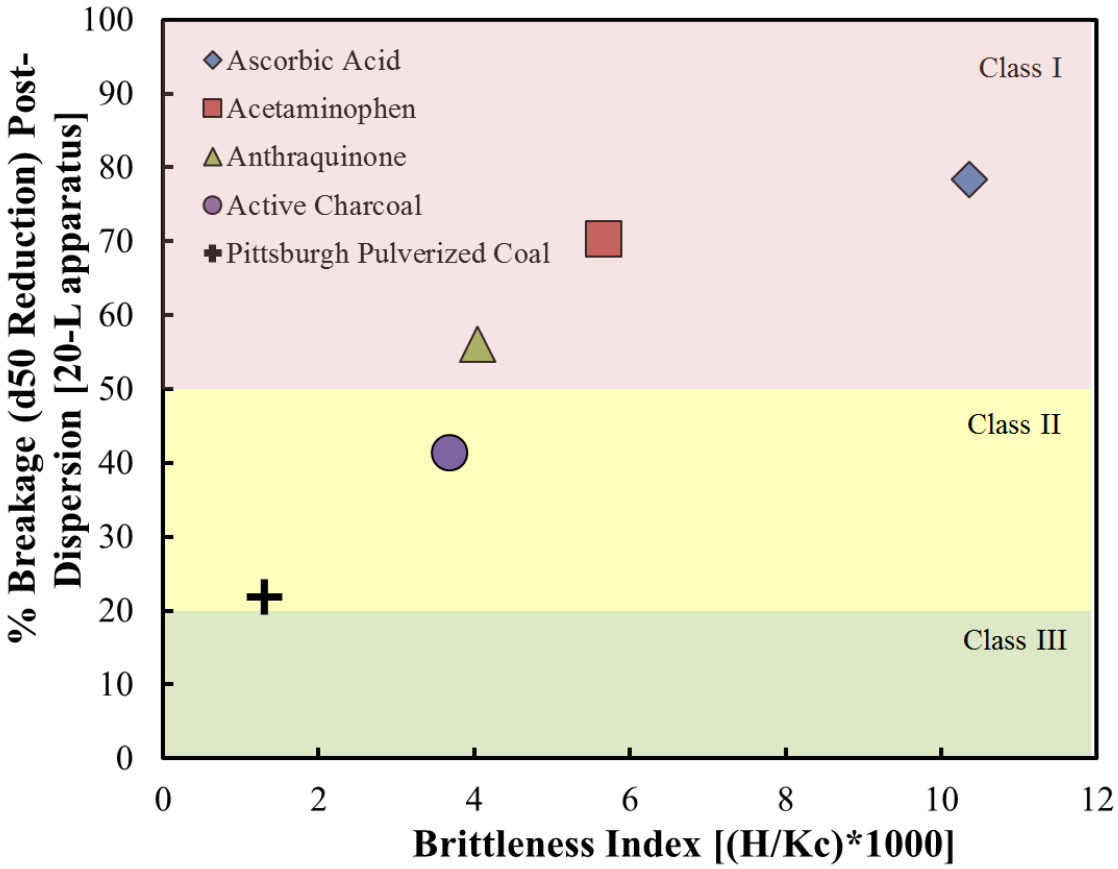

Figure 25 % Particle breakage post-dispersion in 20 L apparatus for the materials vs the brittleness index of the materials [23]. Reprinted with permission from "Classification of particle breakage due to dust dispersion" by Bagaria, P., Li, Q., Dastidar, A., & Mashuga, C., 2019. Powder Technology, 342, 204-213, Copyright (2019) by Elsevier.

Three breakage classes (*BCI, BCII and BCIII*) are proposed based on the particle breakage results (percent decrease in size distribution statistic). In the previous study by Sanchirico et al., [27], a need for two breakage categories, Cat 1 [< 50% breakage] and Cat 2 [> 50% breakage] was defined. Cat 2 includes the dusts that undergo high particle breakage and therefore, can affect the explosion parameters measurement significantly.

This puts emphasis on dusts in Cat 2 to be assessed properly for explosion parameters. However, this is not the case with Cat 1. Cat 1 includes dusts that break moderately (~ 35–40%) and can somewhat influence explosion parameter measurement. It also includes dusts that do not break at all and will have no influence on explosion parameter measurement. Including these dusts (dusts with moderate breakage and dusts with no breakage) in the same category does not allow for a clear categorization of particle breakage and proper risk assessment. Therefore, we included three breakage categories to distinguish dusts with high, medium and low/no breakage.

$$BCI \geq 50\%$$

$$20\% < BCII < 50\%$$

$$BCIII \leq 20\%$$

50% as a threshold value for dusts with high breakage was based on the work by Sanchirico et al., [27]. 20% was decided as a threshold value that can separate dusts with moderate and low/no breakage. This value allows for errors in sample collection post-dispersion. If the shift in particle size distribution is > 20%, particle breakage is the most probable cause (Nanoindentation leads to cracks in the particles with > 20% breakage as observed in this study). But if the shift is < 20%, it can be due to low particle breakage, as well other factors such as some particles sticking to the vessel wall and not being collected for post-dispersion size distribution statistics, or collected particles not being representative of entire batch, etc. The value of 20% sets a good threshold value to encompass these factors.

Table 8 and Figure 25 show the statistics of the brittleness index that correlates to the decrease in particle size distribution. Breakage Class I is associated with a brittleness index value ranging above 4×10^3 $m^{-0.5}$. Ascorbic acid, anthraquinone and acetaminophen fall into this class and can yield the most erroneous results when being tested in the dust explosion apparatus because of the significant shift in particle size distribution. Breakage Class II is associated with a brittleness index value ranging between 1.3×10^3 $m^{-0.5}$ - 4×10^3 $m^{-0.5}$. Active charcoal and Pittsburgh pulverized coal fall into this class and are prone to moderate particle size distribution shifting post-dispersion in dust explosion apparatus. This can lead to some error in explosion parameter measurement [28]. Breakage class III materials will have very low brittleness index values. Cornstarch, lycopodium clavatum and polyethylene fall into this class and are the least susceptible to breakage. These materials do not undergo shift in particle size distribution post-dispersion in the dust explosion apparatus and the measured explosion parameters approximately correspond to pre-dispersion size distribution.

5.4. Conclusions

This research studied the shift in particle size distribution due to the dispersion process in the standard 20 L, 36 L and 1 m^3 apparatus for a variety of combustible dusts and correlated the shift in size distribution with the mechanical properties of the dusts. Ascorbic acid, acetaminophen (paracetamol), anthraquinone, active charcoal, Pittsburgh pulverized coal (PPC), cornstarch, lycopodium clavatum and polyethylene were selected for the study. Nanoindentation was used to measure the dust material mechanical

properties (hardness (H) and fracture toughness (K_c)) in order to calculate the brittleness index (H/K_c). The dust brittleness index was correlated to the particle breakage due to dispersion in the standard 20 L dust explosion apparatus. Based on the results, the following conclusions can be made:

- 20 L and 36 L dust explosion apparatus cause significantly more particle breakage than the 1 m^3 apparatus. This is attributed to the reduced force imparted on the particles in the 1 m^3 apparatus as compared to the 20 L and 36 L apparatus. Also, the dust particle force of impact on the vessel wall might be less in the 1 m^3 apparatus than in the 20 L and 36 L apparatus due to the larger volume. This adds to the credibility of the 1 m^3 apparatus ability to generate explosion parameters representative of original particle size distribution.
- Ascorbic acid, acetaminophen, anthraquinone, active charcoal, and PPC undergo significant post-dispersion particle breakage in the 20 L and the 36 L apparatus. The results show the breakage trend as ascorbic acid > acetaminophen > anthraquinone > active charcoal > PPC in the 20 L apparatus. A similar trend is observed in the 36 L apparatus. Cornstarch, lycopodium clavatum and polyethylene do not undergo particle breakage post-dispersion in the 20 L and the 36 L apparatus. This is because of different brittleness propensities of the materials. The 1 m^3 apparatus causes size reduction for ascorbic acid, acetaminophen and anthraquinone. Other materials do not undergo size reduction in the 1 m^3 apparatus.

- The observed trend of the brittleness index (*BI*) was ascorbic acid > acetaminophen > anthraquinone > active charcoal > PPC. Cornstarch, lycopodium clavatum and polyethylene did not undergo breakage on dispersion and no cracks were observed on Nanoindentation testing of these materials. This represents the respective order of susceptibility to breakage and it is in agreement with the particle breakage observed due to dispersion in the dust explosion apparatus. A sigmoidal correlation was found between percent breakage post-dispersion in the 20 L apparatus (most widely used apparatus) and the brittleness index (*BI*).
- Materials were categorized into three breakage classes based on the particle breakage due to dispersion in the 20 L apparatus. Breakage class I materials undergo ≥ 50% reduction in particle size distribution (Brittleness Index range: > $4 \times 10^3\ m^{-0.5}$). Ascorbic acid, anthraquinone and acetaminophen fall into this class and can yield erroneous results when being tested in the dust explosion apparatus due to a significant shift in the particle size distribution. Breakage class II materials experience 20–50% reduction in particle size distribution (Brittleness Index range: $1.3 \times 10^3\ m^{-0.5}$ - $4 \times 10^3\ m^{-0.5}$). Active charcoal and Pittsburgh pulverized coal fall into this class and are prone to moderate particle size distribution shifting post-dispersion in dust explosion apparatus. This can lead to some error in measurement of explosion parameters. Breakage class III materials undergo ≤ 20% reduction in particle size distribution (low Brittleness Index). Cornstarch, lycopodium clavatum and polyethylene fall into the Class III category and are the least susceptible to breakage. These materials do not undergo much

shift in particle size distribution post-dispersion in the dust explosion apparatus and the measured explosion parameters approximately correspond to pre-dispersion size distribution.

This study correlates the brittleness index values and quantifies the effect of mechanical properties (hardness and fracture toughness) on the particle breakage of dusts post-dispersion in the explosion apparatus. It will help the process industries identify dusts susceptible to breakage during testing, which can lead to misleading hazard parameters such as K_{st} and P_{max}, which may not agree with the conditions at the process scale. This can help in better assessment of dust explosion risk by relating the generated explosion parameter results in the testing apparatus to the actual particle size post-dispersion.

CHAPTER VI

CONSEQUENCE OF PARTICLE SIZE REDUCTION DUE TO DUST DISPERSION ON EXPLOSION PARAMETER ASSESSMENT

6.1. Synopsis

The focus of this work is to show the particle breakage in a 1 m^3 apparatus and to quantify the effect of this particle size distribution shift on the minimum ignition energy (*MIE*). Ascorbic acid was dispersed in a 1 m^3 apparatus at a concentration of 500 g/m^3, and significant particle size reduction was observed. Also, *MIE* measurements were conducted for pre-dispersion and 1 m^3 post-dispersion sample of ascorbic acid to quantify the consequence of the dispersion induced particle size reduction. The *MIE* value for post-dispersion ascorbic acid was significantly lower than the pre-dispersion sample. This is important as dust dispersion from processing, upsets or secondary explosions in the process industries (represented by the 1 m^3 apparatus) can lead to reduction in dust particle size distribution making it flammable (lower its *MIE* values); thereby affecting the dust explosion risk assessment of the process.

6.2. Experiments

6.2.1. Apparatus

This study used a 1 m^3 dust explosion apparatus to demonstrate particle breakage due to dust dispersion and cloud turbulence in an industrial facility. The details of 1 m^3 apparatus are described in Chapter V, section 5.2.1. (Figure 5). Kühner MIKE3 Minimum

Ignition Energy (*MIE*) apparatus (Figure 7) was used to study the consequence of particle breakage due to dust dispersion by measuring the pre-dispersion and post-dispersion *MIE* values. The detail about the apparatus and testing procedure is previously described in Chapter I, section 1.2 (Figure 7 and Figure 8).

6.2.2. Material and Methodology

The material used in this study is ascorbic acid. Literature [23] shows that ascorbic acid has a high brittleness index, thereby rendering it susceptible to breakage. This susceptibility will be used to highlight particle breakage of brittle dusts due to turbulent cloud generation or processing in an industrial facility. The data for particle breakage of ascorbic acid in 1 m^3 apparatus is available in the literature (albeit with a slightly different pre-dispersion particle size) [23], and will provide a validation for ascorbic acid particle breakage in this study.

Ascorbic acid (as received) was characterized for pre-dispersion particle size distribution using laser diffraction (Beckman Coulter LS13320) (Figure 26, Table 9). Thereafter, it was dispersed in the 1 m^3 apparatus at 500 g/m^3 concentration. This concentration was chosen as it provides sufficient post-dispersion sample to do particle size distribution analysis and *MIE* testing. In addition, 500 g/m^3 concentration falls within the flammable region for many typical dusts. After dispersing the dust at 500g/m^3 concentration in 1 m^3 apparatus, it was allowed to settle for a sufficient time (~10 mins) and the post-dispersion sample was collected. The post-dispersion sample particle size distribution was measured using laser diffraction (Beckman Coulter LS13320) (Figure

26, Table 9). A comparison between the particle size distribution of pre-dispersion and post-dispersion ascorbic acid was made to determine the extent of particle breakage. After determining the particle breakage of ascorbic acid in the 1 m^3 apparatus, *MIE* testing was conducted using both pre-dispersion and post-dispersion ascorbic acid to quantify change in *MIE* due to particle breakage. It will allow assessing the shift in dust flammability hazard due to particle breakage during dust cloud formation, or solids processing. This will highlight the importance of considering particle breakage due to cloud turbulence or mechanical shear (as simulated in the 1 m^3 apparatus) in dust explosion testing, and solids handling processes for an accurate risk assessment.

6.3. Results

Ascorbic acid was used to quantify the post-dispersion particle breakage in the 1 m^3 apparatus. The pre and post-dispersion particle size distribution is shown in Figure 26, and the statistics (median, *D (3, 2)*, and specific surface area) are shown in Table 9. Additionally, Table 9 also shows the percent change in the median, *D (3, 2)*, and specific surface area values post-dispersion. Figure 26 and Table 9 present significant particle breakage for ascorbic acid post-dispersion in the 1 m^3 apparatus. The median and the *D (3, 2)* decreased by 33% and 88% respectively. The specific surface area increased by 702%. These values are comparable to the data in the literature [23]. This result indicates that for dusts such as ascorbic acid (high brittleness index) [23], generation of dispersion cloud turbulence or mechanical shear due to processing in an industrial facility (simulated in 1 m^3 apparatus) can cause significant particle breakage. This particle breakage can lead

to a significant increase in the surface area of the dust, thereby increasing the flammability and explosion hazard. Additionally, particle breakage in the 1 m^3 apparatus can affect dust explosion testing. Since the particle size distribution affects explosion parameters, size reduction due to dispersion in the 1 m^3 apparatus can lead to misleading results due to association of explosion parameters with pre-dispersion particle size distribution. This can affect the dust explosion risk assessment.

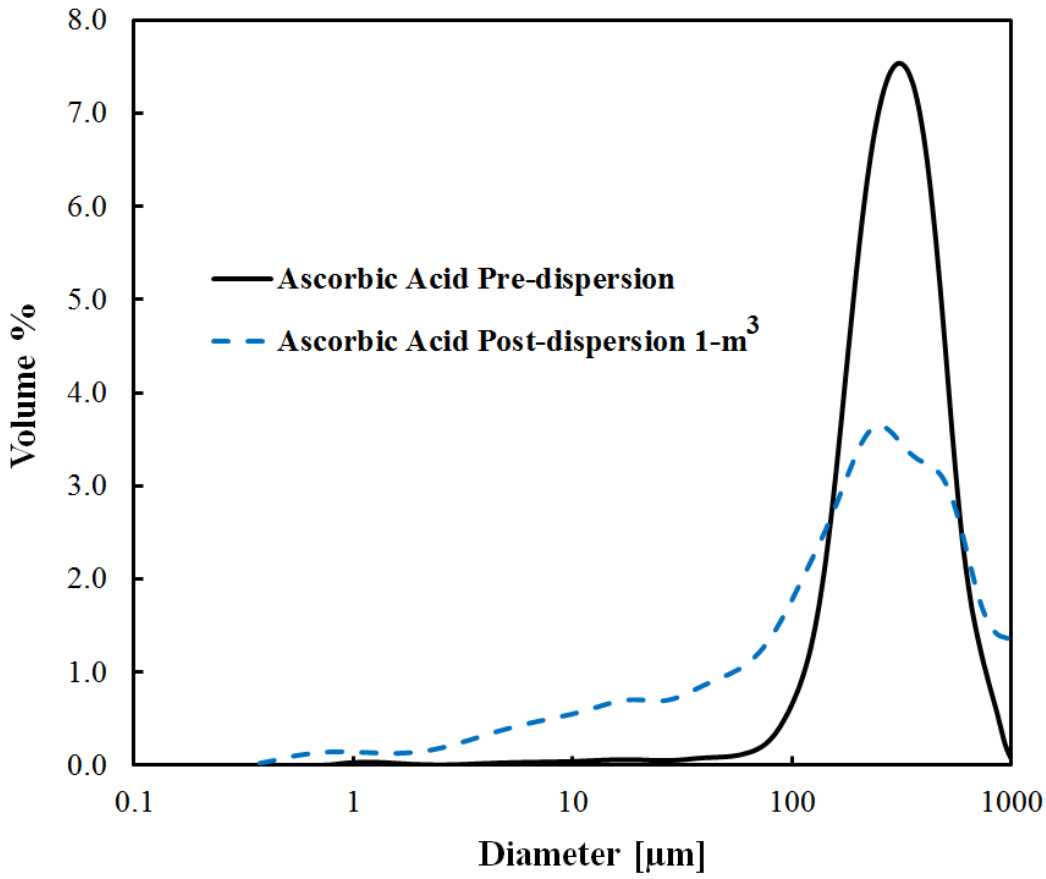

Figure 26 Particle size distribution of pre-dispersion and post- dispersion (1 m^3 apparatus) ascorbic acid at 500 g/m^3.

After quantifying particle breakage for ascorbic acid post-dispersion in the 1 m^3 apparatus, the *MIE* measurements for pre-dispersion and post-dispersion ascorbic acid was conducted using Kühner MIKE3 Minimum Ignition Energy (*MIE*) apparatus. The results show pre-dispersion ascorbic acid did not ignite even at 1000 mJ (inductance = 0 mH, time delay = 120 ms), indicating that the *MIE* for the pre-dispersion dust is greater than 1000 mJ (Figure 27). The post-dispersion ascorbic acid ignited at 300 mJ, but did not ignite at 100 mJ (inductance = 0 mH, time delay = 120 ms), indicating the *MIE* of post-dispersion dust is between 100 mJ and 300 mJ (Figure 28). Equation 1 [25] is used to estimate a single *MIE* value from the data shown in Figure 28 for the post-dispersion ascorbic acid. The estimated value is found to be 200 mJ.

Table 9 Size statistics for pre and post-dispersion ascorbic acid using the standard 1 m^3 apparatus at 500 g/m^3.

Sample and Statistics (dispersion at 500 g/m^3)		**Median/ d_{50} [µm]**	**% Decrease Median/ d_{50}**	***D (3, 2)* [µm]**	**% Decrease *D (3, 2)***	***SSA* [cm^2/ mL]**	**% Increase *SSA***
Ascorbic acid	Pre-dispersion	322	-	179	-	335	-
	Post-dispersion 1 m^3	216	33	22	88	2690	702

D (3, 2): the surface-weighted mean diameter
SSA: the specific surface area
% Change = [(|Original Sample Data-Post Dispersion Data|)/Original Sample Data]*100

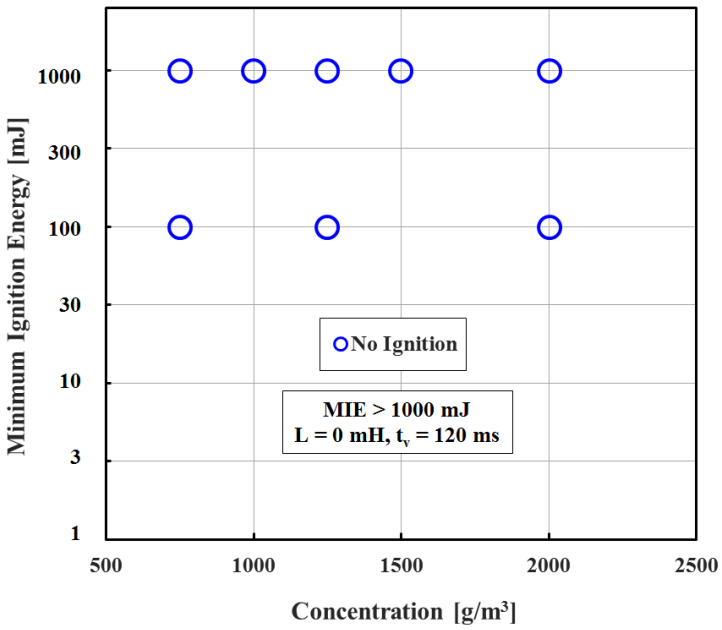

Figure 27 Minimum ignition energy test data for pre-dispersion ascorbic acid.

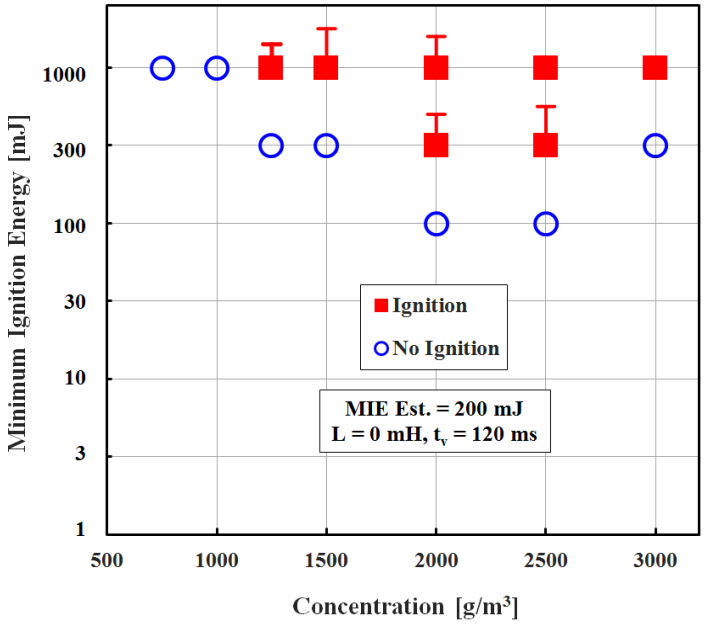

Figure 28 Minimum ignition energy test data for post-dispersion (1 m^3 apparatus) ascorbic acid.

A significant decrease in the *MIE* value is observed for the post-dispersion ascorbic acid. This is due to particle breakage from the dispersion cloud turbulence in the 1 m^3 apparatus, which generates smaller particles, thereby increasing the surface area available for ignition and combustion. This is an important result and highlights an area of potential error in the current dust risk assessment process. Current risk assessment does not consider dusts with large particle size (> 420 µm) as a combustible dust hazard (NFPA 61, NFPA 704) [[95]-[98]]. For dusts < 420 µm, explosion risk assessment is conducted based on ASTM standards, in which the dust is sieved to < 75 µm for conservative explosion parameter measurement. However, the current risk assessment process does not account for particle breakage due to cloud turbulence or dust processing steps. This can severely affect the risk assessment for a dust explosion [Figure 29]. Brittle dusts with particle size > 420 µm can break due to dispersion or processing in a facility, thereby reducing the size of dust to significantly less than 420 µm, making the dust an explosion/deflagration hazard. Also, during a dust explosion risk assessment as per ASTM standards, dusts are sieved to 75 µm and then explosion properties (*MIE*, P_{max}, K_{st}) are measured for conservative approach. However, even 75 µm dusts can break into smaller particles due to dispersion cloud turbulence and processing steps in a facility [18][23], thus lowering the *MIE* and increasing explosion hazard.

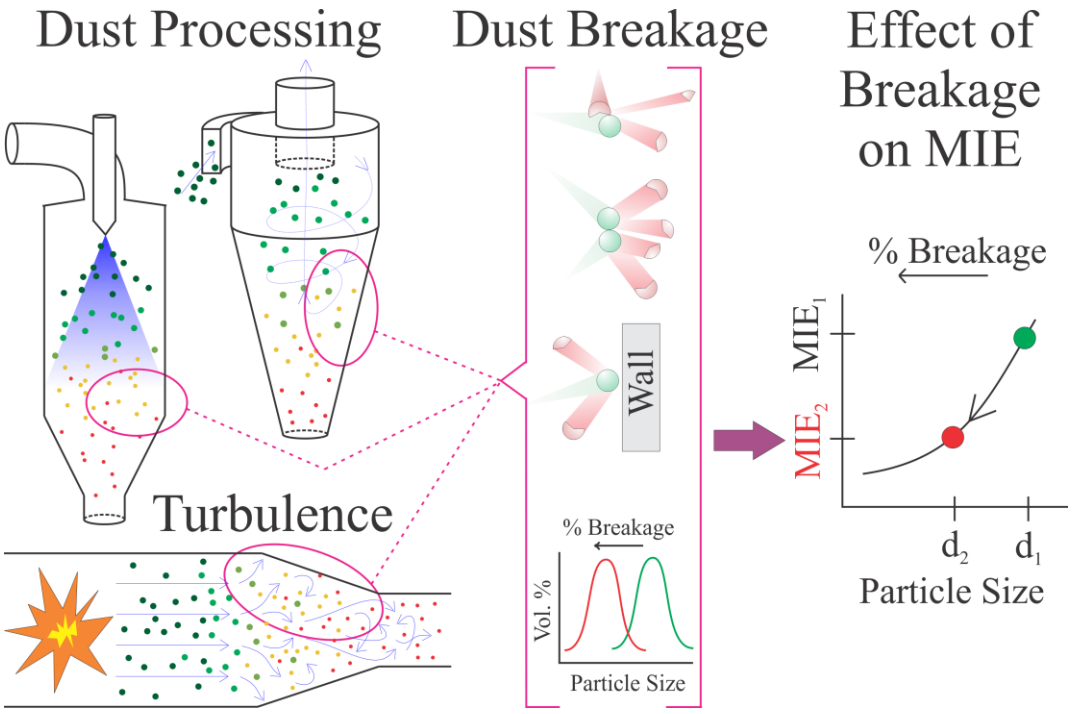

Figure 29 Particle breakage due to processing and the impact on *MIE*.

6.4. Conclusions

This research studied the dust particle breakage due to dispersion cloud turbulence and processing in a facility using a 1 m^3 dust explosion apparatus. This apparatus was used because it replicates an industrial scenario of cloud generation and turbulence levels. Ascorbic acid was used to demonstrate particle breakage due to dispersion cloud turbulence in a 1 m^3 apparatus. Thereafter, *MIE* measurements were conducted for pre-dispersion and post-dispersion ascorbic acid samples to quantify the change in *MIE* due to particle breakage post-dispersion. The following can be concluded based on the results:

- Significant particle breakage occurs for ascorbic acid post-dispersion in the 1 m^3 apparatus. This implies that for ascorbic acid (or similar dusts with high brittleness index [23]), dust cloud generation or processing can lead to particle breakage. This can result in small particles, thereby increasing the explosion hazard.
- Particle breakage leads to an increased dust flammability/explosion hazard. The *MIE* of ascorbic acid reduces significantly due to particle breakage post-dispersion in the 1 m^3 apparatus. This is due to small particle generation, which provides larger surface area for combustion.
- Particle brittleness and breakage due to dispersion cloud generation or dust processing need to be considered for improved dust explosion risk assessment. Current risk assessment process leads to inaccurate assessment due to inconsideration of dust particle breakage. Dusts with particle size > 420 µm would not be considered a combustible hazard according to standards [[95]-[98]], however particle breakage can lead to a significant fraction < 420 µm resulting in a combustible dust hazard. Explosion properties measurements conducted on dust with particles < 75 µm are thought to be conservative. However, even < 75 µm dust can break [18][23], which can lower the *MIE* of the dust and lead to misleading explosion results.

CHAPTER VII

EFFECT OF PARTICLE MORPHOLOGY ON DUST EXPLOSION HAZARD

7.1. Synopsis

Chapters III-VI focused on particle breakage (size distribution aspect) of dust explosion, whereas this chapter will focus on the particle shape/morphology aspect of dust explosion. The aim of this work is to show that particle shape/morphology has an important role to play in influencing the *MIE* of the dust. Two samples of aluminum dust (spherical shaped and irregular shaped) with similar size distribution, polydispersity and chemical composition were taken for the study. *MIE* testing was conducted for these two samples of aluminum using Kühner MIKE3 *MIE* apparatus. It was found that irregular shaped aluminum dust has lower *MIE* compared to spherical shaped aluminum dust. This is attributed to the higher specific surface area of irregular shaped aluminum dust. This study highlights the importance of particle shape/morphology as an important factor that affects dust explosion parameter and makes a case to include particle shape/morphology in dust explosion risk assessment.

7.2. Experiments

7.2.1. Apparatus

Kühner MIKE3 Minimum Ignition Energy (*MIE*) apparatus (Figure 7) was used to study the impact of dust particle shape/morphology on dust explosion hazard by measuring the *MIE* values of dusts with different particle shape. The detail about the

apparatus and testing procedure is previously described in Chapter I, section 1.2 (Figure 7 and Figure 8).

7.2.2. Material and Methodology

Aluminum dust was used to investigate the influence of particle shape/morphology on the minimum ignition energy (*MIE*). Aluminum has a wide industrial application [99] which includes improving the optical properties of pigments [100][101], enhancing combustion and performance of propellants [102][103], pyrotechnic [104], paints and coating [105], *etc.* Aluminum dust has been involved in many dust explosion incidents [9][38][106][107], which has prompted many investigations [22][[36]-[38]][41][44][76][103][[108]-[114]]. Most of these investigations focused on studying the *burning velocity, K_{st}, P_{max}, MIE,* and other combustion characteristics with the aspects of particle size as an important parameter. However, the aspect of aluminum particle shape/morphology on explosion parameters is yet to be explored.

Two samples of aluminum were taken to study the impact of particle shape/morphology on *MIE*. The first sample consisted of spherical shaped particles and the second sample included irregular shaped particles. SEM imaging of the two aluminum samples was done using JEOL JSM-7500F ultra high resolution field emission scanning electron microscope (FE-SEM) and it depicts the difference in particle shape/morphology between the two aluminum samples [Figure 30]. The sample with spherical-shaped aluminum particles was procured from Henan Yuan Yang Aluminum Industry Co. Ltd. The sample with the irregular-shaped aluminum particles was procured

from ECKA Granules Australia Pty Ltd. The chemical compositions of these samples are: spherical (>99.5% Al) and irregular (99.77% Al, 0.035% Si, 0.108% Fe, and 0.005% Ti). The samples were sieved to < 75 µm to comply with the ASTM E 2019 standard for *MIE* testing. Before the *MIE* testing of spherical shaped and irregular shaped aluminum dust, both these samples were processed (sieved and blended, no milling to avoid changes in particle shape/morphology) to yield similar particle size distribution as seen in Figure 31 and Table 10. Particle size distribution was done using Beckman Coulter LS13320 Laser Diffraction. Similar particle size distribution is required to eliminate the impact of particle size on *MIE*. Both these samples were then dried in the oven for 8 hours at 60^0C to remove moisture and then stored in sealed containers in a desiccator for *MIE* testing. *MIE* testing was conducted using Kühner MIKE3 *MIE* apparatus as per the ASTM E 2019 standard described in Chapter I (see section 1.2.). The inductance was set at 0 mH and time delay was set as 120 ms.

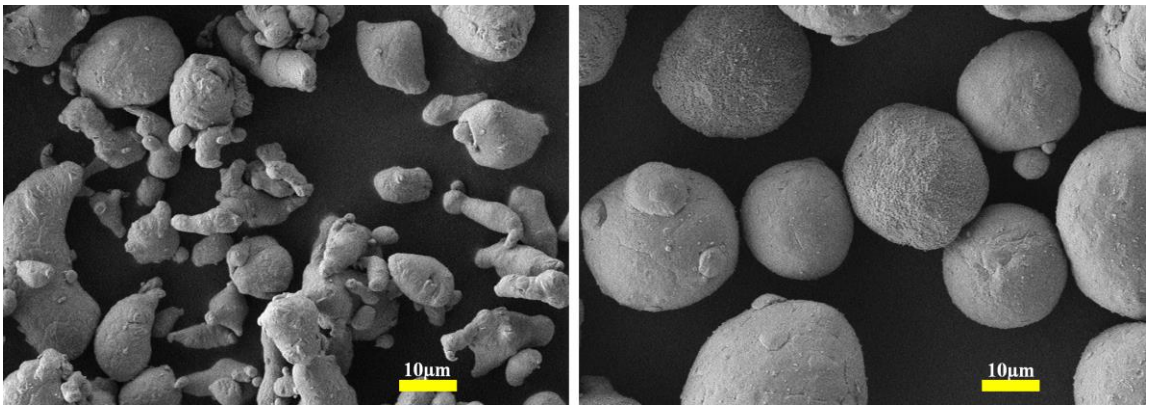

Figure 30 SEM image of irregular shaped (left) and spherical shaped (right) aluminum dust.

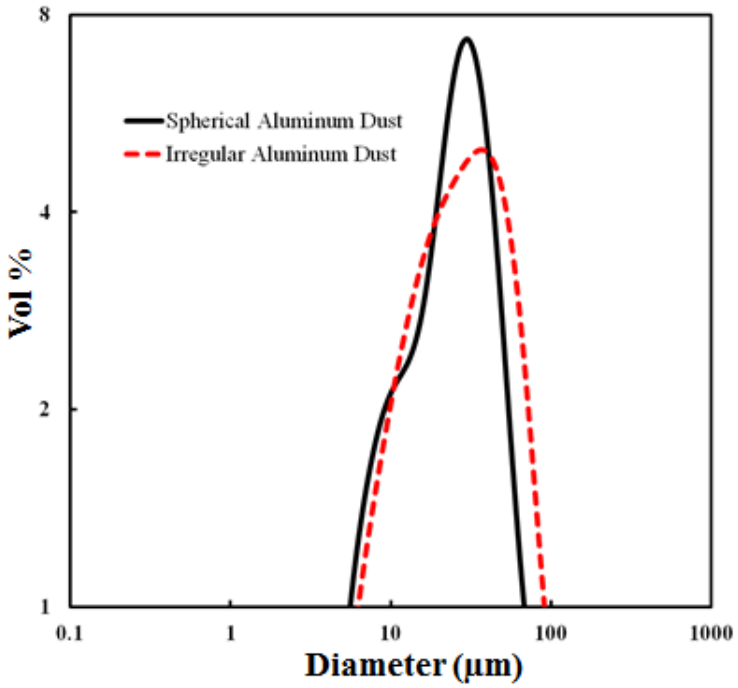

Figure 31 Particle size distributions for spherical shaped and irregular shaped aluminum dust.

Table 10 Size distribution statistics for irregular shaped and spherical shaped aluminum dust.

Sample and Statistics	Irregular Shaped Aluminum	Spherical Shaped Aluminum
Mean (µm)	34.64	31.56
Median/d_{50} (µm)	28.78	27.52
***D (3, 2)* (µm)**	16.18	19.39
Polydispersity (σ_D)	1.99	1.60
Specific Surface Area (cm^2/ml)	3707	3095

7.3. Results

In order to evaluate the impact of particle shape/ morphology on *MIE* without any influence of particle size, spherical and irregular shaped aluminum dust were processed

to yield similar particle size distribution as shown in Figure 31 and Table 10. The size distribution statistics show that mean, median and *D (3, 2)* values of both the samples are very similar. Polydispersity *(σ_D)*, an important parameter to influence explosion characteristics [22], is defined as equation 9:

$$\sigma_D = \frac{d90 - d10}{d50} \quad \text{Eq. 9}$$

Particle size distributions of the two aluminum samples (Figure 31, and Table 10) show that the polydispersity for irregular shaped sample and spherical shaped sample is close (1.99 for irregular shaped aluminum dust and 1.60 for spherical shaped aluminum dust). These values of polydispersity are close enough to not affect the *MIE* of the dust [22]. While the sample preparation technique, chemical composition and particle size characteristics of spherical and irregular shaped aluminum dust were similar, the major difference between these two dust samples was the specific surface area (surface area per unit volume). The specific surface area for the sample containing irregular shaped dust was higher than the sample with spherical aluminum particles as seen in Table 10. Higher specific surface area leads to easier combustion of dust [115]. Based on higher specific surface area of the sample with irregular shaped particles, it was hypothesized that the ignition/combustion probability of irregular shaped particles would be higher than spherical particles, with less ignition energy required to ignite irregular shaped particles.

After making the particle size distribution of irregular shaped and spherical shaped aluminum dust similar, the *MIE* measurements for these dusts were carried out using Kühner MIKE3 Minimum Ignition Energy (*MIE*) apparatus. The results show that irregular shaped aluminum dust ignited at 100 mJ but did not ignite at 30 mJ energy level

(inductance = 0 mH, time delay = 120 ms), indicating that the *MIE* for the irregular shaped aluminum dust is between 30 mJ and 100 mJ (Figure 32). The spherical shaped aluminum dust ignited at 300 mJ, but did not ignite at 100 mJ (inductance = 0 mH, time delay = 120 ms), indicating the *MIE* of spherical shaped aluminum dust is between 100 mJ and 300 mJ (Figure 33). Equation 1 [25] is used to estimate a single *MIE* value from the data shown in Figure 32 and Figure 33 for the irregular shaped and spherical shaped aluminum dust, respectively. The *MIE* value for irregular shaped aluminum dust is found to be 82 mJ, whereas the *MIE* value of spherical shaped aluminum dust is found to be 130 mJ.

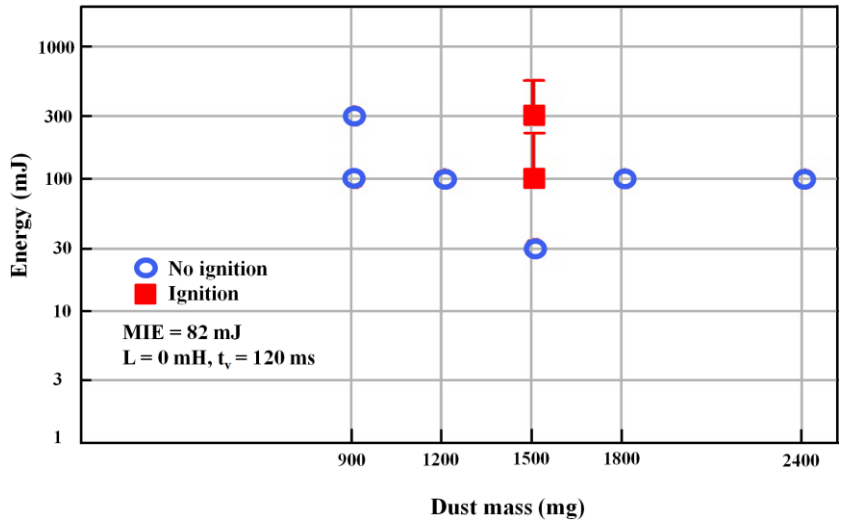

Figure 32 Minimum ignition energy test data for irregular shaped aluminum dust.

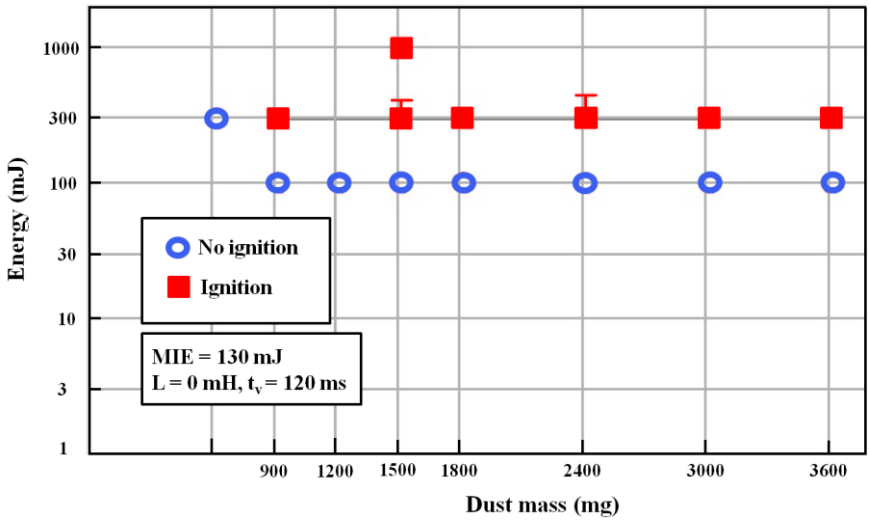

Figure 33 Minimum ignition energy test data for spherical shaped aluminum dust.

It is seen that *MIE* of irregular shaped aluminum dust is significantly lower than spherical shaped aluminum dust. It is expected because the specific surface area of irregular shaped aluminum dust is higher than spherical shaped aluminum dust, thereby enhancing the heat transfer and increasing the flammability. Also, irregularities in the particle shape leads to localized hotspots inducing ignition [116] and leading to increased flammability hazard. Further insight into lower *MIE* of irregular shaped particles compared to spherical shaped particles can be provided using Biot number (*Bi*). It characterizes the heat transfer process and is essentially the ratio of the conductive heat resistance (within the particle) to the convective heat resistance (within the external medium). Biot number is given as equation 10:

$$Bi = \frac{hLc}{k} = \frac{\frac{Lc}{k}}{\frac{1}{h}} = \frac{conductive\ heat\ resistance}{convective\ heat\ resistance} \qquad \text{Eq. 10}$$

Where, h is the external heat transfer coefficient, k is the thermal conductivity of the particle, and Lc is the characteristic dimension (usually taken as volume/surface area). Given that testing conditions are very similar for irregular shaped and spherical shaped dust with similar chemical composition and size distribution, h and k should be very similar for both the dusts. The major difference arises from the different characteristic dimension (Lc) of the samples. Lc for irregular shaped dust is lower than spherical shaped dust because of higher specific surface area of irregular shaped dust. This implies that conductive heat resistance is lower for irregular shaped dust compared to spherical shaped dust. Lower conductive heat resistance of irregular shaped dust will cause more heat transfer within the particle than spherical shaped dust. Typically, aluminum dust has a layer of aluminum oxide on the particle surface, with aluminum trapped inside the oxide layer. More heat transfer within the irregular shaped dust due to lower conductive resistance will allow inside aluminum to expand and crack the oxide layer easily, thus initiating ignition. This highlights the important role of specific surface area in influencing *MIE*. Different particle shape/morphology of dusts (even with same size distribution) has different specific surface area, which impacts the *MIE* significantly.

The results dictate the importance of particle shape/morphology in influencing *MIE* of the dusts and the requirement of its inclusion in dust explosion risk assessment. There are many models that have been developed to predict the *MIE* of the dusts [55] [76] [[117]-[120]]. Mostly, these models factor in the particle size, dust concentration, particle density, specific heat etc. However, particle shape/morphology is often ignored with the assumption of spherical particles. This research highlights the importance of

particle shape/morphology on the *MIE* of dusts and makes a case to include it in prediction models for better *MIE* assessment. Additionally, understanding the role of particle shape/morphology on *MIE* of the dust will help provide guidance to prevent the risk of dust explosion by handling/processing dusts in their less hazardous form.

7.4. Conclusions

This research studied the effect of particle shape/morphology on the minimum ignition energy (*MIE*) of combustible dusts. Spherical shaped aluminum dust and irregular shaped aluminum dust with similar chemical composition, size, and polydispersity were selected for the study. *MIE* testing was carried out in Kühner MIKE3 *MIE* apparatus as per the ASTM E 2019 standard. The results show that the *MIE* of irregular shaped dust is significantly less than the *MIE* of spherical shaped dust. It is seen that particle shape/morphology has significant impact on the *MIE* of the dust samples, with specific surface area playing a key role in influencing the dust explosion parameter. Irregular shaped particle has a larger specific surface area, which leads to lower conductive heat resistance, thereby facilitating ignition of the dust. The study demonstrates the importance of including particle shape/morphology in the same bracket as particle size, chemical composition etc. for risk assessment. Considering particle shape/morphology as a factor that influences *MIE* can help improve the *MIE* prediction models as well as provide guidance for handling dust in its less hazardous form.

CHAPTER VIII

CONCLUSIONS AND FUTURE WORK

8.1. Conclusions

Dust dispersion process can lead to reduction in particle size distribution which can affect the explosion parameters and risk assessment. For dust explosion risk assessment, particle size distribution is considered an important factor; however particle shape/morphology is often ignored, even though it can affect the dust explosion parameters. This dissertation reports the effect of dust dispersion and particle morphology on dust deflagration hazard. In **Chapter I**, the threat of dust explosion to process industries is highlighted and the motivation and requirement for research in the area of dust explosion is provided. Also, **Chapter I** introduces dust explosion, the explosion parameters required for risk assessment, and the standards and apparatus used to measure the dust explosion parameters. **Chapter II** provides the background of this dissertation. It includes literature review and highlights the gaps existing in the literature. In addition, **Chapter II** provides the problem statement, objectives and significance of this research.

In **Chapter III**, the performance of a novel dust dispersion system in the 36 L dust explosion apparatus is compared to a standard 20 L dust explosion apparatus dispersion system for particle breakage. The role of dispersion nozzle and cloud turbulence on particle breakage is examined. The dependence of particle breakage on dust concentration is investigation. Finally, the behavior of nanomaterial post-dispersion is studied. It is observed that particle breakage with the novel dispersion system in the 36

L apparatus is similar to the standard 20 L apparatus. Both dispersion nozzle and dispersion cloud turbulence contribute significantly to particle breakage during dust dispersion process. It is seen that dust cloud concentration is inversely related to particle breakage. Also, nanomaterial (CNFs) de-agglomerates post-dispersion generating large surface area, thereby increasing dust explosion hazard.

Chapter IV is devoted to study the particle breakage due to dispersion in the MIKE3 Minimum Ignition Energy (*MIE*) apparatus. The particle size distribution curves (obtained using laser diffraction) and the SEM images for the samples show that MIKE3 *MIE* apparatus does not cause particle breakage. However, there is a significant shift in size distribution upon dispersion for electrostatic dust. Also, Chapter IV shows that change in size distribution due to dispersion for electrostatic dusts in the *MIE* apparatus can significantly alter the *MIE* measurement, thereby affecting risk assessment.

In **Chapter V**, particle breakage in the standard 20 L, the 36 L and the standard 1 m^3 apparatus is quantified and compared. Particle breakage trend in different types of dust material is studied. Mechanical properties (hardness and fracture toughness) that affect particle breakage are quantified for these dusts using Nanoindentation. The mechanical properties of the dusts are used to measure the brittleness index (brittleness index = hardness / fracture toughness). The brittleness index is correlated to the particle breakage in the 20 L apparatus and the dusts are categorized into breakage classes. It is seen that that the 20 L and the 36 L apparatus cause significantly more particle breakage than the standard 1 m^3 apparatus. Different percent (%) breakage is observed for different dusts indicating the influence of material mechanical properties on particle breakage. A

sigmoidal correlation between brittleness index and particle breakage is seen. Dusts are categorized into three breakage class, ($BCI \geq 50\%$, $20\% < BCII < 50\%$, $BCIII \leq 20\%$) with a range of brittleness index associated with each class. **Chapter V** will help the process industries identify dusts susceptible to breakage during testing, which can lead to misleading explosion parameters such as K_{st} and P_{max}, and help improve the explosion risk assessment.

Chapter VI describes the consequence of particle breakage due to dispersion on the minimum ignition energy (*MIE*). It shows that dust dispersion during dust processing (cyclones, spray dryers *etc.*, as simulated in 1 m^3 apparatus) or dust explosion testing can lead to significant reduction in particle size distribution of dust. This reduction in particle size distribution reduces the *MIE* of the dust and increases the flammability hazard. **Chapter VI** highlights the need of considering particle brittleness and breakage due to dispersion for improved dust explosion risk assessment by putting NFPA standards (which defines combustible dust as < 420 μm) into perspective.

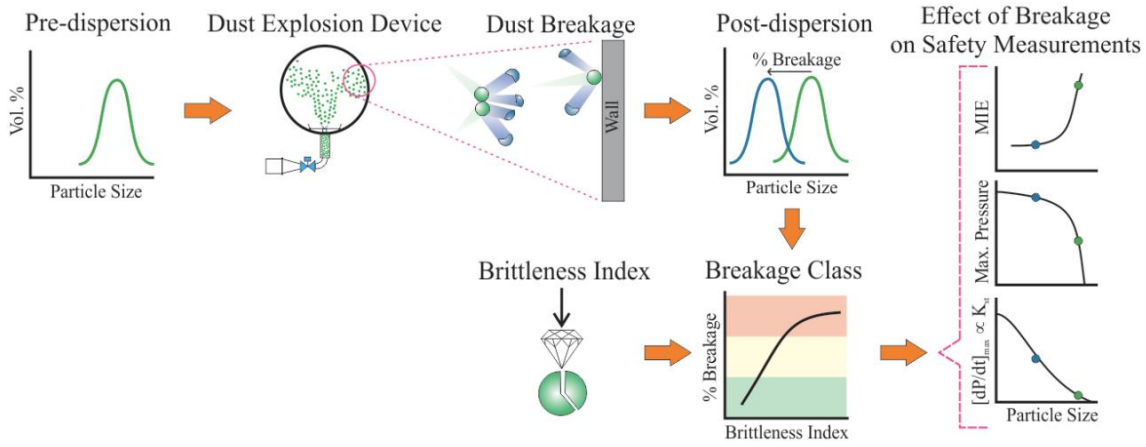

Figure 34 Particle breakage due to dispersion and its effect on explosion parameters [23]. Reprinted with permission from "Classification of particle breakage due to dust dispersion" by Bagaria, P., Li, Q., Dastidar, A., & Mashuga, C., 2019. Powder Technology, 342, 204-213, Copyright (2019) by Elsevier.

Chapters III-VI focus on the particle size distribution aspect of dust explosion (Figure 34), whereas **Chapter VII** reports the particle shape/morphology aspect of dust explosion. In **Chapter VII**, the effect of particle shape/morphology on the minimum ignition energy of dust is studied. Spherical dust and irregular shaped dust, with a similar particle size distribution and polydispersity, were used to demonstrate the difference in *MIE* caused by particle shape. Significant difference in *MIE* value was found with specific surface area (cm^2/ml) playing an important role in influencing *MIE*.

The research in this dissertation will result in improved ASTM, NFPA testing standards and lead to accurate risk assessment for better safety measures.

8.2. Future work

A lot of work has been done in this research to study effect of dust dispersion and morphology on dust deflagration hazards, yet there are still some areas that need further investigation.

This research has shown that dispersion process can cause dust cloud particle size distribution to change thereby affecting the explosion parameter measurement. Analysis of post-dispersion dust sample to quantify particle breakage and then conducting experiments to measure explosion parameters is a good way to associate measured explosion parameters to post-dispersion particle size distribution. A more comprehensive way to get dust cloud particle size distribution, and cloud turbulence in dust explosion apparatus is by using real time optical monitoring laser techniques (Malvern, Digital In-Line Holography (DIH), Particle Image Velocimetry (PIV)). Laser techniques have been previously deployed in the *MIE* apparatus for ignition, flame propagation, thermal and concentration gradient characterization [[77]-[80]]. Having an optical pathway in the dust explosion apparatus (20 L, 36 L, 1 m^3 and *MIE* apparatus) will allow measurement of particle size distribution, and turbulence as the cloud is being formed and enhance the understanding of dust cloud dynamics. Dust cloud dynamics as a function of density and concentration can be resolved using laser monitoring techniques. This will aid in understanding fundamentals behind dust cloud formation and improved risk assessment.

The consequence of particle breakage due to dispersion or processing techniques such as spray drying, cyclone separators *etc.* (as simulated in 1 m^3 apparatus) on explosion parameters should be studied. Chapter VI demonstrates that particle breakage

due to dispersion or processing techniques can decrease the *MIE* of the dust and render a non-combustible dust (as per NFPA standards) as combustible. Additional work is required to understand the effect of particle breakage due to dispersion or processing on other explosion parameters such as P_{max} and K_{st}. Quantifying the changes in P_{max} and K_{st} values due to particle breakage during dispersion or processing will allow process industries to better understand the hazards of dust explosion and improve the risk assessment process.

The effect of particle morphology/shape on dust cloud formation characteristics and explosion parameters P_{max} and K_{st} would be an interesting extension of this dissertation. Particle shape/morphology affects dust flowability and surface area [22], which can influence cloud formation and combustion characteristics. Optical techniques (DIH, PIV) can be used in the MIKE3 *MIE* apparatus to measure cloud concentration during ignition, turbulence, flight pattern as a function of particle shape. This will highlight the role of particle morphology on dust cloud formation characteristics, which eventually affects explosion parameters. Chapter VII shows a significant impact of particle shape/morphology on the *MIE* of dust sample. A logical extension would be to understand the role of particle shape/morphology on P_{max} and K_{st}. Studying the impact of particle morphology on P_{max} and K_{st} will provide guidance to improve P_{max} and K_{st} prediction models by including shape as factor. It will also allow process industries to moderate explosion risk by handling the dust in their least hazardous shape.

Chapter IV revealed the interaction between acetaminophen (electrostatic dust) and Hartmann tube (made of glass) to show that electrostatic dust particles can stick to

Hartmann tube and not participate in dust cloud formation, which may yield erroneous *MIE* results. Understanding the interaction between different dusts and tube material in MIKE3 *MIE* apparatus would be an interesting future work. Different dusts can be selected from the spectrum of triboelectric series (positive, neutral and negative) to disperse in MIKE3 *MIE* apparatus. The dispersion tube can be made of different material in the spectrum of triboelectric series such as glass (positive), polycarbonate (neutral) and polyvinyl chloride (negative) [121]. This will enhance understanding of interaction between dusts and dispersion tube material. The results will provide guidance on selection of tube material depending on specific dust so that dust particles do not stick to the dispersion tube and participate in cloud formation. It will allow accurate *MIE* measurement and improve the risk assessment procedure.

REFERENCES

[1] Cheremisinoff, N. P. (2014). Dust Explosion and Fire Prevention Handbook: A Guide to Good Industry Practices. John Wiley & Sons.

[2] Combustible Dust: Safety and Injury Prevention, Awareness Training Program, Instructors Manual, Version 1. Kirkwood Community College Community Training and Response Center. Susan Harwood Grant Number SH-17797-08-60-F-19. Retrieved from: https://www.osha.gov/dte/grant_materials/fy08/sh-17797-08/cd_instructor_manual.pdf. Accessed on: 12th December, 2016.

[3] Bresland, J. (2008, July 29). Oral Testimony of John S. Bresland, Chair and CEO, U.S. Chemical Safety Board, before the U.S. Senate Committee on Health, Education, Labor and Pensions Subcommittee on Employment and Workplace Safety.

[4] Final Investigation Report: AL Solutions, Inc., New Cumberland, WV (Metal Dust Explosion and Fire Case Study) (2014, July). U.S. Chemical Safety and Hazard Investigation Board (CSB). Report No. 2011-3-I-WV. Retrieved from: http://www.csb.gov/assets/1/19/final_case_study_7.161.pdf. Accessed on: 12th December, 2016.

[5] Keizer, G. (2012, January 13). Apple confirms aluminum dust caused Chinese factory explosions. Computerworld. Retrieved from: http://www.computerworld.com/article/2501382/apple-mac/apple-confirms-aluminum-dust-caused-chinese-factory-explosions.html. Accessed on 12th December, 2016.

[6] Final Investigation Report: US Ink/Sun Chemical Corporation (Ink Dust Explosion and Flash Fires in East Rutherford, New Jersey) (2015, January). U.S. Chemical Safety and Hazard Investigation Board (CSB). Report No. 2013-01-I-NJ. Retrieved from: http://www.csb.gov/file.aspx?DocumentId=688. Accessed on: 12th December, 2016.

[7] Yu, R. (2014, December 30). China Dust Blast Explosion Death Toll Nearly Doubles. The Wall Street Journal. Retrieved from: http://www.wsj.com/articles/china-dust-blast-explosion-death-toll-nearly-doubles-1419957615. Accessed on 12th December, 2016.

[8] Color Play Asia fire claims another life, after five months (2015, November 15). Taipei Times. Retrieved from: http://www.taipeitimes.com/News/taiwan/archives/2015/11/30/2003633680. Accessed on: 12th December, 2016.

[9] Eckhoff, R. K. (2003). Dust explosions in the process industries: identification, assessment and control of dust hazards. Gulf Professional Publishing.

[10] Occupational Safety and health Administration (OSHA). Combustible Dust. Retrieved from: https://www.baghouse.com/combustible-dust-protection-chart-osha/. Accessed on: 2nd February, 2019.

[11] Abbasi, T., & Abbasi, S. A. (2007). Dust explosions–Cases, causes, consequences, and control. Journal of hazardous materials, 140(1), 7-44.

[12] Taveau, J. (2011). Secondary dust explosions: How to prevent them or mitigate their effects? Process Safety Progress, 31(1), 36-50.

[13] P.R. Amyotte, R.K. Eckhoff, Dust explosion causation, prevention and mitigation: An overview, Journal of Chemical Health and Safety, 17 (2009) 15-28.

[14] Bagaria, P., Zhang, J., & Mashuga, C. (2018). Effect of dust dispersion on particle breakage and size distribution in the minimum ignition energy apparatus. Journal of Loss Prevention in the Process Industries, 56, 518-523.

[15] Eckhoff, R. K. (2006). Differences and similarities of gas and dust explosions: a critical evaluation of the European 'ATEX' directives in relation to dusts. Journal of loss prevention in the process industries, 19(6), 553-560.

[16] Di Sarli, V., Russo, P., Sanchirico, R., & Di Benedetto, A. (2014). CFD simulations of dust dispersion in the 20 L vessel: effect of nominal dust concentration. Journal of Loss Prevention in the Process Industries, 27, 8-12.

[17] Khalil, Y. F. (2013). Experimental determination of dust cloud deflagration parameters of selected hydrogen storage materials: complex metal hydrides, chemical hydrides, and adsorbents. Journal of Loss Prevention in the Process Industries, 26(1), 96-103.

[18] Bagaria, P., Zhang, J., Yang, E., Dastidar, A., & Mashuga, C. (2016). Effect of dust dispersion on particle integrity and explosion hazards. Journal of Loss Prevention in the Process Industries, 44, 424-432.

[19] ASTM E1226, 2010. Standard Test Method for Explosibility of Dust Clouds. ASTM International, West Conshohocken, PA (2010)

[20] O. Kalejaiye, P.R. Amyotte, M.J. Pegg, K.L. Cashdollar, Effectiveness of dust dispersion in the 20 L Siwek chamber, J. Loss Prev. Process Indust., 23 (1) (2010) 46-59

[21] P. Zeeuwen, The 1 M3 Vessel For Determination Of Explosion Severity - Why Use It?, DEKRA Insight. http://dekra-insight.com/images/focus-articles/fa-The_1M3_Vessel_for_Determination_of_Explosion_Severity_us_8.5x11_2016.pdf, 2016 (accessed 25th December, 2017)

[22] Castellanos, D.Y. (2013). The Effects of Particle Size and Crystallinity on the Combustion Behavior of Particulated Solids. Texas A&M University

[23] Bagaria, P., Li, Q., Dastidar, A., & Mashuga, C. (2019). Classification of particle breakage due to dust dispersion. Powder Technology, 342, 204-213.

[24] Fauske& Associates. LLC. *MIE* Testing for Combustible Dust Safety: With or Without Inductance? Retrieved from: http://www.fauske.com/blog/bid/397157/mie-testing-for-combustible-dust-safety-with-or-without-inductance. Retrieved on: 14th September, 2017.

[25] Kühner,A., Cesana,C., &Siwek, R. (2010). Operating Manual MIKE 3.4 Kühner AG: CH-4127 Birsfelden, Switzerland.

[26] Du, B., Huang, W., Liu, L., Zhang, T., Li, H., Ren, Y., & Wang, H. (2015). Visualization and analysis of dispersion process of combustible dust in a transparent Siwek 20 L chamber. Journal of Loss Prevention in the Process Industries, 33, 213-221.

[27] Sanchirico, R., Di Sarli, V., Russo, P., & Di Benedetto, A. (2015). Effect of the nozzle type on the integrity of dust particles in standard explosion tests. Powder Technology, 279, 203-208.

[28] Mittal, M. (2014). Explosion characteristics of micron-and nano-size magnesium powders. Journal of Loss Prevention in the Process Industries, 27, 55-64.

[29] B.R. Lawn, D.B. Marshall, Hardness, Toughness and Brittleness: an Indentation Analysis, J. Am. Ceram. Soc., 62 (1979) 347-350

[30] B. Lamy, Effect of brittleness index and sliding speed on the morphology of surface scratching in abrasive or erosive processes, Tribol. Int., 17(1) (1984) 35-38

[31] L.J. Taylor, D.G. Papadopoulos, P.J. Dunn, A.C. Bentham, J.C. Mitchell, M.J. Snowden, Mechanical characterization of powders using nanoindentation, Powder Technol., 143-144 (2004) 179-185

[32] M. Meier, E. John, D. Wieckhusen, W. Wirth, W. Peukert, Influence of mechanical properties on impact fracture: prediction of the milling behaviour of pharmaceutical powders by nanoindentation, Powder Technol., 188 (3) (2009) 301-313

[33] S. Callé, L. Klaba, D. Thomas, L. Perrin, O. Dufaud, Influence of the size distribution and concentration on wood dust explosion: Experiments and reaction modelling, Powder Technology, 157 (2005) 144-148.

[34] M. Hertzberg, I.A. Zlochower, K.L. Cashdollar, Volatility model for coal dust flame propagation and extinguishment, Symposium (International) on Combustion, 21 (1988) 325-333.

[35] R. Soundararajan, P.R. Amyotte, M.J. Pegg, Explosibility hazard of iron sulphide dusts as a function of particle size, Journal of Hazardous Materials, 51 (1996) 225-239.

[36] A. Di Benedetto, P. Russo, P. Amyotte, N. Marchand, Modelling the effect of particle size on dust explosions, Chemical Engineering Science, 65 (2010) 772-779.

[37] O. Dufaud, M. Traoré, L. Perrin, S. Chazelet, D. Thomas, Experimental investigation and modelling of aluminum dusts explosions in the 20 L sphere, Journal of Loss Prevention in the Process Industries, 23 (2010) 226-236.

[38] M. Nifuku, S. Koyanaka, H. Ohya, C. Barre, M. Hatori, S. Fujiwara, S. Horiguchi, I. Sochet, Ignitability characteristics of aluminium and magnesium dusts that are generated during the shredding of post-consumer wastes, Journal of Loss Prevention in the Process Industries, 20 (2007) 322-329.

[39] A. Di Benedetto, P. Russo, Thermo-kinetic modelling of dust explosions, Journal of Loss Prevention in the Process Industries, 20 (2007) 303-309

[40] W. Peukert, Trends in solids process engineering (in German), Chemie Ingenieur Technik 66(10), (1996) 1254-1263

[41] Q. Li, B. Lin, W. Li, C. Zhai, C. Zhu, Explosion characteristics of nano-aluminum powder-air mixtures in 20 L spherical vessels, Powder Technology, 212 (2011) 303-309.

[42] Dufaud, O., Vignes, A., Henry, F., Perrin, L., & Bouillard, J. (2011). Ignition and explosion of nanopowders: something new under the dust. In Journal of Physics: Conference Series (Vol. 304, No. 1, p. 012076). IOP Publishing.

[43] P. Escot Bocanegra, D. Davidenko, V. Sarou-Kanian, C. Chauveau, I. Gökalp, Experimental and numerical studies on the burning of aluminum micro and nanoparticle clouds in air, Experimental Thermal and Fluid Science, 34 (2010) 299-307.

[44] Y. Huang, G.A. Risha, V. Yang, R.A. Yetter, Combustion of bimodal nano/micron-sized aluminum particle dust in air, Proceedings of the Combustion Institute, 31 (2007) 2001-2009.

[45] P.R. Santhanam, V.K. Hoffmann, M.A. Trunov, E.L. Dreizin, Characteristics of Aluminum Combustion Obtained from Constant-Volume Explosion Experiments, Combustion Science and Technology, 182 (2010) 904-921.

[46] P. van der Wel, S. Lemkowitz, B. Scarlett, K. van Wingerden, A Study of Particle Factors Affecting Dust Explosions, Particle & Particle Systems Characterization, 8 (1991) 90-94.

[47] F.S. Lai, D.W. Garrett, L.T. Fan, Study of mechanisms of grain dust explosion as affected by particle size and composition. I. Review of literature, Powder Technology, 32 (1984) 193-202.

[48] H.-C. Wu, H.-J. Ou, D.-J. Peng, H.-C. Hsiao, C.-Y. Gau, T.-S. Shih, Dust E plosion Characteristics of Agglomerated 35 nm and 100 nm Aluminum Particles, International Journal of Chemical Engineering, 2010 (2010) 1-6.

[49] J. Bouillard, A. Vignes, O. Dufaud, L. Perrin, D. Thomas, Ignition and explosion risks of nanopowders, Journal of Hazardous Materials, 181 (2010) 873-880.

[50] Amyotte, P. R. (2014). Some myths and realities about dust explosions. Process Safety and Environmental Protection, 92(4), 292-299.

[51] K.L. Cashdollar, Coal dust explosibility, Journal of Loss Prevention in the Process Industries, 9 (1996) 65-76.

[52] Liu, S. H., Cheng, Y. F., Meng, X. R., Ma, H. H., Song, S. X., Liu, W. J., & Shen, Z. W. (2018). Influence of particle size polydispersity on coal dust explosibility. Journal of Loss Prevention in the Process Industries, 56, 444-450.

[53] I. Glassman, R. Yetter, Combustion, Fourth ed., Elsevier, 2008

[54] A.S. Parker, H.C. Hottel, Industrial & Engineering Chemistry, 28 (1936).

[55] R. Mitsui, T. Tanaka, Simple Models of Dust Explosion. Predicting Ignition Temperature and Minimum Explosive Limit in Terms of Particle Size, Industrial & Engineering Chemistry Process Design and Development, 12 (1973) 384-389.

[56] A.L. Kuhl, M. Boiko, Ignition of Aluminum Particles and Clouds, in: Energetic Materials: High Performance, Insensitive Munitions and Zero Pollution, 2010, pp. 29.21–29.11.

[57] R.S. Lee, D.F. Aldis, D.W. Garrett, F.S. Lai, Improved diagnostics for determination of minimum explosive concentration, ignition energy and ignition temperature of dusts, Powder Technology, 31 (1982) 51-62.

[58] F.-D. Tang, A.J. Higgins, S. Goroshin, Effect of discreteness on heterogeneous flames: Propagation limits in regular and random particle arrays, Combustion Theory and Modelling, 13 (2009) 319-341.

[59] Hartmann, I. (1948). Recent research on explosibility of dust dispersions. Industrial & Engineering Chemistry, 40(4), 752-758.

[60] Jacobson, M., Nagy, J., & Cooper, A. R. (1962). Explosibility of dusts used in the plastics industry. US Department of the Interior, Bureau of Mines.

[61] Jacobson, M., Cooper, A. R., & Nagy, J. (1964). Explosibility of metal powders. Bureau of Mines Washington DC.

[62] Worsfold, M., Amyotte, P., & Marta, M. Fires, explosions and combustible dust hazards. Minerva Safety Management Education. Retrieved from: https://cdn.dal.ca/content/dam/dalhousie/pdf/faculty/engineering/peas/CHEE4773/Fires%

2C%20Explosions%2C%20and%20Combustible%20Dust%20Hazards_4773.pdf. Accessed on 5th February, 2019.

[63] Russo, P., & Di Benedetto, A. (2013). Review of dust explosion modeling. Chemical Engineering Transactions, Vol.31

[64] Thomas, G. O., Oakley, G., & Brenton, J. (1991). Influence of the morphology of lycopodium dust on its minimum ignition energy. Combustion and Flame, 85(3).

[65] Ogle, R. A., Chen, L. D., Beddow, J. K., & Butler, P. B. (1988). An investigation of aluminum dust explosions. Combustion science and technology, 61(1-3), 75-99.

[66] Kuhl, A. L., Leyer, J. C., Borisov, A. A., & Sirignano, W. A. (1989). Dynamics of Deflagrations and Reactive Systems: Heterogeneous Combustion. American Institute of Aeronautics and Astronautics.

[67] Matsuda, T., & Yamaguma, M. (2000). Tantalum dust deflagration in a bag filter dust-collecting device. Journal of hazardous materials, 77(1-3), 33-42.

[68] Rowe, S. (2017). Ashes to Ashes, Dust to Dust…And Dust to Ashes. The Impact of variables on dust explosion properties. Focus Article. Dekra Insight. Retrieved from: https://www.dekra-process-safety.co.uk/images/documents/dekra_fa_the-impact-of-variables-on-dust-explosion-properties.pdf. Accessed on: 6th March, 2019.

[69] The Aluminum Association. (2006). Recommendations for storage and handling of aluminum powders and paste. Retrieved from: https://www.aluminum.org/sites/default/files/Safe%20Handling%20of%20Powder%20and%20Paste.pdf. Accessed on: 5th February, 2019

[70] Zhang, J., Chen, H., Liu, Y., Elledge, H., Mashuga, C. V., & Mannan, M. S. (2015). Dust explosion of carbon nanofibers promoted by iron nanoparticles. Industrial & Engineering Chemistry Research, 54(15), 3989-3995.

[71] Jiang, J., Liu, Y., & Mannan, M. S. (2014). A correlation of the lower flammability limit for hybrid mixtures. Journal of Loss Prevention in the Process Industries, 32, 120-126.

[72] Castellanos, D.Y., Carreto-Vazquez, V. H., Mashuga, C. V., Trottier, R., Mejia, A. F., & Mannan, M. S. (2014). The effect of particle size polydispersity on the explosibility characteristics of aluminum dust. Powder Technology, 254, 331-337.

[73] Ghadiri, M., & Zhang, Z. (2002). Impact attrition of particulate solids. Part 1: a theoretical model of chipping. Chemical Engineering Science, 57(17), 3659-3669.

[74] Burton, D., Lake, P., & Palmer, A. (2011). Properties and Applications of Carbon Nanofibers (CNFs) Synthesized using Vapor-grown Carbon Fiber (VGCF) Manufacturing Technology. Applied Sciences, Inc., Cedarville, OH.

[75] ASTM E2019-03. (2013). Standard test method for minimum ignition energy of a dust cloud in air. West Conshohocken, PA: ASTM International.

[76] Kalkert, N., & Schecker, H. G. (1979). Theoretische Überlegungen zum Einfluß der Teilchengröße auf die Mindestzündenergie von Stäuben. Chemie Ingenieur Technik, 51(12), 1248-1249.

[77] Morrison, K. A., & Alexander, D. R. (1984). Particle concentration measurements by laser imaging for a turbulent dispersion. Particulate Science and Technology, 2(4), 379-395.

[78] Sun, J. H., Dobashi, R., & Hirano, T. (2001). Temperature profile across the combustion zone propagating through an iron particle cloud. Journal of Loss Prevention in the Process Industries, 14(6), 463-467.

[79] Xin-Guang, L., Hong-Guang, D., & Radandt, S. (2007). Measurement of dust concentration in Hartmann bomb. Journal of Northeastern University (Natural Science), 4, 009.

[80] Yu, J., Zhang, X., Zhang, Q., Wang, L., Ji, K., Peng, L., & Gao, W. (2016). Combustion behaviors and flame microstructures of micro-and nano-titanium dust explosions. Fuel, 181, 785-792.

[81] ASTM E2546, Standard Practice for Instrumented Indentation Testing, ASTM International, West Conshohocken, 2015

[82] V. Buskirk, C. Griffith, The Applications of Modern Nanoindentation, Los Alamos National Laboratory. http://permalink.lanl.gov/object/tr?what=info:lanl-repo/lareport/LA-UR-17-222292017, 2017. (accessed 25th December, 2017)

[83] Nanoindenter. Materials Characterization Facility. Retrieved from: http://mcf.tamu.edu/instruments/nanoindenter/. Retrieved on: 22nd September, 2017

[84] V. Di Sarli, R. Sanchirico, P. Russo, A. Di Benedetto, CFD modeling and simulation of turbulent fluid flow and dust dispersion in the 20 L explosion vessel equipped with the perforated annular nozzle, J. Loss Prev. Process Indust., 38 (2015) 204-213

[85] C. Proust, A. Accorsi, L. Dupont, Measuring the violence of dust explosion with the "20 litre sphere" and with the standard "ISO 1 m3 vessel" : systematic comparison and analysis of the discrepancies, J. Loss Prev. Process Indust., 20 (4-6) (2007) 599-606

[86] D. Li, Fracture Toughness Measurement Using Nanoindentation, NANOVEA. http://www.nanovea.com/App-Notes/nanofracturetoughness.pdf, 2014. (accessed 25th December, 2017)

[87] S. Leigh, J.E. Carless, B.W. Burt, Compression characteristics of some pharmaceutical materials, J. Pharm. Sci., 56 (1967) 888-892

[88] X. Mi, Y. Shi, Elastic Properties of Mimetically Synthesized Model Nanoporous Carbon, Mater. Res. Soc. Symp. Proc., 1224 (2010). https://doi.org/10.1557/PROC-1224-FF10-10

[89] Y.A. Yusof, A.C. Smith, B.J. Briscoe, Deformation of food powders by nanoindentation, Int. J. Eng. and Technol., 4 (2) (2007) 154-165

[90] M. Aubertin, F. Hassani, H. Mitri, Rock Mechanics Tools and Techniques: Proceedings of the 2nd North American Rock Mechanics Symposium: NARMS '96, a Regional Conference of ISRM, Canada, 1 (1996)

[91] X. Cao, M. Morganti, B.C. Hancock, V.M. Masterson, Correlating particle hardness with powder compaction performance, J. Pharm. Sci., 99 (10) (2010) 4307-4316

[92] E.A. Silinsh, Organic Molecular Crystals: Their Electronic States, Springer-Verlag, New York, 1980

[93] Polyethylene U.H.M.W., Material Information. http://www.goodfellow.com/E/Polyethylene-UHMW.html, (accessed 25th December, 2017)

[94] T.C. McKay, Physical measurements in sound, light, electricity and magnetism, Stanley-Taylor Company, Berkeley, 1908

[95] NFPA 61, Standard for the Prevention of Fires and Dust Explosions in Agricultural and Food Processing Facilities, National Fire Protection Association (NFPA), (2017)

[96] NFPA 704, Standard System for the Identification of Hazardous Materials for Emergency Response, National Fire Protection Association (NFPA), (2017)

[97] J.D. McKee, Comparative Case Study Analysis of Combustible Dust Explosions: Determining the Need for an OSHA Combustible Dust Standard, Online Theses and Dissertations. 400. https://encompass.eku.edu/etd/400, (2016)

[98] NFPA, Correlating Committee on Combustible Dusts: NFPA 61, NFPA 654, and NFPA 664, National Fire Protection Association (NFPA). https://www.nfpa.org/Assets/files/AboutTheCodes/61/61_A2016_CMD-AAC_FDagenda_01-15.pdf, (2015)

[99] M. Kearns, Development and applications of ultrafine aluminium powders, Materials Science and Engineering A, 375-377 (2004) 120-126.

[100] Y. Zhang, H. Ye, H. Liu, K. Han, Preparation and characterisation of aluminium pigments coated with silica for corrosion protection, Corrosion Science, 53 (2011) 1694-1699.

[101] F.J. Maile, G. Pfaff, P. Reynders, Effect pigments—past, present and future, Progress in Organic Coatings, 54 (2005) 150-163.

[102] K. Jayaraman, S. Chakravarthy, R. Sarathi, Accumulation of nano-aluminium during combustion of composite solid propellant mixtures, Combustion, Explosion, and Shock Waves, 46 (2010) 21-29.

[103] R.J. Gill, C. Badiola, E.L. Dreizin, Combustion times and emission profiles of micron-sized aluminum particles burning in different environments, Combustion and Flame, 157 (2010) 2015-2023.

[104] Pourmortazavi, S. M., Hajimirsadeghi, S. S., Kohsari, I., Fathollahi, M., & Hosseini, S. G. (2008). Thermal decomposition of pyrotechnic mixtures containing either aluminum or magnesium powder as fuel. Fuel, 87(2), 244-251.

[105] González, S., Cáceres, F., Fox, V., & Souto, R. M. (2003). Resistance of metallic substrates protected by an organic coating containing aluminum powder. Progress in organic coatings, 46(4), 317-323.

[106] D.C. May, D.L. Berard, Fires and explosions associated with aluminum dust from finishing operations, Journal of Hazardous Materials, 17 (1987) 81-88.

[107] CSB, Investigation Report. Aluminum Dust Explosion, Hayes Lemmerz International-Huntington, Inc., U.S Chemical Safety and Hazard Investigation Board, 2005.

[108] S. Goroshin, I. Fomenko, J.H.S. Lee, Burning velocities in fuel-rich aluminum dust clouds, Symposium (International) on Combustion, 26 (1996) 1961-1967.

[109] Y. Huang, G.A. Risha, V. Yang, R.A. Yetter, Effect of particle size on combustion of aluminum particle dust in air, Combustion and Flame, 156 (2009) 5-13.

[110] M. Beckstead, Correlating Aluminum Burning Times, Combustion, Explosion, and Shock Waves, 41 (2005) 533-546.

[111] R. Friedman, A. Maček, Ignition and combustion of aluminium particles in hot ambient gases, Combustion and Flame, 6 (1962) 9-19.

[112] R. Siwek, C. Cesana, Ignition behavior of dusts: Meaning and interpretation, Process Safety Progress, 14 (1995) 107-119.

[113] P. van der Wel, J. van Veen, S. Lemkowitz, B. Scarlett, C.. van Wingerden, An interpretation of dust explosion phenomena on the basis of time scales, Powder Technology, 71 (1992) 207-215.

[114] T. Matsuda, M. Yashima, M. Nifuku, H. Enomoto, Some aspects in testing and assessment of metal dust explosions, Journal of Loss Prevention in the Process Industries, 14 (2001) 449-453.

[115] Nifuku, M., & Katoh, H. (2001). Incendiary characteristics of electrostatic discharge for dust and gas explosion. Journal of Loss Prevention in the Process Industries, 14(6), 547-551.

[116] Cairns, M. (2010). Titanium Particle Combustion (Doctoral dissertation, McGill University).

[117] Jost, W. 1950. Zur Theorie der Flammengeschwindigkeit III (Elementare Überlegunen über die Funkenzundung).

[118] Gubin, E.I., and Dik, I.G. (1986) Ignition of a Dust Cloud by a Spark. Combustion, Explosion and Shock Waves, Volume 22, Issue 2, pp.135-141.

[119] Bidabadi, M., Mohammadi, M., Poorfar, A.K., Mollazadeh, S., Zadsirjan, S., 2015. Modeling combustion of aluminum dust cloud in media with spatially discrete sources. Heat Mass Transf. 51, 837–845.

[120] Whitmore, M. W. (1992). Prediction of dust cloud minimum ignition energy for organic dusts from modified Hartmann tube data. Journal of loss prevention in the process industries, 5(5), 305-309.

[121] Lee, B. W., Orr, D. E. The Triboelectric Series. AlphaLab Inc. Retrieved from: https://www.alphalabinc.com/triboelectric-series/. Accessed on 6th February, 2019.